Structural basis for the binding of antifreeze proteins from a snow mold fungus to ice

（担子菌由来不凍タンパク質の構造と機能に関する研究）

by

Jing Cheng

A thesis submitted to the Division of Life Science,

Graduate School of Life Science, Hokkaido University

In conformity with the requirements for the degree of Doctor of Philosophy

Hokkaido University

Sapporo, Hokkaido, Japan

March, 2017

Table of contents

Table of contents i

List of Figures iv

List of Tables vi

List of Abbreviations vii

Chapter 1 General Introduction 1

1.1 Ice binding proteins (IBPs) 2

1.2 Biotechnological applications of IBPs 2

1.3 Functional diversity of IBPs 3

1.3.1 Antifreeze 3

1.3.2 Ice recrystallization inhibition (IRI) 4

1.3.3 Ice nucleation 7

1.3.4 Ice adhesion 8

1.4 Structural diversity of AFPs 9

1.4.1 Fish AFPs 9

1.4.1 Insect AFPs 11

1.4.2 Plant AFPs 13

1.4.3 Microbial AFPs 14

1.5 Ice as a heterogeneous ligand 17

1.6 Determining the planes of ice to which AFPs bind 19

1.7 Moderately active vs. hyperactive AFPs 20

1.8 The mechanism by which AFPs bind to ice 21

1.9 AFP isoforms 23

1.10 AFPs from a snow mold fungus, *Typhula ishikariensis* 24
1.11 X-ray crystal structure of *Tis*AFP6 27
1.12 Aims and objectives 29
Chapter 2 Hydrophobic ice-binding sites confer hyperactivity of an antifreeze protein from a snow mold fungus 31
2.1 Abstract 33
2.2 Introduction 34
2.3 Materials and methods 38
2.3.1 Expression and purification of wild-type *Tis*AFPs and their mutants 38
2.3.2 Thermal hysteresis measurements and ice crystal morphology 41
2.3.3 FIPA analysis 42
2.3.4 Crystallization and X-ray structure analysis of *Tis*AFP8 43
2.3.5 Ice-lattice matching method 43
2.3.6 Docking model of the ice-AFP interaction 45
2.3.7 Circular-dichroism (CD) spectroscopy 45
2.4 Results 46
2.4.1 Purification of recombinant *Tis*AFP wild type and mutants 46
2.4.2 Antifreeze activity of *Tis*AFP8 46
2.4.3 FIPA analysis 50
2.4.4 Overall structure of *Tis*AFP8 50
2.4.5 Ice binding site of *Tis*AFP8 54
2.4.6 Site-directed mutagenesis of the putative IBS of *Tis*AFP8 57
2.4.7 Characterization of the waters on the β-sheet and loop region of *Tis*AFP8 62
2.4.8 Ice-docking model 64

2.5 Discussion 66
2.5.1 General comparison between *Tis*AFP8 and *Tis*AFP6 66
2.5.2 Mutations on hydrophobic residues of *Tis*AFP8 caused TH decrease 67
2.5.3 *Tis*AFPs may recognize ice through a compound IBS 67
2.5.4 Bound waters on the compound IBS of *Tis*AFP8 form an ice-like network 68
2.5.5 *Tis*AFP8 matches ice lattice better 68
2.5.6 *Tis*AFP8 has a more hydrophobic IBS 69
2.5.7 Biological implications 70
2.6 Supplemental data 73
2.6.1 pH dependence study of *Tis*AFP8 73
2.6.2 Ice recrystallization inhibition (IRI) assay 75
2.7 Acknowledgements 77
Chapter 3 General discussion 78
3.1 *Tis*AFPs adsorb to ice surface through the anchored clathrate water mechanism 79
3.2 Hyperactive *Tis*AFP8 Vs moderately active *Tis*AFP6 81
3.3 Biological implications 82
Acknowledgements 84
References 85

List of Figures

Figure 1.1 Simple model of adsorption-inhibition mechanism. 5

Figure 1.2 Schematic representation of thermal hysteresis. 6

Figure 1.3 X-ray crystal structures of fish AFPs. 10

Figure 1.4 X-ray crystal structures of insect AFPs. 12

Figure 1.5 X-ray crystal structures of other AFPs. 15

Figure 1.6 Amino acid sequence alignment of homologous AFPs to *Tis*AFP6. 16

Figure 1.7 Hexagonal unit cell of ice lattice (I_h) and representative ice planes involving in AFP interactions. 18

Figure 1.8 Sclerotium and fruit body of *Typhula Ishikariensis.* 25

Figure 1.9 Amino acid sequence alignments of *Tis*AFP isoforms. 26

Figure 1.10 X-ray crystal structure of *Tis*AFP6. 28

Figure 1.11 Regular and repetitive IBSs of hyperactive AFPs Vs complex IBSs of homologous AFPs to *Tis*AFP6. 30

Figure 2.1 Purification of recombinant *Tis*AFP8 wild type. 39

Figure 2.2 Crystal image of *Tis*AFP8. 44

Figure 2.3 SDS-PAGE analysis of purified wild-type *Tis*AFPs and their mutants. 47

Figure 2.4 Antifreeze properties of *Tis*AFP8. 49

Figure 2.5 Crystal structure of *Tis*AFP8. 53

Figure 2.6 Comparison of the IBS of *Tis*AFP8 and *Tis*AFP6. 55

Figure 2.7 Site-directed mutants introduced to the IBS of *Tis*AFP8. 58

Figure 2.8 Site-directed mutants introduced to the IBS of *Tis*AFP6. 59

Figure 2.9 CD spectra of wild-type (WT) *Tis*AFP8 and mutants. 60

Figure 2.10 Ice crystal bursts in the presence of each mutant. 61

Figure 2.11 Superposing of the ice-like waters on *Tis*AFP8 to the basal plane of the ice lattice. 63

Figure 2.12 Docking of *Tis*AFP8 and *Tis*AFP6 to the basal plane of ice. 65

Figure S2.1 Effect of pH on TH activity and ice crystal morphology of *Tis*AFP8. 74

Figure S2.2 Inhibition of ice recrystallization by *Tis*AFP8. 76

Figure 3.1 Crystal packing of TisAFP8 observed in the asymmetric unit of the crystal. 80

List of Tables

Table 2.1 Primer sequences used for the construction of the expression plasmids of wild-type *Tis*AFP8 and mutants, as well as *Tis*AFP6 S212A mutant. 40

Table 2.2 Summary of the yield of each protein. 48

Table 2.3 Summary of data collection and refinement statistics. 51

Table 2.4 Comparison of exposed nonpolar ASA. 71

List of Abbreviations

ACW, anchored clathrate water

AFGP, antifreeze glycoprotein

AFP, antifreeze protein

CD, circular dichroism

*Cf*AFP, *Choristoneura fumiferana* antifreeze protein

*Col*AFP, *Colwellia* sp. Strain SLW05 antifreeze protein

*Dc*AFP, *Dendroides Canadensis* antifreeze protein

FIPA, fluorescence-based ice plane affinity

*Fc*AFP, *Fragilariopsis cylindrus* antifreeze protein

*Ff*AFP, *Flavobacterium frigoris* PS1 antifreeze protein

IBP, ice-binding protein

IBS, ice-binding site

INP, ice nucleation protein

IR, ice recrystallization

IRI, ice recrystallization inhibition

*Le*AFP, *Leucosporidium* sp. AY30 antifreeze protein

*Lp*AFP, *Lolium perenne* antifreeze protein

MD, molecular dynamics

*Mp*AFP, *Marinomonas primoryensis* antifreeze protein

Mw, molecular weight

NMR, nuclear magnetic resonance

PDB, Protein Data Bank

PVC, polyvinyl chloride

QAE-Sephadex-binding, quaternary-amino-ethyl-Sephadex-binding

RMSD, root mean squared deviation

RTX, Repeats-In-Toxin

*Ri*AFP, *Rhagium inquisitor* antifreeze protein

SDS-PAGE, sodium dodecyl sulfate-polyacrylamide gel electrophoresis

SP-Sephadex-binding, sulfopropyl-Sephadex-binding

TH, thermal hysteresis

T_f, freezing point

*Tis*AFP, *Typhula ishikariensis* antifreeze protein

T_m, melting point

*Tm*AFP, *Tenebrio molitor* antifreeze protein

UV, ultraviolet

sfAFP, snow flea antifreeze protein

Chapter 1 General Introduction

1.1 Ice binding proteins (IBPs)

To survive at subzero temperatures, many living organisms have developed several strategies to help them overcome extremely cold temperatures, among which ice binding proteins (IBPs) are well known as a result of cold adaptation. The first IBPs were discovered from the blood of Antarctic Notothenioid fishes in the late 1960s and were the antifreeze glycoproteins (AFGPs) [1]. Since the discovering of the first AFGP, other IBPs are found to be expressed by various organisms, including fishes, plants, insects and microorganisms.

So far, at least four IBP subclasses are documented: antifreeze proteins (AFPs), ice-recrystallization (IR) inhibition proteins, ice nucleation proteins (INPs) and a newly discovered ice adhesion protein [2]. AFPs are termed as those IBPs that function to protect an organism from freezing. IR inhibition proteins are serving to inhibit the process of ice recrystallization by controlling the size and aggregation of ice crystals rather than to prevent water from freezing [3]. INPs allow water to freeze at high subzero temperatures and prevent supercooling of the solution, which are membrane-associated and tend to aggregate [4, 5, 6]. An AFP (*Mp*AFP) from an Antarctic bacterium, *Marinomonas primoryensis*, functions as an ice adhesion protein by helping the bacterium to adhere to the underside of sea or lake ice and obtain oxygen and nutrients [2].

1.2 Biotechnological applications of IBPs

Taking a cue from the characteristics of IBPs, researchers are working on the potential applications of IBPs in industry, medicine and agriculture [7]. The applications are numerous

and include using IBPs as: additives to improve the quality, texture and shelf life of frozen food during freezing storage, transport and thawing [8, 9]; as cryoprotectants in cryopreservation of cells, tissues and organs [10, 11], and as adjuvants in cancer cryosurgery [12]. Besides, IBPs can also be used to: acquire transgenic plants and animals that possess the ability to cold acclimate by IBP gene transfer [13]; inhibit frost and ice formation on various surfaces [14]; control the growth of hydrocarbon hydrates in oil and gas pipelines [15, 16].

To introduce IBPs into foods, people face with a risk that an allergic reaction in individuals sensitive to that IBP will be provoked or not. Fish type III AFP has been proved that it is unlikely to induce allergic responses in humans [17]. One try has been made in the food industry that Unilever, the global consumer marketing products giant, sells ice creams containing fish AFPs [18]. However, the success rate of these applications varies. For example, *Drosophila melanogaster*, transformed with the hyperactive insect AFP gene from the spruce budworm, *Choristoneura fumiferana*, cannot tolerate cold shock [19]. To improve the success rate of AFP biotechnological applications, we need to better understand that how AFPs function in their host at the molecular level.

1.3 Functional diversity of IBPs

1.3.1 Antifreeze

Species containing IBPs can be classified as two categories: freeze resistance and freeze tolerance. Freeze resistant species (such as marine fishes and insects) have to prevent their body fluids from freezing altogether. For example, marine fishes encounter seawater which has a freezing point of -1.9 °C and is much colder than that of fish blood. To avoid freezing, marine

fishes produced AFPs to bind to the surface of seed ice crystals and control their growth by an adsorption-inhibition mechanism [20]. The binding of AFPs causes increased local curvatures in the ice front, which is energetically less favorable for water molecules to add to the ice lattice (Fig. 1.1 C). Thus it results in a non-colligative depression of the freezing point (T_f) and a slight elevation of the melting point (T_m) due to the Gibbs-Thomson effect [21]. The difference between T_f and T_m is termed as thermal hysteresis (TH), which is widely utilized to quantify antifreeze protein (Fig. 1.2).

Adsorption of AFPs to ice crystals also leads to a modification of crystal morphology due to the specific binding of AFPs, which is usually a defined and unchanging shape within the TH gap. This ice crystal morphology is a reproducible characteristic of the particular AFP type. However, there are no common morphological features shared by all hyperactive or by all moderately active AFPs (see details in Chapter 1.7). Moderately active AFPs produce elongated hexagonal bipyramid shaped ice crystals during growth in the hysteresis gap, while hyperactive AFPs induce more varied crystal shapes [22]. For example, *Tm*AFP from an insect *Tenebrio molitor* produces lemon shaped ice crystals. The ice crystal morphology induced by *Cf*AFP from spruce budworm, *Choristoneura fumiferana*, has been described as hexagonal disc shape [22]. However, Bar-Dolev *et al*. found that unlike in the presence of moderately active AFPs, the ice crystal morphologies produced by hyperactive AFPs from insects and bacteria are formed during melting, in which a definitive shape is acquired once the crystal is small enough [23].

1.3.2 Ice recrystallization inhibition (IRI)

Ice recrystallization is a process that large ice grains form at the expense of smaller ones due to Ostwald ripening process. And ice recrystallization generally occurs readily in a condition

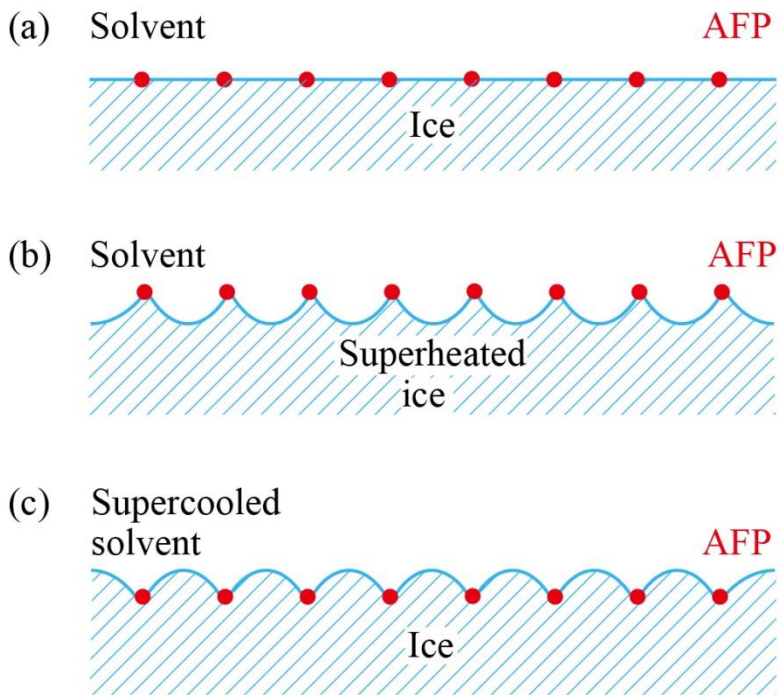

Figure 1.1 Simple model of adsorption-inhibition mechanism.

(a) AFPs (red spheres) bind to ice (indicated) at the temperature near Tm (≈0 °C). At this stage, the ice-water interface is assumed to be flat in between the adsorbed AFPs. (b) Simple model of melting-inhibition operating through Gibbs-Thomson effect, causing negative curvatures. (c) Simple model of freeing-inhibition operating through Gibbs-Thomson effect, causing positive curvatures. Adsorbed AFPs limit the ice growth to the areas between AFPs. Therefore, ice is forced into an energetically unfavorable state, where waters are difficult to join the ice lattice and further growth of ice is arrested until explosive growth occurs.

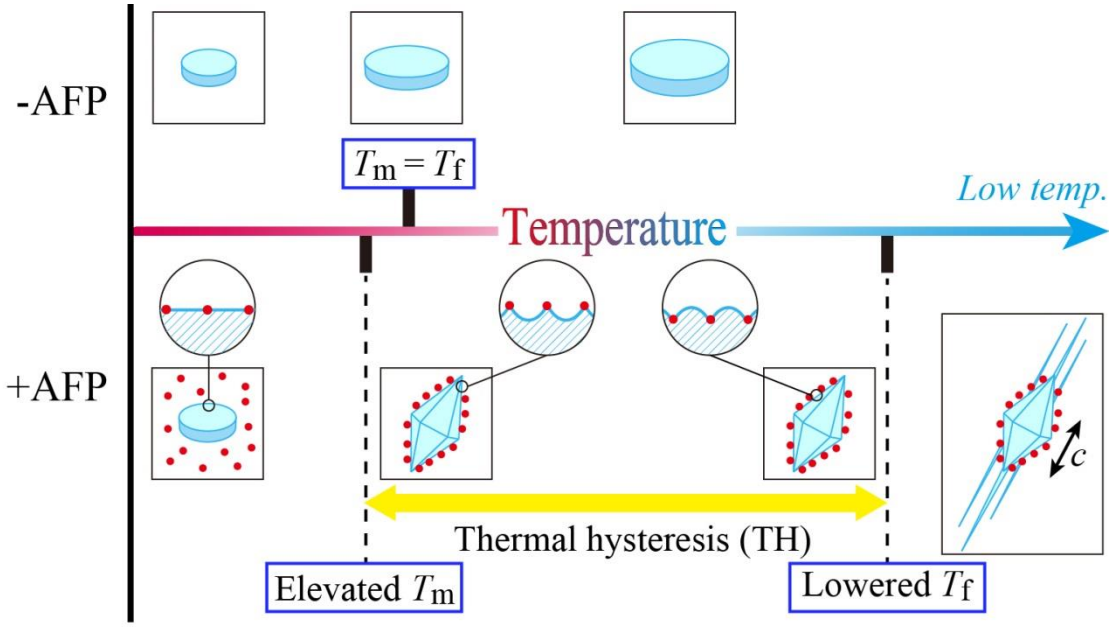

Figure 1.2 Schematic representation of thermal hysteresis.

The upper side of the horizontal temperature scale shows the situation when AFPs are absent in solution and the freezing point (T_f) equals to the melting point (T_m). Ice crystals grow or shrink in the form of round disk (light blue) when temperature fluctuates beyond the T_m or T_f. The lower side illustrates the case where AFPs are present in solution. AFPs (red dots) adsorb onto the ice surface, develop facets on ice, slightly raise the T_m and lower the T_f. Generally, in the presence of moderately active AFPs, ice crystals grow into two directions along the *c*-axis. Ice crystals bound by hyperactive AFPs grow in a dendritic pattern (normal to the *c*-axis) below the T_f.

when the temperature fluctuates diurnally or during the spring freeze-thaw circle, which is just below the melting point. Under most freezing conditions, ice forms as a multicrystalline mass. Grain boundaries between ice grains tend to be strained and unstable [24]. At high sub-zero temperatures, an appreciable amount of liquid is present around the ice grains. And there is a tendency for ice to recrystallize, resulting in a less total surface area of ice and an energetically favorable state [24].

AFPs allow freeze resistant species to supercool and avoid freezing by adsorbing onto the surface of ice crystals and halting their growth. However, freeze tolerant organisms can survive freezing of their extracellular water, for which supercooling has to be avoided because it would ultimately lead to the rapid, uncontrolled growth of ice [25]. Ice crystals formed in the extracellular space tend to recrystallize at several degrees below the melting point. Therefore, freeze tolerant organisms (overwintering plants such as carrots and grasses) produce IBPs to inhibit ice recrystallization and minimize the damage caused by it in frozen tissue and help themselves tolerate freeze rather than resist it [26, 27]. These IBPs show weak TH activity but have effective IRI activity. One IBP from ryegrass was reported to be better at IRI activity [28].

IRI is observed at much lower AFP concentrations than TH. TH requires millimolar AFP concentrations, however, only micromolar concentrations are needed for IRI [3]. Although all IBPs to date are found to possess both TH and IRI activity simultaneously, it seems that both TH and IRI are driven by the same adsorption-inhibition mechanism to confer freeze resistance and freeze tolerance, respectively.

1.3.3 Ice nucleation

INPs show an exact opposite function to AFPs, which initiate ice growth at high subzero temperatures [29]. Due to the large size (typically greater than 120 kDa) and tendency to

aggregate, there are currently no determined structures for INPs. Several predicted model structures of INPs suggest that the class of INPs and some hyperactive AFPs (such as *Mp*AFP) have a similar β-solenoid structure, but the size of INPs is on a much larger scale [30, 31]. Moreover, it has been postulated that INPs can function to trigger ice nucleation by organizing waters into the ice-like clathrate structures [31], similar to the anchored clathrate water (ACW) mechanism of AFPs [32].

1.3.4 Ice adhesion

One novel function of IBP has been recently discovered as ice adhesin. This ice adhesion protein (*Mp*AFP) was isolated from an Antarctic Gram-negative bacterium, *Marinomonas primoryensis*, and is exceptionally large (ca.1.5 MDa) with Ca^{2+}-dependent antifreeze activity [33, 34]. The protein is divided into five distinct regions (RI-V), all of which show dependence of millimolar Ca^{2+} to fold correctly [2]. The N-terminal region I (RI) is thought to bind the protein to the outer membrane of the bacterium [2]. Region II (RII) is made up of ～120 tandem 104-residue repeats and accounts for the majority of the whole protein, forming a ～0.6 μm rod-like structure in order to project the ice-binding domain (RIV) away from the bacterial cell surface to help it to contact sea or lake ice [35]. Region IV (RIV) is 322-residue long and contains 13 tandem Repeats-In-Toxin (RTX)-like repeats, in which the antifreeze activity of *Mp*AFP resides. RIV is thought to serve to adhere to the underside of ice [2]. Region V (RV) also contains RTX-like repeats and may be responsible for directing the protein out of the bacterial cell as a non-cleavable signal sequence through the type I secretion pathway [2]. It was suggested that the host bacterium develops the AFP-like domain within this adhesin to adsorb to ice, finally obtaining oxygen and nutrients.

1.4 Structural diversity of AFPs

To date, dozens of nuclear magnetic resonance (NMR) and X-ray crystal structures of AFPs from polar fishes, insects, plants, algae, fungi and bacteria have been reported. Although they share a common capability of binding to ice, AFPs are found to have an extraordinary diversity on their amino acid sequence and tertiary structure. This remarkable divergence is considered as the result of convergent evolution, in which the AFPs arose fairly recently and independently from different progenitors under strong selective pressure and an abrupt shift in environmental conditions (subzero environment) [36, 37]. AFPs are classified broadly into several types according to the features of their three-dimensional structures, which are described as follows.

1.4.1 Fish AFPs

The first AFPs were the antifreeze glycoproteins (AFGPs), derived from Antarctic Notothenioid fishes and discovered over 50 years ago [1]. Marine fishes produce AFPs to prevent their blood from freezing and survive in subzero environment. Typically, most of the fish AFPs exhibit TH activities of 0.5-1.5 °C at millimolar concentrations, classified as moderately active AFPs (see details in Chapter 1.7).

Currently, fish AFPs have been classified into five types [AFP type I~IV and AFGP]. NMR and/or X-ray derived structures are available for all fish AFPs except type IV AFP and AFGP. Most type I AFPs are long, simple alanine-rich amphipathic α-helices with the molecular weight (Mw) of ca. 3.3-5 kDa (Fig. 1.3a) [38, 39]. Recently, a new type I AFP homologue was discovered and characterized from the plasma of winter flounder *Pseudopleuronectes americanus* [40]. The crystal structure of this large type I AFP (Maxi) was determined by X-ray

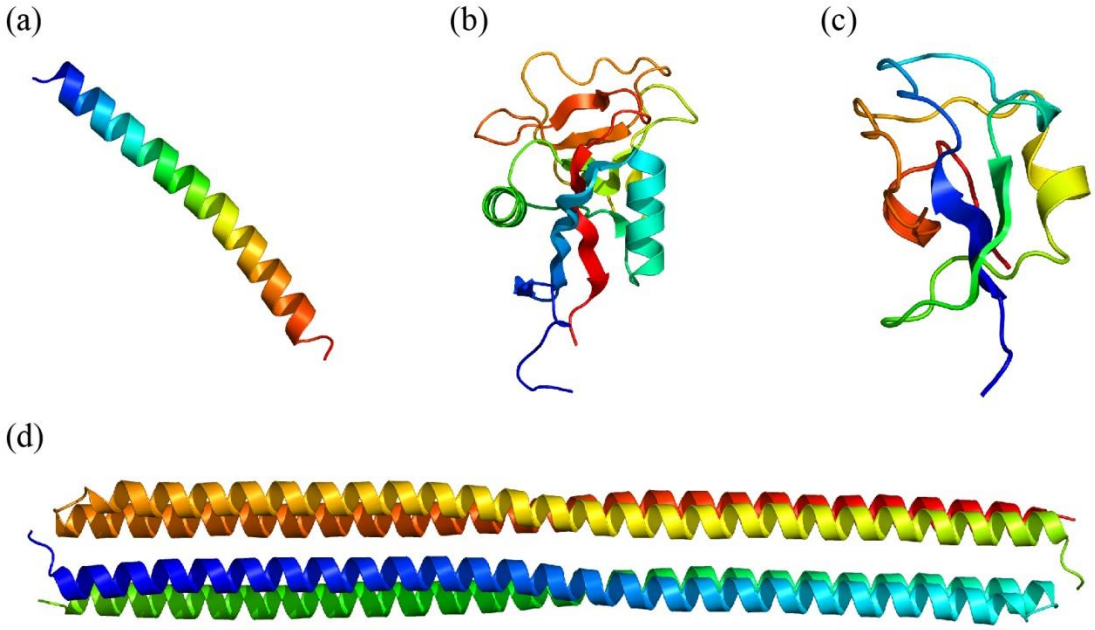

Figure 1.3 X-ray crystal structures of fish AFPs.

(a) Type I AFP from winter flounder [Protein Data Bank (PDB) code: 1WFA. (b) Type II AFP from longsnout poacher (PDB code: 2ZIB). (c) Type III AFP from ocean pout (PDB code: 1HG7). (d) Hyperactive type I AFP from winter flounder: Maxi (PDB code: 4KE2). All structures are represented in cartoon and created by PyMOL.

crystallography, which is a dimeric four-helix bundle (Fig. 1.3d) [41]. Type II AFPs are cysteine-rich disulfide-stabilized globular proteins and homologs of the carbohydrate-recognition domain of C-type lectins (Mw ~14 kDa) (Fig. 1.3b) [42, 43]. Type III AFPs are compact globular proteins consisting mainly of short β-strands connected by large loops (Mw ~ 6.5 kDa) (Fig. 1.3c) [44, 45, 46]. Type IV AFP is proposed to be relatively Gln-rich, highly helical and have a four-helic bundle structure [47]. AFGP is a glycoprotein formed from a repeat of glycotripeptide Ala-Ala-Thr, with side-chain of the Thr residues modified with a disaccharide group (Mw ~ 3-24 kDa) [48].

1.4.1 Insect AFPs

Most insect AFPs show potent TH activities, which can be categorized into hyperactive AFPs. The first structures of hyperactive AFPs were reported over ten years ago. They were two non-homologous, β-helical AFPs produced by the beetle, *Tenebrio molitor* (*Tm*AFP) (Fig. 1.4a) [49] and the moth, spruce budworm, *Choristoneura fumiferane* (*Cf*AFP) (Fig. 1.4b) [50]. *Tm*AFP is a small protein (8.4 kDa) that folds into a right-handed β-helix and consists of seven tandem 12-residue repeats. With an Mw of 9 kDa, *Cf*AFP folds into a left-handed β-helical structure that contains four 15-residue loops. Two parallel arrays of Thr residues align down the ice-binding site (IBS). This kind of TXT motifs is found in both *Tm*AFP and *Cf*AFP, where X is cysteine for *Tm*AFP and any inward pointing amino acid for *Cf*AFP. The average distances between Thr residues in the neighboring and within TXT motifs are 4.5 Å and 7.4 Å respectively, closely matching the spacing of oxygen atoms on both the primary prism and basal planes of ice.

The longhorn beetle *Rhagium inquisitor* produces *Ri*AFP to survive harsh freezing conditions in Siberia and can supercool to below -25 °C [51]. The crystal structure of the 13-kDa *Ri*AFP

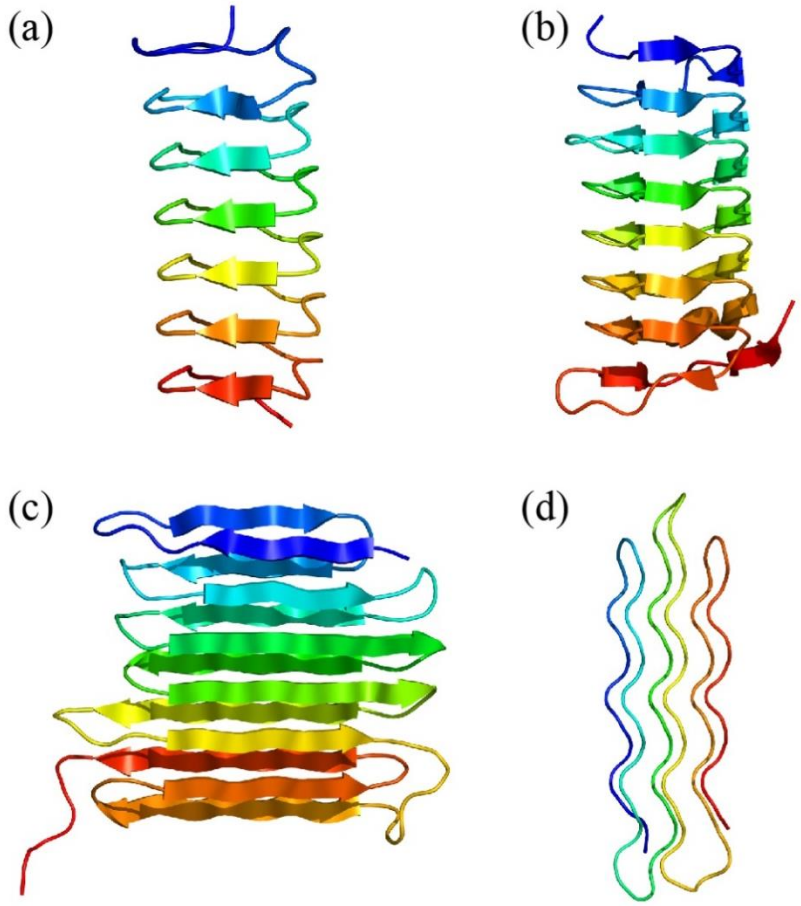

Figure 1.4 X-ray crystal structures of insect AFPs.

(a) *Tm*AFP from the beetle, *Tenebrio molitor* (PDB code: 1EZG). (b) *Cf*AFP from spruce budworm, *Choristoneura fumiferane* (PDB code: 1M8N). (c) *Ri*AFP from the long beetle, *Rhagium inquisitor* (PDB code: 4DT5). (d) sfAFP from snow flea (PDB code: 2PNE). All structures are represented in cartoon and created by PyMOL.

was determined and reveals a tight, two-layered β-sandwich with an extremely extensive IBS (Fig. 1.4c) [52]. Four arrays of Thr residues comprise the IBS of *Ri*AFP, comprising the TXTXTXT ice-binding motifs.

Hyperactive sfAFP was discovered in snow fleas (*Hypogastrum harveyi*), composed of two isoforms [53]. The X-ray structure of the small isoform was determined by chemical protein synthesis and racemic protein crystallization (Fig. 1.4d) [54]. This 6.5-kDa Gly-rich protein is made up of six antiparallel left-handed polyproline type II helices that stack into two groups. This forms a brick-like structure with hydrophilic and hydrophobic faces on the opposite sides of the protein. The predicted model of the large isoform (15.7 kDa) shows the similar structure with the small isoform [55].

Recently, an AFP with no known homologs was discovered from Lake Ontario midge (*Chironomidae*) [56]. The structure of the major isoform of this midge AFP was modeled as a tightly wound left-handed solenoid fold, in which 16 cysteine residues are disulfide bonded to brace the solenoid coil. The putative IBS was predicted to locate in the most regular, flattest, most hydrophobic and tyrosine-rich surface [56] and identified by site-directed mutagenesis [57]. The recombinant midge AFP shows intermediate TH activity between moderately active and hyperactive AFPs and binds to a shallow pyramidal plane angled nearer the basal plane than the pyramidal plane bound by moderate AFPs [57].

1.4.2 Plant AFPs

Freeze tolerant organisms are thought to produce AFPs with weaker TH but higher IRI activity to minimize the damage caused by ice recrystallization. *Lp*AFP from the perennial ryegrass *Lolium perenne* is a 118-residue protein with an Mw of 11 kDa and shows high IRI but low TH activity [28]. The structure of *Lp*AFP was the first crystal structure of a plant AFP,

revealing a left-handed β-roll structure (Fig. 1.5a) [58].

1.4.3 Microbial AFPs

Recently, more AFPs were isolated and characterized from a wider range of organisms, including bacteria and fungi. *Mp*AFP (34 kDa) from a bacterium shows high TH activity (2 °C) and is a part of an exceptionally large protein (1.5 MDa) [2, 33, 34]. The X-ray crystal structure of this 34 kDa domain has been solved, revealing a right-handed Ca^{2+}-bound parallel β-helical fold (Fig. 1.5b) [32]. Two arrays of Thr and Asx (usually Asn) residues from the xGTGND Ca^{2+}-bound turns project outward and comprise the regular and flat IBS of 34-kDa domain. A novel role has been given to the entire *Mp*AFP that it simply binds the bacterium to ice, rather than prevents ice growth or recrystallization [2].

The first fugal protein (*Tis*AFP) with ice-binding activity was found in a snow mold fungus, *Typhula ishikariensis* [59]. Since then, a distinct class of AFPs, comprised of homologous AFPs to *Tis*AFP, was identified from various microorganisms, including fungi [60, 61], diatoms [62-65], bacteria [66-68] and even a copepod [69]. AFPs from this microbial family have similar molecular sizes (~ 25 kDa) and share approximately 40-50 % amino acid sequence identity (Fig. 1.6). The wide distribution of the homologous AFPs supports the hypothesis that these AFP genes were acquired by horizontal gene transfer from bacteria [70, 71].

To date, four crystal structures have been reported for this AFP family, which are *Tis*AFP6 (see details in Chaper 1.11) [72], *Le*AFP from an Arctic yeast *Leucosporidium* sp. AY30 (Fig. 1.5c) [73], *Ff*AFP from an Antarctic bacterium *Flavobacterium frigoris* PS1 (Fig. 1.5d) [74], and *Col*AFP an Antarctic bacterium *Colwellia* sp. strain SLW05 (Fig. 1.5d) [75]. They share a right-handed triangular β-helical structure reinforced by a long α-helix, forming a semipear-shaped structure. The regular ice-binding motifs, such as Thr-X-Thr or Thr-X-Asx, are

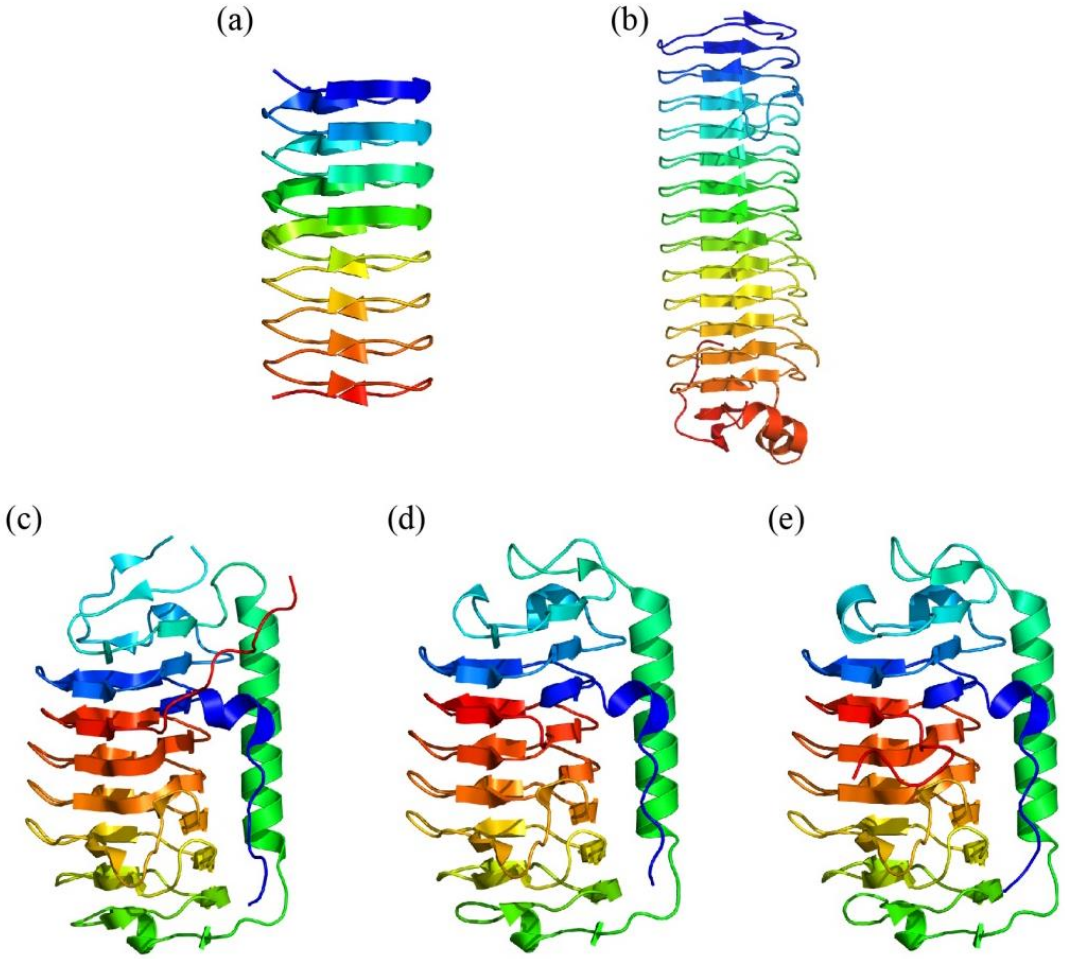

Figure 1.5 X-ray crystal structures of other AFPs.

(a) *Lp*AFP from perennial ryegrass, *Lolium perenne* (PDB code: 3ULT). (b) *Mp*AFP from an Antarctic bacterium, *Marinomonas primoryensis* (PDB code: 3P4G). (c) *Le*AFP from an Arctic yeast, *Leucosporidium* sp. AY30 (PDB code: 3UYU). (d) *Ff*AFP from an Antarctic bacterium, *Flavobacterium frigoris* PS1 (PDB code: 4NU2). (e) *Col*AFP from an Antarctic sea ice bacterium, *Colwellia* sp. Strain SLW05 (PDB code: 3WP9). All structures are represented in cartoon and created by PyMOL.

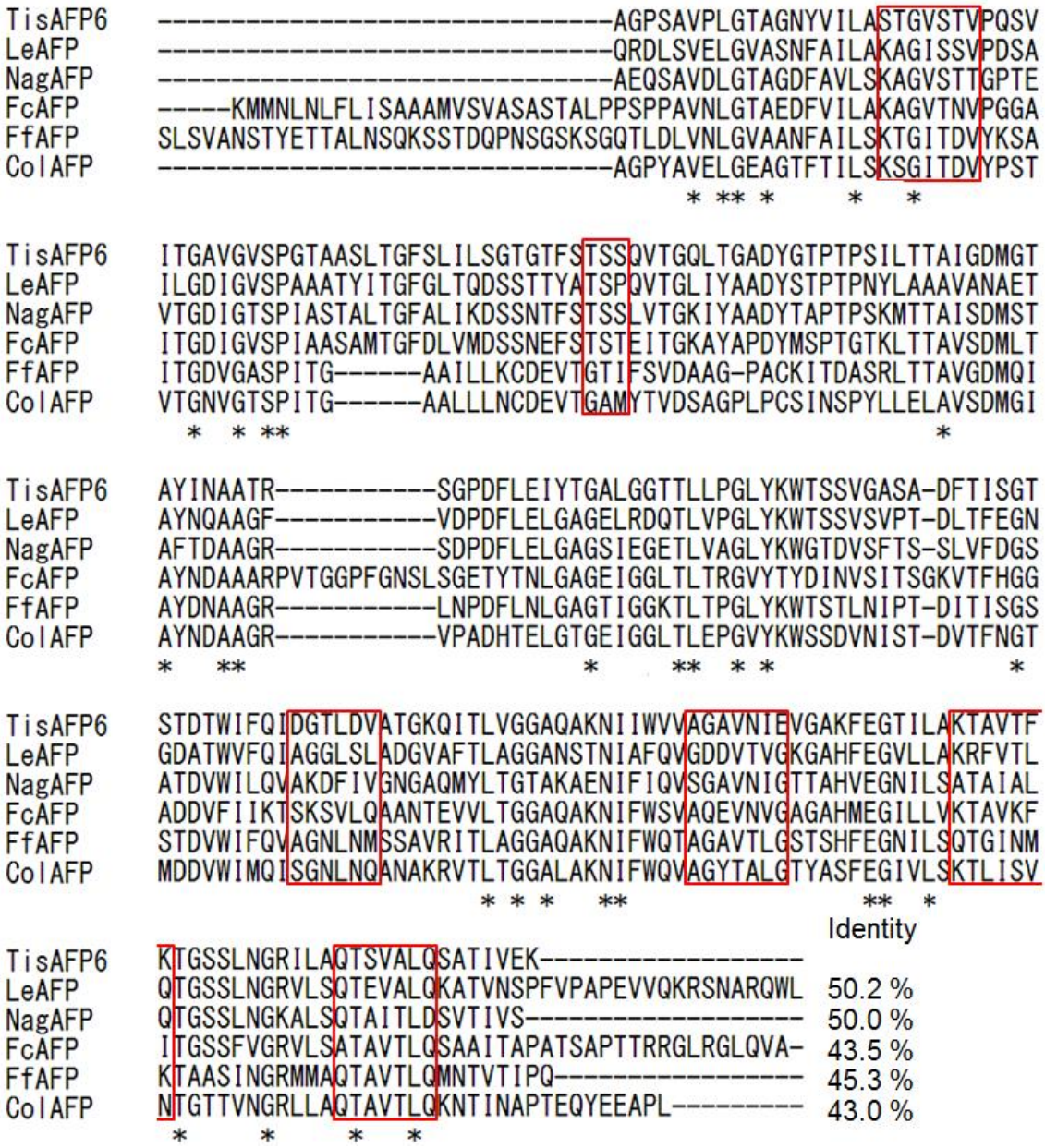

Figure 1.6 Amino acid sequence alignment of homologous AFPs to *Tis*AFP6.

*Tis*AFP6, an isoform from *Typhula ishikariensis*; *Le*AFP, an IBP from *Leucosporidum* sp. AY 30; *Nag*AFP, an AFP from *Navicula glaciei*; *Fc*AFP, an AFP from *Fragilariopsis cylindrus*; *Ff*AFP, an AFP from *Flavobacterium frigoris* PS1; *Col*AFP, *Colwellia* sp. strain SLW05. The asterisks under the alignment show the conserved residues between all six species. Residues on the putative IBS of *Tis*AFP6 are shown in red boxes. Identities of these homologous AFPs to *Tis*AFP6 are shown.

absent in the IBSs of this microbial AFP family. *Le*AFP appeared to be glycosylated and dimeric in solution [73]. One intramolecular disulfide bond was existed in both the structure of *Col*AFP [75] and *Ff*AFP [74]. The above microbial AFP family, in which proteins are homologous to *Tis*AFP, was designated as type I IBPs, where the authors used the term "IBP" instead of "AFP" [64].

A new type IBP was isolatedf from a unicellular Antarctic alga, *Chlamydononas* [76]. This snow alga produces four isoforms with molecular masses of 36.2-37.1 kDa. Bearing no resemblance to type I IBPs, this IBP have a repeating TXT motif, which has been implicated in ice binding in insect AFPs and may also been involved in ice binding of this snow alga IBP. As a result, Raymond *et al*. designated it as type II IBP [64].

1.5 Ice as a heterogeneous ligand

Ice can exit in a large number of different crystalline forms, more than any other known materials [77]. Hexagonal ice (ice I_h), which is six-fold symmetry, forms at atmospheric temperatures and pressures and is the form of all natural snow and ice on Earth. Ice I_h assume hexagonal plates with four axes (a_1, a_2, a_3, c), where all *a*-axes are perpendicular to the *c*-axis and the *c*-axis coincides with the hexagonal symmetrical axis of the ice lattice (Figure 1.7). The top and bottom faces are basal planes {0001}, which are normal to the *c*-axis. The six equivalent side faces are called primary prism planes {10-10}. Secondary prism planes {11-20} parallel to the *c*-axis similarly, while incline at an angle to the primary prism planes. Planes that form an angle with the c-axis (≠0 °C and ≠90 °C) are called pyramidal. Here pyramidal planes {20-21} are indicated in Figure 1.7.

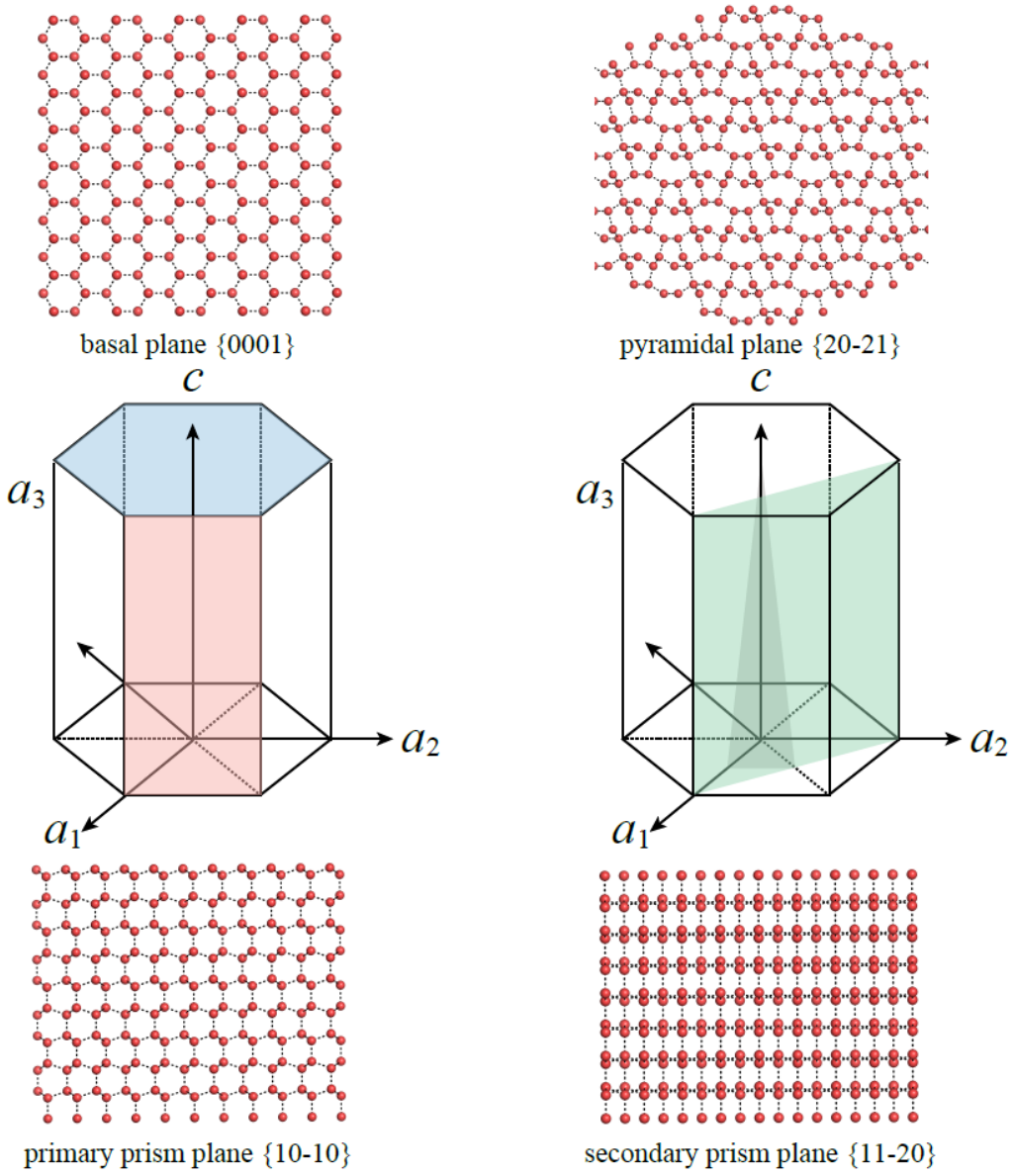

Figure 1.7 Hexagonal unit cell of ice lattice (I_h) and representative ice planes involving in AFP interactions.

The *c*- and *a*-axes of the unit cell are labeled. The one on the left shows the basal plane (shaded blue) and the primary prism plane (shaded pink). The one on the right shows the pyramidal plane (shaded grey) and the secondary prism plane (shaded green). Oxygen atoms on each plane are shown as red spheres. The Miller indices of each plane are indicated. Hydrogen bonds are shown as black dashed lines.

Nada *et al*. reported that the growth velocity from the basal plane is slower than both the primary and secondary prism plane, preventing the sideways growth of ice crystals. Growth from the secondary prism is larger than that from the primary prism faces. During growth on the secondary prism plane, the secondary prism plane disappears and the primary prism plane appears, allowing the axial growth of ice crystals and leading to the formation of hexagonal ice crystals [78].

Different AFPs bind to different planes or sets of planes, which present different patterns of oxygen atoms (Fig. 1.7). The spacing of oxygen atoms on the primary prism planes {10-10} is 4.52 Å along the *a*-axis and 7.35 Å along the *c*-axis, respectively. Oxygen atoms on the basal plane repeat at 4.52 Å along the *a*-axis and 7.8 Å along the *c*-axis.

1.6 Determining the planes of ice to which AFPs bind

The identification and observation of the ice planes to which AFPs bind had puzzled researchers for a long time until the development of ice-etching technique established by Knight *et al*. [21]. In this technique, a single ice crystal of known orientation is attached to a temperature-controlled brass cold finger and immersed into a cylindrical, insulated container of dilute AFP solution. After grown in several hours into a single ice crystal hemisphere (ca. 6 cm in diameter), the crystal is removed from the solution and transferred to a cold room. The ice surface is then carefully scraped to remove residual surface AFPs and evaporated for several hours. Finally, white etched patches appear on the surface where AFPs are incorporated into the crystal, and simultaneously AFP-unbound areas become mirror smooth.

A modification of this ice etch technique was made by Granham *et al*. [79, 80], which is

termed fluorescence-based ice plane affinity (FIPA) analysis. In the new modified technique, AFPs are fluorescently labeled with a chimeric tag or a covalent dye, providing us a more sensitive detection of AFP-bound ice planes in a shortened experimental time.

1.7 Moderately active vs. hyperactive AFPs

Since the discovery of AFGPs, AFPs have been identified in a wide range of organisms, such as fishes, plants, arthropods, and microorganisms. Based on their antifreeze activities, AFPs are categorized into two sub-groups: moderately active and hyperactive AFPs. Most AFPs isolated from marine fishes have TH values of 0.5–1.5 ℃ at millimolar concentrations [22]. In combination with the colligative effects of solutes, moderate fish AFPs will depress the freezing point of the blood below the freezing point of seawater (-1.9 °C). There is one exception that one fish AFP derived from the plasma of the winter flounder (*Pleuronectes americanus*) exhibits hyperactive TH activity comparable to the AFPs from insects [40]. More recently, purified insect and microorganism AFPs show hyper TH activities, which are 5 °C or higher at micromolar concentrations and more than ten times effective on a concentration basis at TH [22]. The higher TH activities of hyperactive AFPs have been attributed to their affinity for the basal plane of ice [22]. Moderately active AFPs bind only prism/pyramidal planes of ice crystal, leaving the basal planes uncovered [21, 79, 81]. Then the ice crystals are typically shaped into hexagonal bipyramids. When the TH gap of moderately active AFPs is exceeded, the ice crystals grow rapidly (burst) along the *c*-axis. In addition, hyperactive AFPs are capable of binding multiple planes of ice, including the basal plane. This additional binding to the basal plane by hyperactive AFPs provides better coverage of the ice crystal, resulting in an explosive

rapid growth normal to the *c*-axis and greater TH activity [22, 82].

1.8 The mechanism by which AFPs bind to ice

It has been difficult to deduce the mechanism by which AFPs bind to ice at the molecular level, partly due to the unavailable, stable AFP/ice complex for structural investigation. Early research based on AFGP and type I AFP structures suggested that the hydrogen bonding interaction through the regularly spaced hydroxyl groups with oxygen atoms in the ice lattice is the main driving force for AFPs to bind to ice crystals [83-85]. However, this hypothesis could not explain the mutagenesis experiments where the central two Thr residues of type I AFP were replaced with Val or Ser [86, 87]. The Val mutant preserved almost comparable activity to that of wild type, while the Ser mutant was virtually inactive. As the IBSs of AFPs were shown to be more hydrophobic than other surfaces of the protein [45, 88], this led to a suggestion that hydrophobic effect could be a significant contributor in adsorbing AFPs on the ice surface. In this mechanism, the release of the constrained waters on the IBS into the bulk solvent results in a gain of large entropy, which might drive the binding of AFPs to ice lattice.

Along with the determination of the structures of hyperactive insect AFPs, water molecules located on each IBS of them are found to be regularly ice-like spaced. In the crystal structure of *Tm*AFP [49], *Cf*AFP [89, 90] and *Ri*AFP [52], ordered water molecules are hydrogen-bonded to the IBS and located in the trough created by the outward-pointing Thr residues. However, due to the flat and hydrophobic feature of the IBSs, AFPs tend to crystallize with their IBSs. Therefore, the ordered waters might be constrained or displaced and cannot represent their true structure in solution. Before proving directly experimental evidence, several molecular dynamics (MD)

simulations were carried out to investigate the possibility whether AFPs order water molecules on their IBSs before binding to ice. Nutt and Smith [91] investigated the structural and dynamic features of waters around the three faces of *Cf*AFP, including the IBS. They observed ordered structure and slowed down dynamics of water molecules around the IBS at low temperature. Therefore, they postulated that the ice-like structure of waters ordered by the AFP could merge with the quasi-liquid layer of ice. Then the AFP is incorporated into the growing surface of ice. The authors termed this mechanism "pre-ordering-binding" mechanism.

The crystal structure of *Mp*AFP supports the above hypothesis directly [32]. Four *Mp*AFP molecules were packed within the unit cell of the crystal. Arranged ice-like water molecules aligned down one and one third of the four proteins, where were well exposed to the solvent. These water molecules were ordered into an ice-like lattice via the hydrophobic effect by the relative hydrophobicity of the IBS, and then anchored to the AFP via hydrogen bonds. Besides, these waters matched well to both the basal and primary prism planes of ice crystals, allowing *Mp*AFP to binding these planes. This mechanism was termed "anchored clathrate water" (ACW) mechanism. Recently, the interior organized water molecules were found in the crystal structure of Maxi, anchored to backbone via hydrogen bonds and stabilizing the four helix-bundle fold [41]. These waters extended outward to the protein surface and were likely to be involved in ice binding, supporting the ACW mechanism.

However, as described above, due to the tendency of IBSs to pack against each other in the crystal, it is restricted to test the generality of the ACW mechanism. In the crystal structure of the most active isoform (QAE1) of type III AFP, the primary prism plane IBS was partially exposed to the solvent, on which five water molecules were ice-like [92]. Whereas the pyramidal prism plane IBS was involved in crystal packing. Sun *et al*. solved the crystal structure of a fusion protein of type III AFP from *Macrozoarces americanus* with

maltose-binding protein (MBP), making the pyramidal prism plane IBS more exposed to solvent [93]. By combining with molecular dynamics (MD) simulations, waters on both IBSs revealed that they matched well with their target ice planes. The utilization of fusion protein method makes it possible to force the IBS of AFPs to expose to solvent, providing more potential evidence for ACW mechanism.

1.9 AFP isoforms

Many different organisms are found to produce a family of AFPs, contributing to total antifreeze activity [94]. It has been reported that fish type I AFP [95, 96], type III AFP [97-99], plant AFP [100], insect AFP [101, 102] and fungi AFP [59, 71] consist of multiple isoforms. Bayer-Giraldi *et al*. assumed that the occurrence of multigene family of *Fc*AFP from a polar diatom *Fragilariopsis cylindrus* probably contribute to its application to the extreme habitat of sea ice [71, 103].

Variation in antifreeze activity has been also reported for AFP isoforms. For type III AFP from Japanese notched-fin eel pout (*Zoarces elongatus*), 13 isoforms with approximately 48 % of sequence identity were identified and categorized into SP- and QAE-Sephadex binding groups, and the latter were further subdivided into QAE1 and QAE2 subgroups [99]. TH activities for QAE1, QAE2 and SP isoforms were 0.60 °C, 0.11°C and almost zero, respectively, at the concentration of 1.0 mM. Besides, the authors also found that the TH activity of the less active SP isoforms showed concentration dependence in the presence of 0.2 mM QAE1 isoform. This kind of manner that multiple isoforms co-operatively enhance antifreeze activity was also reported for *Dc*AFP isoforms from overwintering larvae of the beetle *Dendroides canadensis*

[104]. However, it is still unclear that how slight variations in amino acid sequence result in the significantly different antifreeze activities of homologous AFPs.

1.10 AFPs from a snow mold fungus, *Typhula ishikariensis*

Snow mold fungus---*Typhula ishikariensis*, is a pathogen that grows and attacks dormant plants at low temperature under snow cover (Fig. 1.8). Gray snow mold caused by *T. ishikariensis* is mostly found in the turf industry, affecting a wide range of turfgrasses. To survive the cold, wet conditions, *T. ishikariensis* secretes *Tis*AFPs to the extracellular space via a cleavable N-terminal signal sequence [59, 105]. *Tis*AFPs prepared from mycelial culture is a mixture of seven isoforms (termed *Tis*AFP2-8) with high sequence identity. *Tis*AFP isoform6 (*Tis*AFP6) exhibits a TH activity of 0.3 °C at a concentration of 0.16 mM with a rapid ice crystal growth along its crystallographic *c*-axis under T_{f2}, which is comparable with the moderately active AFPs. Among the seven isoforms, *Tis*AFP8 shows the lowest sequence identity of 83.4 % with *Tis*AFP6. While others of *Tis*AFP2, 3, 4, 5, 7 show 87.0 %, 99.1 %, 97.3 %, 99.6 % and 99.1 % sequence identity with *Tis*AFP6, respectively (Fig. 1.9). Besides, *Tis*AFP8 displays the highest TH activity of 2.0 °C at 0.17 mM. Under T_f seed ice crystal in *Tis*AFP8 solution bursts into dendrite-like pattern with a hexagonal symmetry perpendicular to the *c*-axis [105]. These observations are similar to those found in other hyperactive AFPs [22, 50].

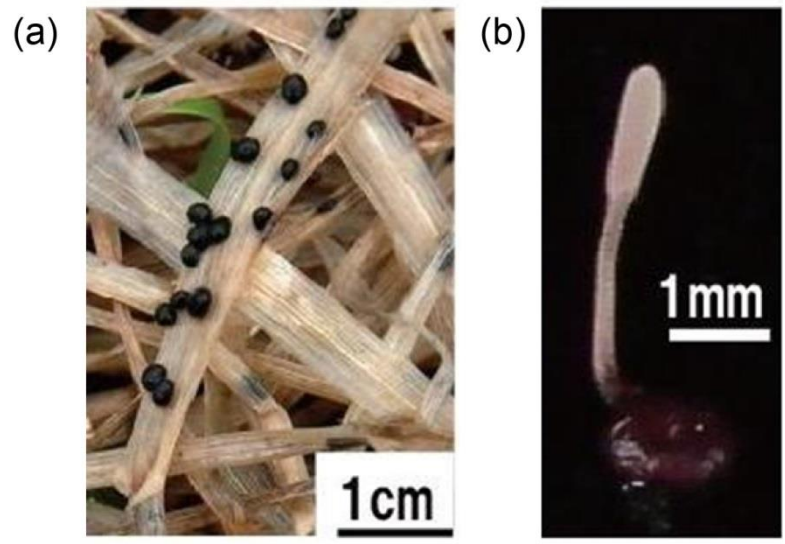

Figure 1.8 Sclerotium and fruit body of *Typhula Ishikariensis.*

(a) Sclerotium (black ones) of *Typhula ishikariensis.* (b) Fruit body of *Typhula ishikariensis.*

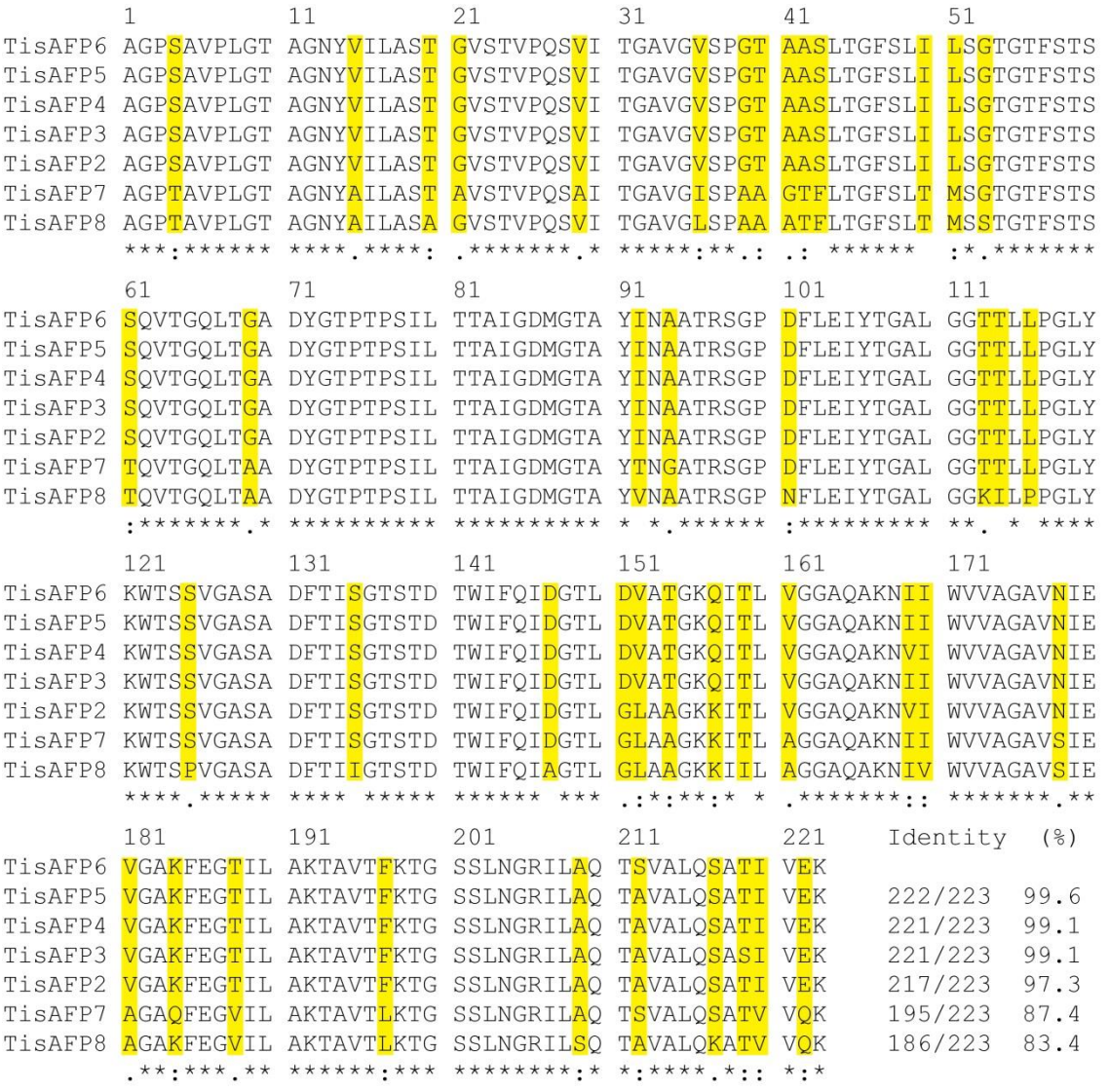

Figure 1.9 Amino acid sequence alignments of *Tis*AFP isoforms.

Each sequence is available in DDBJ/EMBL/GenBank under the accession code of Q76CE6 for *Tis*AFP6, Q76CE5 for *Tis*AFP5, Q76CE4 for *Tis*AFP4, Q76CE3 for *Tis*AFP3, Q76CE2 for *Tis*AFP2, Q76CE7 for *Tis*AFP7 and Q76CE8 for *Tis*AFP8.

1.11 X-ray crystal structure of *Tis*AFP6

In our laboratory, we recently solved the X-ray crystal structure of one isoform---*Tis*AFP6 [72]. *Tis*AFP6 is composed of 223 amino acid residues with a molecular weight of 22 kD [59]. *Tis*AFP6 mainly consists of a right-handed irregular β-helix with six loops (Fig. 1.10a). A long α-helix lies parallel to the β-helix axis. The N-terminal β-helical loop β1 is adjacent to the C-terminal loop β6 within the β-solenoid, which means that the six β-helical loops are aligned in an irregular order, β1-β6-β5-β4-β3-β2 (Fig. 1.10a). *Tis*AFP6 owns a triangular cross-section, in which the six helical loops constitute three parallel β-sheets (face a, b, c) and the b face has been assumed to be the ice-binding face probed by steric mutations (Fig. 1.10a). What's more, neither tandem repeats in the sequence nor the TXT/TXN motifs is present in *Tis*AFP6 and other isoforms, which are known in hyperactive AFPs, like *Tm*AFP [49], *Cf*AFP [50], and *Mp*AFP [32]. It leads to an irregular ice-binding face of *Tis*AFP6. The whole structure of *Tis*AFP6 reveals a semipear-shaped structure (Fig. 1.10b).

The hydrophobicity of the core of β-helix is one of the important elements that stabilize the β-helical fold of *Tis*AFP6. Side chains of inward-pointing residues direct into the core of the β-helix and hydrophobic ones among them are considered to take an important role in stabilizing the β-helical fold (Fig. 1.10c). And side chains of outward-pointing residues in the IBS point out to the ice crystal when binding and could directly effect on the interaction of AFPs and ice crystals.

For *Tis*AFP6, a set of 56 crystallographic waters were found on the putative ice-binding face. Although compared with *Mp*AFP, not all of these water molecules are perfectly aligned in an ice-like arrangement. Several waters of them are located in an interval which closely matches the distance between oxygen atoms on several planes of ice crystals.

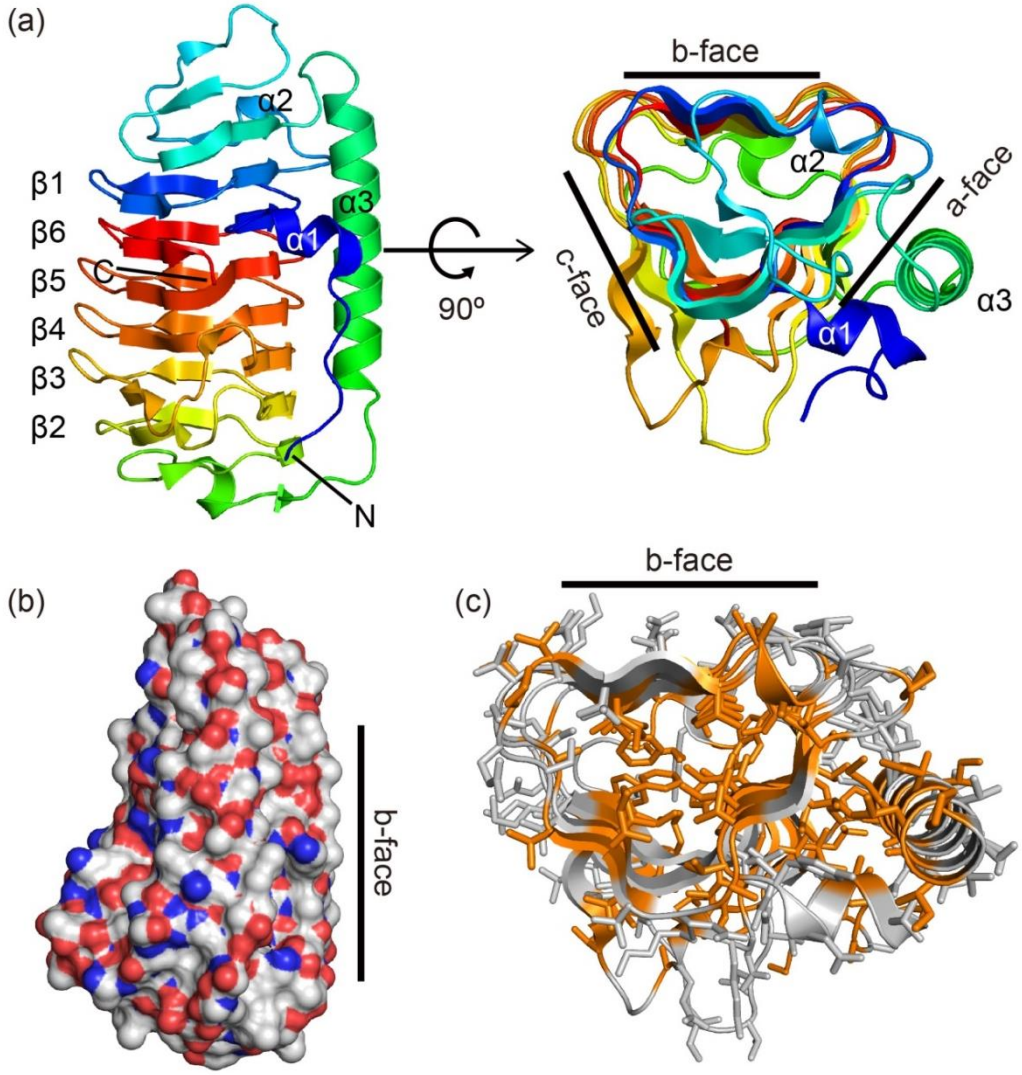

Figure 1.10 X-ray crystal structure of *Tis*AFP6.

(a) Ribbon representation of *Tis*AFP6 in spectral color gradation from blue (N terminus) to red (C terminus). The protein adopts a right-handed β-helical fold and has a triangular cross-section with three parallel sheets (face a, b, c). The N- and C-terminus are labeled. The six turns of the β-helix are aligned in an irregular order, β1-β6-β5-β4-β3-β2. The three α-helices are labeled. (b) Surface representation of *Tis*AFP6 with the b face (IBS) viewed side on. *Tis*AFP6 appears to have a flat IBS and pear-shaped other side. Carbon is in grey, nitrogen is in blue and oxygen is in red. (c) Ribbon representation of *Tis*AFP6 viewing along the axis of the β-helix. All side chains are shown as sticks, within which hydrophobic ones (Phe, Ala, Leu, Met, Ile, Trp, Pro, Val) are colored orange.

1.12 Aims and objectives

Since the discovery of the first AFGP in 1960s, AFPs have been uncovered a remarkable structural and functional diversity. Structure analysis shows that the IBSs of AFPs share a common feature to be flat and hydrophobic, rendering the ability of organizing ice-like waters on the ice-binding surface of an AFP. This suggests that all AFPs adsorb onto ice through a common mechanism. Experimental evidence has been provided to support the ACW mechanism by Garnham *et al*. [32].

Hyperactive AFPs from insects and bacterium bind to ice crystals by well-ordered ice-binding motifs, which usually consist of two arrays of Thr residues in insect AFPs and Thr-X-Asx in *Mp*AFP (Fig. 1.11a-d). However, microbial AFPs which are homologous AFPs to *Tis*AFP6 do not have this kind of regular, repetitive structural motifs (Fig. 1.11e-h). Besides, the coexistence of hyperactive and moderately active AFPs in this microbial AFP family suggests a non-repetitive IBS could also contribute to hyperactive TH activity, where *Tis*AFP6 and *Le*AFP display moderately active TH activities, and *Ff*AFP and *Col*AFP are found to be hyperactive AFPs. Nevertheless, a general mechanism that explains how hyperactive microbial AFPs interact with ice crystals with a non-repetitive IBS remains unclear.

To answer the above question, I focused on another isoform from *Typhula ishikariensis*, *Tis*AFP8, which shows characteristics of hyperactive AFPs [105] and high sequence identity with moderately active *Tis*AFP6, and performed functional and structural analyses upon these two isoforms.

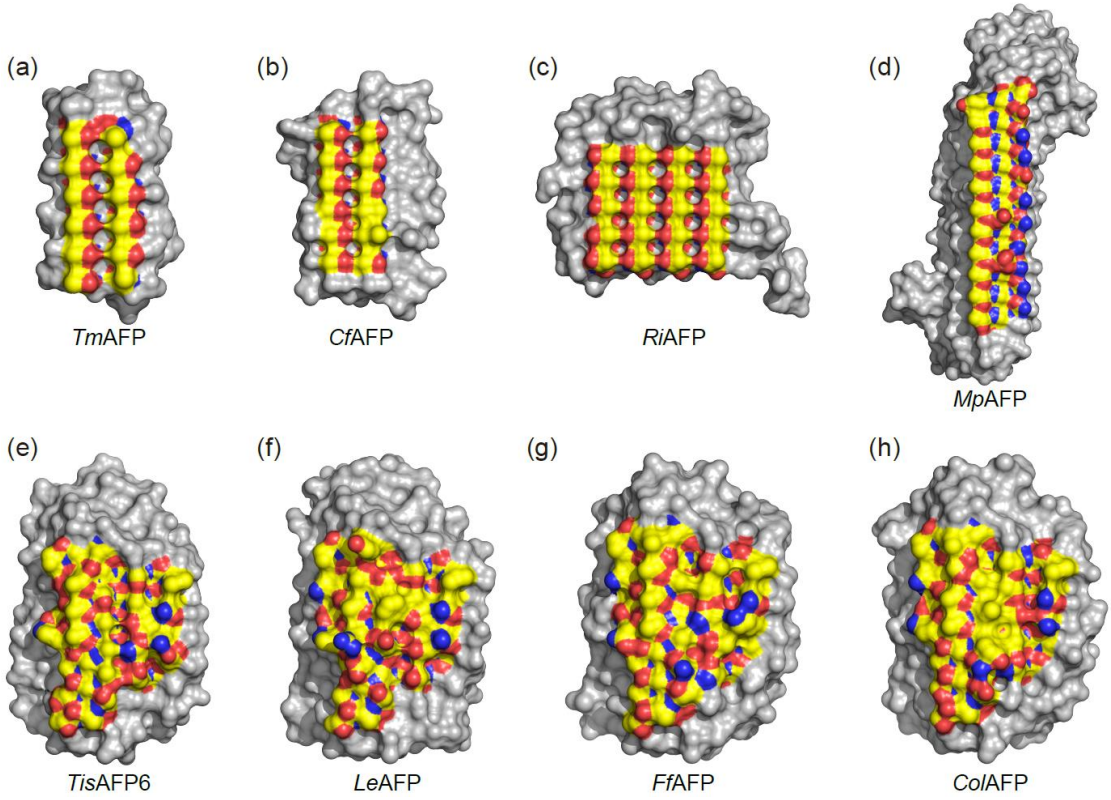

Figure 1.11 Regular and repetitive IBSs of hyperactive AFPs Vs complex IBSs of homologous AFPs to *Tis*AFP6.

Residues on IBSs are colored yellow for C atoms, red for O atoms and blue for N atoms. (a-d) Space-filling views of hyperactive AFPs derived from insects and bacterium showing the regularity of their IBSs resulting from the alignment of Thr-X-Thr ice-binding motifs in *Tm*AFP and *Cf*AFP, Thr-X-Thr-X-Thr-X-Thr motifs in *Ri*AFP and Thr-Gly-Asx motifs in *Mp*AFP. (e-h) Homologous AFPs (*Le*AFP, *Ff*AFP and *Col*AFP) to *Tis*AFP6 lack the repetitive ice-binding motifs, resulting in complex and non-repetitive IBSs.

Chapter 2 Hydrophobic ice-binding sites confer hyperactivity of an antifreeze protein from a snow mold fungus

Preface:

This chapter was published in Biochemical Journal: Cheng, J., Hanada, Y., Miura, A., Tsuda, S. and Kondo, H. (2016) Hydrophobic ice-binding sites confer hyperactivity of an antifreeze protein from a snow mold fungus. *Biochem. J*. 473, 4011-4026.

Jing Cheng, Sakae Tsuda and Hidemasa Kondo designed research. Jing Cheng, Yuichi Hanada, Ai Miura, Sakae Tsuda and Hidemasa Kondo performed experiments. Jing Cheng and Hidemasa Kondo analyzed data and wrote the paper.

2.1 Abstract

Snow mold fungus, *Typhula ishikariensis*, secretes seven antifreeze protein isoforms (denoted *Tis*AFPs) that assist in the survival of the mold under snow cover. Here, the X-ray crystal structure of a hyperactive isoform, *Tis*AFP8, at 1.0 Å resolution is presented. *Tis*AFP8 folds into a right-handed β-helix accompanied with a long α-helix insertion. *Tis*AFP8 exhibited significantly high antifreeze activity that is comparable with other hyperactive AFPs despite its close structural and sequence similarity with the moderately active isoform *Tis*AFP6. A series of mutations introduced into the putative ice-binding sites (IBSs) in the β-sheet and adjacent loop region reduced antifreeze activity. A double mutant A20T/A212S, which compose a hydrophobic patch between the β-sheet and loop region, caused the greatest depression of antifreeze activity of 75 %, when compared with that of the wild-type protein. This shows that the loop region is involved in ice binding and hydrophobic residues play crucial functional roles. Additionally, bound waters around the β-sheet and loop region IBSs were organized into an ice-like network and can be divided into two groups that appear to mediate separately *Tis*AFP and ice. The docking model of *Tis*AFP8 with the basal plane via its loop region IBS reveals a better shape complementarity than that of *Tis*AFP6. In conclusion, we present new insights into the ice-binding mechanism of *Tis*AFP8 by showing that a higher hydrophobicity and better shape complementarity of its IBSs, especially the loop region, may render *Tis*AFP8 hyperactive to ice binding.

2.2 **Introduction**

Organisms that are exposed to sub-zero temperatures are protected from freezing damage by the presence of antifreeze proteins (AFPs), which bind to ice, modify its behavior and prevent its further growth. Ice growth is restricted to the exposed ice surface area between the bound AFPs, leading to an increase in the micro-curvature of the ice front, which is energetically less favorable for water molecules to join the ice [106]. This unfavorable energy term leads to a non-colligative depression of the freezing point (T_f) and a slight elevation of the melting point (T_m) owing to the Gibbs–Thomson effect [20]. The gap between the nonequilibrium T_f and T_m is termed thermal hysteresis (TH), which is a definitive evaluation of the antifreeze activity. In the temperature range of the TH gap, ice crystal morphology is modified typically to hexagonal bipyramidal or a lemon-like shape. AFPs also inhibit ice recrystallization, which is the gradual growth of ice grains under T_f at the expense of small ones. These unique properties of AFPs are attributed to their specific affinity towards ice crystals, which would be beneficial for diverse applications, such as cell/tissue cryopreservation, food storage and gas hydrates growth inhibition in oil and gas pipelines [11, 107, 15]. To shed light on cold-adaptation strategies and make further study on applications, therefore, it is crucial to elucidate the molecular mechanisms between AFPs and ice through a detailed analysis of their antifreeze activity in combination with structural and molecular biology studies.

AFPs are categorized into moderately active and hyperactive based on their antifreeze activities. Purified insect and microorganism AFPs exhibit “hyper-” TH activities, which are up to ~5 °C or higher at micromolar concentrations, whereas moderately active AFPs from fish and plant species exhibit THs of 0.5–1.0 °C at millimolar concentrations [22, 108, 33, 28]. Variation in antifreeze activity has also been reported for AFP isoforms. For type III AFPs from the

Japanese notched-fin eel pout (*Zoarces elongatus*), 13 isoforms with approximately 48%sequence identity have been identified and categorized into SP- and QAE-Sephadex binding groups, and the latter were further subdivided into QAE1 and QAE2 subgroups [99]. TH activities for QAE1, QAE2 and SP isoforms were 0.60 °C, 0.11 °C and almost zero, respectively, at 1.0 mM. Multiple isoforms were reported to enhance co-operatively antifreeze activity [99, 104]. However, it is still unclear how slight variations in amino acid sequence evoke significant differences in antifreeze activities of homologous AFPs.

Hyperactive AFPs found in arthropods and bacteria exhibit a β-helical fold composed of highly repetitive sequences. The ice-binding site (IBS) of hyperactive AFPs is constructed of a well-ordered motif, which consists of two arrays of Thr residues in insect AFPs [49, 50] and Thr-X-Asx in *Mp*AFP from the Antarctic bacterium *Marinomonas primoryensis* [33]. These ice-binding motifs facilitate the interaction of AFPs with both the basal and prism planes of hexagonal ice crystals [33, 49, 50, 109]. The affinity of hyperactive AFPs toward the basal plane is a key determinant for their hyper antifreeze activity. Crystal structure analysis of *Mp*AFP showed that water molecules that bind to the IBS are ordered into an ice-like pattern and match perfectly to the ice lattice of the basal and primary prism planes [32]. Highly ordered water molecules are also found in the crystal structure of a large type I AFP isoform from the winter flounder *Pseudopleuronectes americanus* (Maxi) [41]. Maxi, which exhibits more than 2 °C of TH at 0.4 mg/ml [40], folds into a dimeric four-helix bundle that is stabilized by interior ordered water molecules. These water molecules occupy the interface between helices to form polypentagonal networks, which extend the outside of the dimer and are likely to be involved in ice binding. These observations indicate that IBSs anchor clathrate waters with an ice-like structure, which resembles the quasi-liquid layer of water around the ice surface [32, 41, 110, 91]. The anchored clathrate waters then merge with the quasi-liquid layer and turn to ice to

promote AFPs to match specific ice planes. Therefore, structural information describing AFPs and bound water is essential for obtaining a detailed understanding of the binding manner of other AFPs to ice crystals.

Typhula ishikariensis, a snow mold fungus that grows under snow cover, secretes *Tis*AFPs to the extracellular space via a cleavable N-terminal signal sequence [59, 105]. The *Tis*AFPs prepared from a mycelial culture is a mixture of seven isoforms of 223 residues, sharing high sequence identity with each other. Within all the isoforms, *Tis*AFP8 shows the lowest sequence identity (83.4 %) with *Tis*AFP6, whose structure was solved. However, the detailed antifreeze activities and structural differences between them have not been well studied. Homologous AFPs to *Tis*AFP have been identified from fungus, diatom, yeast and bacteria, which form a unique protein family [61, 62, 66]. The wide distribution of these homologous AFPs, therefore, supports the hypothesis that these AFP genes were propagated by horizontal gene transfer [70, 71]. It should be noted here that a concomitant of hyper and moderately active species have been reported only for the microbial AFP family. *Ff*AFP from an Antarctic bacterium *Flavobacterium frigoris* PS1 and *Col*AFP from an Antarctic bacterium *Colwellia* sp. strain SLW05 were reported as hyperactive AFPs. *Ff*AFP can depress the freezing point by ~2.2 ℃ at 5 μM [74] and *Col*AFP displays a TH activity of ~4 ℃ at 0.14 mM [75]. Additionally, *Nag*AFP from the Antarctic sea ice diatom *Navicular glaciei* has a TH activity of 3.22 ℃ at 1.6 mM [111]. *Le*AFP from Arctic yeast *Leucosporidium* sp. AY30 is moderately active with a TH of 0.42 ℃ at 0.4 mM [112]. In the presence of *Fc*AFP from a polar diatom *Fragilariopsis cylindrus*, the freezing point depression is comparable to that of other moderately active AFP, which is 0.9 ℃ at 0.23 mM [103].

Currently, four crystal structures have been reported for the AFP family: *Tis*AFP6 [72], *Le*AFP [73], *Ff*AFP [74] and *Col*AFP [75]. These reports have revealed that AFPs fold into a

monomeric right-handed β-helix with a triangular cross-section that forms a semi-pear-shaped structure [72]. Mutagenesis experiments based on the crystal structure reveal that the IBS of these AFPs is located on the flattest surface of the β-helix. All of the family members, however, lack regular ice-binding motifs on their IBSs, which suggest that a non-repetitive structure could be ascribed to their hyperactivities. Bound waters located in the troughs within the IBS seem to help anchor AFPs to ice planes. Hanada *et al*. proposed for *Col*AFP that a compound IBS combining a flat surface of the β-helix with the adjoining loop region might confer its potent antifreeze activity [75]. Do *et al*. suggested that the hyperactivity of *Ff*AFP can be explained by its free accessibility as a monomer owing to the lack of the C-terminal region and flatter IBS, and relatively more regular ice-binding motif residues (T-A/G-*X*-T/N) when compared with that of *Le*AFP [74]. Nevertheless, a general mechanism that explains how hyperactive microbial AFPs interact with ice planes in the absence of a repetitive ice-binding motif as seen for insect AFPs remains unclear.

Here we report the antifreeze activity and crystal structure of *Tis*AFP8 and compare its structure with other known structures in order to understand their ice-binding modes. The results show that *Tis*AFP8 functions as a hyperactive β-helical AFP with a larger hydrophobic IBS than moderately active *Tis*AFP6. Water molecules around the IBS of *Tis*AFP8 are aligned into an ice-like pattern, which seems to anchor the protein onto the ice surface. Our research suggests that the potent antifreeze activity of *Tis*AFP8 is ascribed to the relatively high hydrophobicity of the IBS, especially the loop region. In addition, high shape complementarity between the loop region IBS and the basal plane may also confer hyperactivity to *Tis*AFP8.

2.3 Materials and methods

2.3.1 Expression and purification of wild-type *Tis*AFPs and their mutants

cDNA encoding *Tis*AFP8 (DDBJ/EMBL/GenBank accession no. Q76CE8) was inserted into *Pichia* expression vector pPICZα (Invitrogen Co., CA, USA), as described previously [105]. The recognition site for *Nde* I was introduced by the KOD-plus mutagenesis kit (Toyobo, Osaka, Japan). The *Tis*AFP8 DNA was then cleaved from pPICZα by *Nde* I and *Not* I, and inserted into the expression vector pET-20b (+) (Novagen, Madison, WI, USA). The nucleotide sequence that encodes a mature *Tis*AFP8 (Ala^{1}-Lys^{223}) was confirmed by DNA sequencing and the expression vector was transformed into *Escherichia coli* strain BL21 (DE3). Transformants were plated onto a Luria–Bertani (LB) agar plate containing 100 μg/ml ampicillin and grown overnight. A single colony was inoculated into 50 ml LB medium with 100 μg/ml ampicillin and cultured at 37 °C overnight with agitation. This culture was transferred into 1 L of fresh medium and cultured at 30 °C until the OD_{600} reached 0.4–0.8. Expression of *Tis*AFP8 was then induced by isopropyl-β-D-thiogalactopyranoside with a final concentration of 0.5 mM. The culture was incubated at 15 °C for a further 24 h, and the cells were harvested by centrifugation at 3000 *g* for 15 min at 4 °C (Fig. 2.1a).

The cell pellet was lysed by sonication in 20 mM Tris-HCl (pH 7.4) containing 100 mM NaCl and 1 mM EDTA (Fig. 2.1b). The cellular debris was removed by centrifugation at 11,000 *g* for 30 min at 4 °C. The supernatant was loaded into dialysis tubing with a molecular weight cut-off (MWCO) of 14, 000 and dialyzed against 10 mM Gly-HCl (pH 3.0) (Fig. 2.1c). Most of the impurities, including *E. coli* proteins, were precipitated during dialysis (Fig. 2.1d). The precipitates were removed by centrifugation at 11, 000 g for 15 min at 4 °C and filtration with a 0.20 μm pore-sized filter (Fig. 2.1e). The dialysate was then loaded onto an Econo-pac High S

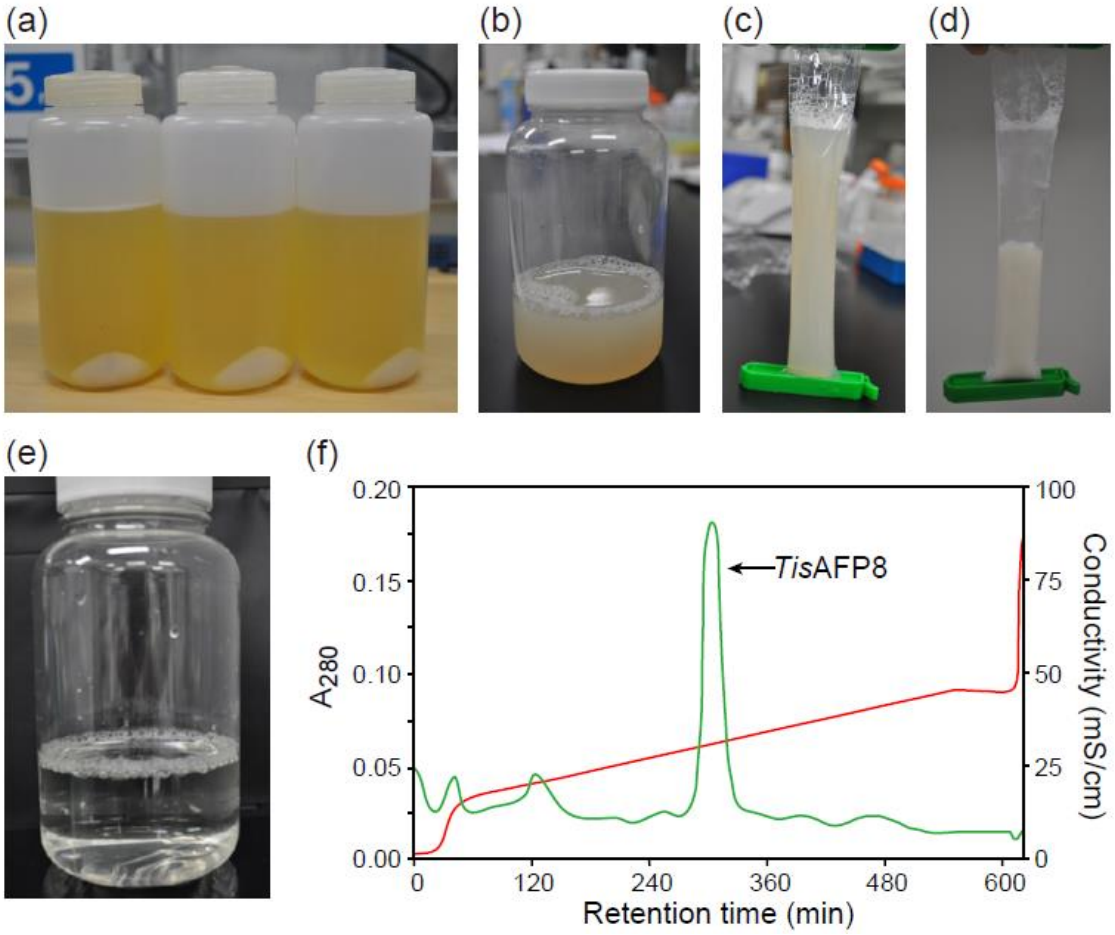

Figure 2.1 Purification of recombinant *Tis*AFP8 wild type.

(a) LB culture medium of recombinant *Tis*AFP8 wild type after centrifugation. (b) *E. coli* cells lysate after sonication. The disruptions of cells were repeated three times. (c) (b) before dialysis against glycine-HCl (pH 3.0) buffer. (d) (b) after dialysis against glycine-HCl (pH 3.0) buffer. (e) The supernatant of (d). (f) A representative chromatogram of *Tis*AFP8 wild type purification with High-S resin. Green: absorbance at 280 nm. Red: conductivity. *Tis*AFP8 wild type was detected in a peak indicated by an arrow.

Table 2.1 Primer sequences used for the construction of the expression plasmids of wild-type *Tis*AFP8 and mutants, as well as *Tis*AFP6 S212A mutant. The underlined bold letters are corresponding to each mutation site.

Protein	Primer sequence
*Tis*AFP8 wild type	5′-GCTGGTCCCACCGCTGTG-3′
	5′-CATATGTCTTTTCTCGAGAGATACCCCTTCTTC-3′
A20T	5′-**ACT**GGAGTTTCCACTGTCCCACAATCTGTT-3′
	5′-AGAAGCCAAGATGGCGTAATTTCCTGCGGT-3′
P125S	5′-**TCT**GTAGGAGCCTCCGCT-3′
	5′-AGAAGTCCATTTATATAAACCTGGAGGTAA-3′
A147D	5′-**GAT**GGAACGTTAGGACTTGCAGCTGGTAAG-3′
	5′-AATTTGGAAAATCCATGTATCCGTTGAGGT-3′
G151D	5′-**GAT**CTTGCAGCTGGTAAGAAGATTATCTTG-3′
	5′-TAACGTTCCAGCAATTTGGAAAATCCATGT-3′
L152V	5′-**GTT**GCAGCTGGTAAGAAGATTATCTTGGCA-3′
	5′-TCCTAACGTTCCAGCAATTTGGAAAATCCA-3′
S178N	5′-**AAC**ATAGAAGCCGGTGCCAAGTTTGAGGGA-3
	5′-CACTGCGCCAGCAACAACCCAGACAATGTT-3′
A212S	5′-**TCT**GTTGCTTTGCAAAAAGCCACCGTT-3′
	5′-GGTCTGAGACAATATTCGACCATTAAGACT-3′
*Tis*AFP6 S212A	5′-**GCT**GTCGCTCTGCAGTCCGCTACCATTGTG-3′
	5′-AGTCTGCGCCAGAATCCTTCCGTTGAGGGA-3′

column (Bio-Rad, Hercules, CA, USA) equilibrated with the same buffer after removing precipitates. The bound protein was eluted with a linear gradient of 0–400 mM NaCl (Fig. 2.1f). Fractions showing TH activity were pooled and dialyzed against 25 mM ammonium bicarbonate (pH 7.9). The dialysate was applied onto an Econo-pac High Q column. Flow-through containing *Tis*AFP8 was collected and its purity was confirmed by SDS-PAGE. The purified protein was concentrated using Amicon Ultra-4 centrifugal filter units. Protein concentration was determined by OD_{280} with the calculated molar adsorption coefficient (1.083 M^{-1} cm^{-1}) for *Tis*AFP8.

Each *Tis*AFP8 mutant and *Tis*AFP6 mutant were prepared using the KOD-plus mutagenesis kit (Toyobo, Osaka, Japan) with primers presented in Table 2.1. The nucleotide sequences of mutants were confirmed by DNA sequencing. All mutants were expressed in *E. coli* cells BL21 (DE3) and purified using the same procedure described for purification of the wild-type *Tis*AFP8.

2.3.2 Thermal hysteresis measurements and ice crystal morphology

The TH of *Tis*AFP8 wild type and mutants was measured by a photomicroscope system, as described previously [113]. Briefly, the system is mainly composed of a Leica DMLB 100 photo-microscope (Leica Microsystems AG, Wetzlar, Germany) and a Linkam THMS 600 temperature controller (Linkam Scientific Instruments Ltd., Tasworth, UK). The sample solution of 1 µl in a glass capillary tube was frozen rapidly at ~−20 °C and then warmed slowly until a single ice crystal was prepared. Again the sample was cooled at a rate of 0.1 °C/min. The change in ice crystal morphology was recorded by a CCD camera. The freezing point of the solution was determined as the temperature when rapid growth of the ice crystal was observed. Each AFP sample was dissolved in 25 mM ammonium bicarbonate (pH 7.9) and TH

measurements were repeated at least three times for various concentrations between 0 and 0.3 mM.

2.3.3 FIPA analysis

FIPA analysis was performed as described previously [80]. At first, polyvinyl chloride (PVC) cylindrical molds (4.5 cm diameter, 3−4 cm high and 4 mm thick) with a tiny notch (1 mm wide, 2 mm high) on the bottom were sealed to a metal pan. Then the pan was placed into a temperature-controlled ethylene glycol bath cooled to –0.5 ℃ and 0.22 μm filtered and degassed water was added to the pan but outside of the molds. After the water had slowly entered into the molds and reached to –0.5 ℃, a small piece of ice was added to the pan, outside of the molds to nucleate ice growth. Ice crystals were finally prepared after filling the molds with water, dropping the temperature of the bath and 3−4 days of incubation. Then ice crystals were observed under cross-polarized light to determine if they were single crystals or not.

One milliliter of 1.1 mg/ml *Tis*AFP8 was fluorescently labeled with 50 μl of 10 mg/ml 6-(tetramethylrhodamine-5-(and-6)-carboxamido) hexanoic acid, succinimidyl ester (product code T-6105, Invitrogen) in 100 mM $NaHCO_3$ (pH 8.5). The solution was mixed on a rotator at room temperature for 3 h. The mixture was dialyzed against ultra-pure water to remove unreacted fluorescent dye. A single ice crystal with a known crystal orientation was mounted onto a brass cold finger and immersed into 35 ml of fluorescent-labeled *Tis*AFP8 solutions (0.022 mg/ml, 1 μM). The crystal was grown for 2–3 h at −8 ℃ to a hemispherical shape and then removed from the cold finger. Fluorescence on the ice hemisphere, which displays AFP-bound ice planes, was visualized under a UV light in a cold room of −1 ℃. The effect of pH (pH 3.0–10.0) was examined by diluting fluorescently labeled *Tis*AFP8 solutions to a concentration of 0.022 mg/ml (1 μM) with 25 mM glycine-HCl (pH 3.0), 25 mM acetate-NaOH

(pH 4.0), 25 mM acetate-NaOH (pH 5.0), 25 mM MES-NaOH (pH 6.0), 25 mM HEPES-NaOH (pH 7.0), 25 mM ammonium bicarbonate (pH 7.9), 25 mM Tris-HCl (pH 9.0) and 25 mM glycine-NaOH (pH 10.0).

2.3.4 Crystallization and X-ray structure analysis of *Tis*AFP8

The hanging-drop vapor-diffusion method was used for crystallization of *Tis*AFP8 with a concentration of 35 mg/ml [114]. The crystal of *Tis*AFP8 used for data collection was grown in a plate-like shape under 0.1 M MES monohydrate (pH 6.5), 1.6 M ammonium sulfate and 10% v/v 1, 4-dioxane at 20 °C (Fig. 2.2). Diffraction data were collected on beamline BL-17A at the Photon Factory (High Energy Accelerator Research Organization, KEK, Tsukuba, Japan) with 0.98000 Å radiation, and processed using HKL-2000 [115] and CCP4 suite [116]. The structure of *Tis*AFP8 was determined by molecular replacement method using PHENIX [117], with the coordinates of *Tis*AFP6 (PDB ID: 3VN3), which shows 83.4 % sequence identity with *Tis*AFP8, as the search model. The molecular model of TisAFP8 was built using Coot [118] and refined using PHENIX and REFMAC [119].

2.3.5 Ice-lattice matching method

In order to evaluate structural similarity between the ice lattice and the bound water molecules determined in the present study, two sets of the coordinates were superposed by referring to the work of Sun *et al* [93]. A set of surface waters on the putative ice-binding site (IBS) including the β-sheet and loop region of *Tis*AFP8 were sampled for the calculation. A referential hexagonal ice structure was generated in a box with dimensions of ~40 × 40 × 40 Å, which accommodated all of the sampled waters. A sampled water molecule that most likely matched the ice lattice was superposed onto the ice water at the center of the ice box, which was

Figure 2.2 Crystal image of *Tis*AFP8.

Large single crystals grew to maximum dimensions in a plate-like shape under 0.1 M MES monohydrate (pH 6.5), 1.6 M ammonium sulfate and 10% v/v 1, 4-dioxane at 20 °C.

used for the origin of the coordinate. The water anchored to the hydroxyl group of Thr^{193} was selected as the rotation center. The surface water molecules were rotated around orthogonal *x*-, *y*- and *z*-axes (polar angle) with intervals of 2° for each axis using the program PDBSET in the CCP4 suit. At each rotation angle the distances between surface waters and the proximate ice waters were recorded by the program NCONT in CCP4, and the root-mean-square deviation (RMSD) was evaluated by an in-house FORTRAN program. The rotated coordinates of surface waters with the lowest RMSD were used for superposing with the ice lattice.

2.3.6 Docking model of the ice-AFP interaction

Molecular models of *Tis*AFP8 bound with various ice planes was searched by the docking program HEX 8.0.0 [120]. Default search parameters were applied for all docking runs with a correlation type = shape + electrostatics, post processing = OPLS minimization and a final search = 30. The surface complementarity between AFPs and the basal planes was evaluated by the shape correlation (*S*c) value calculated by the program SC in the CCP4 suite. The *S*c value was used as an indicator of geometric complementarity of protein/protein interfaces, which ranges from 0.0 to 1.0 [44]. The *S*c value of 1.0 defines a perfect match between two binding molecules.

2.3.7 Circular-dichroism (CD) spectroscopy

CD spectra were measured on a J-720 spectropolarimeter (Jasco, Tokyo, Japan) with a quartz cuvette of 0.1 cm optical path length. *Tis*AFP8 and its mutant solutions of 0.3 mg/ml in 10 mM sodium phosphate buffer (pH 7.4) were measured. Spectral data were collected from 190 to 260 nm at room temperature. The scan was repeated four times and averaged.

2.4 Results

2.4.1 Purification of recombinant *Tis*AFP wild type and mutants

Recombinant *Tis*AFP wild type and mutants were purified in two steps, cation exchange chromatography (High-S) followed by anion exchange chromatography (High-Q). SDS-PAGE of each purified *Tis*AFP wild type and mutant revealed a single band clear of any other contaminants (Fig. 2.3). The total amount of purified *Tis*AFP8 wild type from 1 L culture medium was 3.5 mg. Yields of other mutants from 1 L culture medium were also listed in Table 2.2.

2.4.2 Antifreeze activity of *Tis*AFP8

Thermal hysteresis (TH) activity of purified recombinant *Tis*AFP8 as a function of the protein concentration is shown in Fig. 2.4a. *Tis*AFP8 exhibited a TH activity of 2.0 °C at 0.11 mM (Fig. 2.4a), which is consistent with the previous report by Xiao *et al*. [105] and was almost 10-fold higher than that of *Tis*AFP6 at the same concentration. As seen in hyperactive AFPs, the seed ice crystal in the presence of *Tis*AFP8 maintained its original shape during the TH gap. The crystal grew rapidly (burst) in six directions with a dendritic pattern perpendicular to the *c*-axis at T_f (Fig. 2.4b, top row). At a low concentration (9 μM), the ice crystal turned into a lemon-like shape within the TH gap and expanded along the *a*-axis, resulting in flat basal planes (Fig. 2.4b, central row). The morphology and TH activity indicated that *Tis*AFP8 is a member of hyperactive AFPs and possesses basal plane affinity, which is a hallmark of hyperactive AFPs [22]. In contrast, *Tis*AFP6 showed TH activity of ~0.3 °C at 0.11 mM and an elongation of the crystal along the *c*-axis, which is comparable with moderate AFPs (Fig. 2.4b, bottom row).

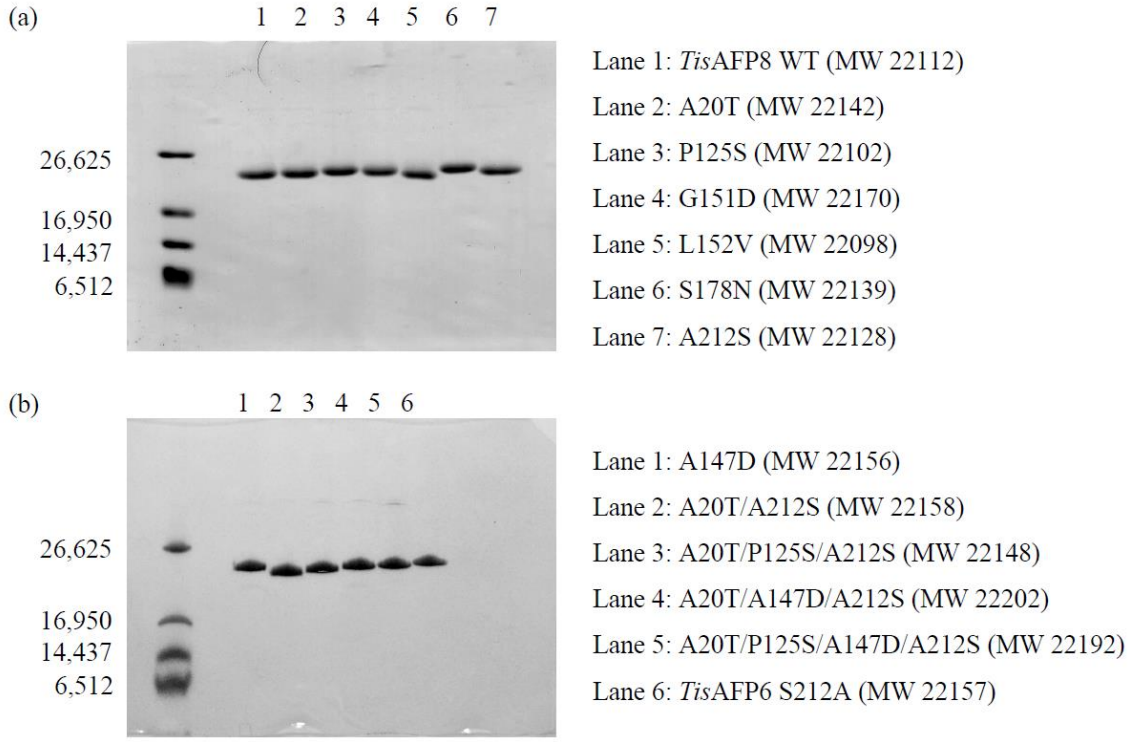

Figure 2.3 SDS-PAGE analysis of purified wild-type *Tis*AFPs and their mutants.

(a) SDS-PAGE analysis of purified *Tis*AFP8 wild type (lane 1), A20T (lane 2), P125S (lane 3), G151D (lane 4), L152V (lane 5), S178N (lane 6) and A212S (lane 7). (b) SDS-PAGE analysis of purified A147D (lane 1), A20T/A212S (lane 2), A20T/P125S/A212S (lane 3), A20T/ A147D/A212S (lane 4), A20T/ P125S/A147D/A212S (lane 5) and *Tis*AFP6 S212A (lane 6). Molecular weight of each protein was indicated. Polypeptide SDS-PAGE molecular weight standards (Bio-Rad) were used as the molecular weight marker.

Table 2.2 Summary of the yield of each protein.

Protein	Yield (mg/L)
*Tis*AFP8 wild type	3.5
A20T	5.8
P125S	29.0
A147D	11.9
G151D	12.1
L152V	2.9
S178N	6.3
A212S	11.0
A20T/A212S	15.3
A20T/P125S/A212S	11.5
A20T/A147D/A212S	35.8
A20T/P125S/A147D/A212S	21.5
*Tis*AFP6 S212A	0.8

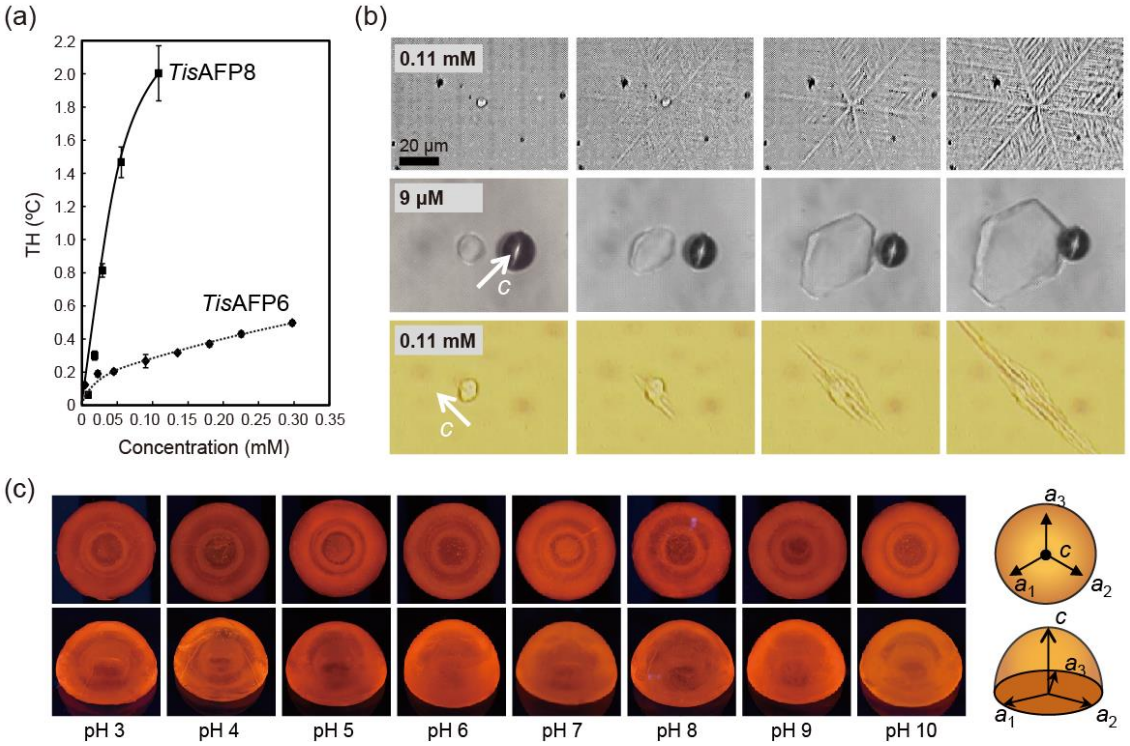

Figure 2.4 Antifreeze properties of *Tis*AFP8.

(a) TH activity of *Tis*AFP8 (solid line) and *Tis*AFP6 (dash line) as a function of protein concentration. Each point was measured at least three times and averaged. Standard deviations are shown as vertical bars. (b) Ice crystal growth patterns in the AFP solutions. The top row shows the rapid growth of an ice crystal in 0.11 mM *Tis*AFP8 solution. Images were taken within 1 s. The middle row shows the slow growth of an ice crystal in the presence of 9 μM *Tis*AFP8. Four frames encompass a period of 6 s. The bottom row shows the two-direction growth of an ice crystal in a *Tis*AFP6 solution at 0.11 mM and intervals of 10 s. Scale bars = 20 μm. (c) Single-ice hemispheres grown in solutions of fluorescently labeled *Tis*AFP8 (1 μM) under different pH conditions, which are oriented with the basal plane perpendicular to the cold finger. The upper panels: top-down views of ice hemispheres under UV light. The lower panels: oblique views of the same hemispheres.

2.4.3 FIPA analysis

FIPA analysis is used for visualization of AFP-bound ice planes. Figure 2.4c shows the illuminated images of single ice hemispheres grown in 1 μM fluorescently labeled *Tis*AFP8 solutions at various pH conditions. At each pH condition, fluorescence was observed throughout the entire ice hemisphere without individual patches, which shows the accumulation of *Tis*AFP8 toward the basal planes and the primary prism planes of the ice crystal, as well as surfaces between these planes. This is the same pattern reported for known hyperactive AFPs from insects [52, 55], bacteria (*Mp*AFP and *Col*AFP) [32, 75] and fish (Maxi) [41], suggesting that *Tis*AFP8 is categorized into the hyperactive AFP with high affinity to ice planes. In contrast, we previously reported that *Tis*AFP6 adsorbs onto the basal and prism plane with separate fluorescent patches in FIPA analysis [72], despite its moderate antifreeze activity. This observation for *Tis*AFP6 can be explained by a slow accumulation process over the time period of the FIPA experiment (3–4 h) [122], which may overcome the apparent lower affinity of *Tis*AFP6 to the basal plane.

2.4.4 Overall structure of *Tis*AFP8

The crystal structure of *Tis*AFP8 was determined at 1.0 Å resolution using molecular replacement. The coordinates were deposited in the Protein Data Bank (PDB) under ID 5B5H. Statistics for data collection and refinement are summarized in Table 2.3. The overall structure of *Tis*AFP8 is a β-helical fold with dimensions of ~52 × 31 × 28 Å, which is consist of a large right-handed β-helical domain and an additional long α-helix (Fig. 2.5). The β-helical domain is assembled by six helical turns, which constitute three parallel β-sheets (face a, b, c) and a triangular cross-section. The six helical turns are irregularly stacked in the order of β1-β6-β5-β4-β3-β2, thus the N- and C-terminal regions of polypeptide chain adjoin in a

Table 2.3 Summary of data collection and refinement statistics.

Data collection	
Space group	$P2_12_12$
Unit-cell parameters (*a*, *b*, *c*), (Å)	48.39, 104.85, 35.63
Number of molecules in asymmetric unit	1
V_M (Å^3 Da^{-1}) [123]	1.92
Solvent content (%) [123]	36.0
Beam line	Photon Factory BL-17A
Wavelength (Å)	0.98000
Resolution range (Å)	52.4–1.0 Å
R_{merge} [*,†]	0.091 (0.419)
Observed reflections	867539
Independent reflections	83006
Completeness (%) [*]	84.5 (24.6)
$\langle I/\sigma(I)\rangle$ [*]	4.8 (1.5)
Refinement	
R factor [*,‡]	0.120 (0.355)
Free *R* factor [*,‡,§]	0.136 (0.414)
R.M.S bond lengths (Å)	0.028
R.M.S bond angles (°)	2.269
Residues	223
Number of non-hydrogen atoms	
Protein	1568
Solvent	315
Ramachandran plot (%) [¶]	
Residues in favored regions	99.0
Residues in allowed regions	1.0
Residues in outliner regions	0.0
Average B factor (Å^2)	10.0

[*] Values in parentheses are for the highest resolution shell (1.06–1.00 Å for data collection and 1.03–1.00 Å for refinement)

[†] $R_{merge} = \Sigma\Sigma_j|\langle I(h)\rangle - I(h)_j| \; / \; \Sigma\Sigma_j\langle I(h)\rangle$, where $\langle I(h)\rangle$ is the mean intensity of a set of equivalent reflections.

[‡] R factor $= \Sigma||F_{obs}(h)| - |F_{calc}(h)||/ \; \Sigma \; |F_{obs}(h)|$, where F_{obs} and F_{calc} are the observed and calculated structure factors, respectively.

[§] A randomly chosen 4.9% of the data were used to calculate the free R factor [124].

[¶] Statistics were obtained from MolProbity [125].

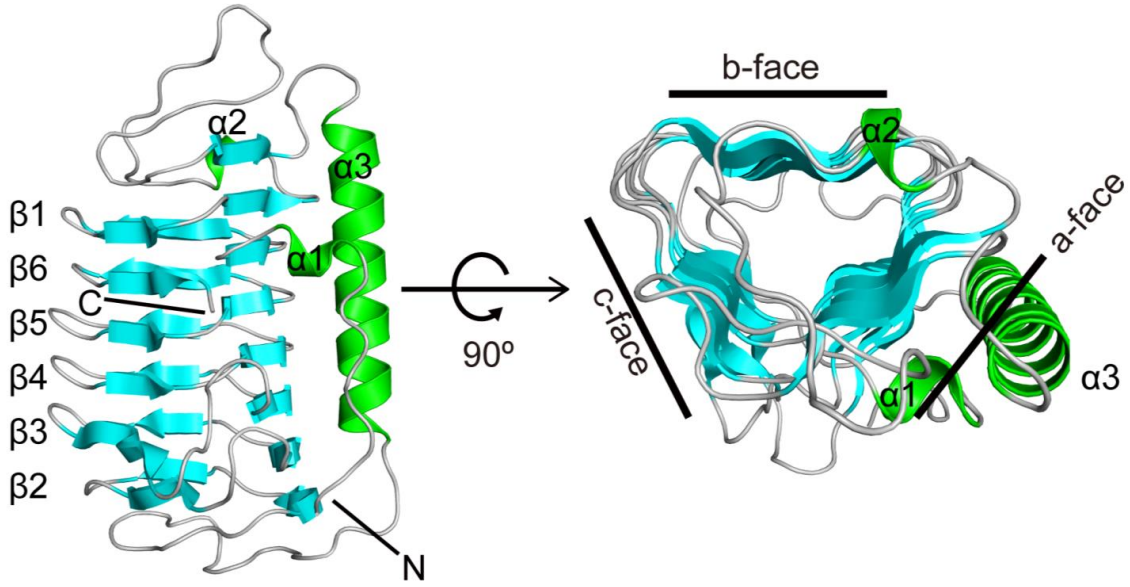

Figure 2.5 Crystal structure of *Tis*AFP8.

The overall structure of *Tis*AFP8 is shown in schematic representation. The protein adopts a right-handed β-helical fold and has a triangular cross-section with three parallel sheets (face a, b, c). β sheets are cyan, α helices are green and loops are grey. The N- and C-termini are labeled. The six turns of the β-helix are aligned in an irregular order, β1-β6-β5-β4-β3-β2.

"head-to-tail" manner in the middle of the β-helix. The unique stacking topology for the β-helical structure has been only reported for crystal structures of the AFP family including *Tis*AFP, *Le*AFP, *Ff*AFP and *Col*AFP. A several loop segments cap each end of the β-helix to stabilize the helical structure. The six helical units differ in length and are derived from residues as follows: β1, 17 residues (Ile16 to Gly32); β6, 18 residues (Arg206 to Lys223); β5, 18 residues (Val188 to Gly205); β4, 21 residues (Lys167 to Gly187); β3, 28 residues (Thr139 to Ala166); β2, 21 residues (Gly118 to Ser138). The bottom three helical units (β4, β3, β2) have additional 4- to 10-residue insertions, which form extended loops between β-strands on the same side of the protein, causing a bulge-like structure at the β-helical surface and a semi-pear-shaped structure. The β-helical fold is stabilized by the intramolecular hydrogen-bonding network and hydrophobic residues stacked inside the helix. The RMSD between all Cα atoms of *Tis*AFP8 and *Tis*AFP6 is 0.38 Å, which indicates high structural similarity between the two AFP isoforms and the overall structure of *Tis*AFP8 is not affected by crystal packing forces.

2.4.5 Ice binding site of *Tis*AFP8

In our previous report, the ice-binding site (IBS) of *Tis*AFP6 was the β-sheet of the b-face (termed the β-sheet IBS), which is the flattest side of the β-helix, by site-directed mutagenesis [72].

In Fig. 2.6, we compared the amino acid sequence and 3D structure of the β-sheet IBS and the adjacent loop region of *Tis*AFP8 and *Tis*AFP6. In this region, the repetitive ice-binding TXT or TXN motifs found in hyperactive insect AFPs or bacterium AFP [49, 50, 32] are absent in both *Tis*AFP8 (Fig. 2.6a) and *Tis*AFP6 (Fig. 2.6d). The putative β-sheet IBS of *Tis*AFP8 is composed mainly of five parallel β-strands with 5- or 6-residues (shown in yellow in Fig. 2.6a).

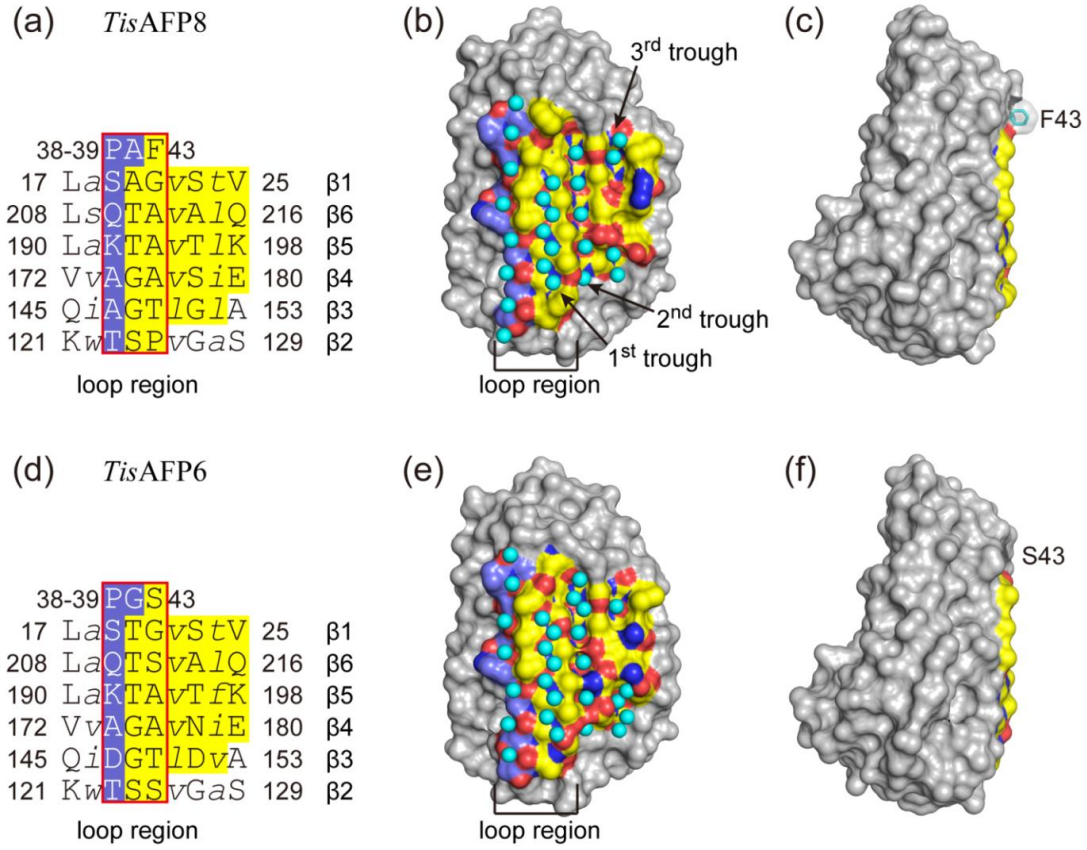

Figure 2.6 Comparison of the IBS of *Tis*AFP8 and *Tis*AFP6.

(a, d) Amino acid residues of the IBS of *Tis*AFP8 and *Tis*AFP6. Letters shaded in yellow are residues in the β-sheet IBS. The adjacent row is shaded in slate. Residues in the loop region are indicated in the red box. Italic lowercase letters represent inward-pointing residues. Residues with outward-pointing side chains are represented in uppercase letters. (b, e) Front view of the IBS of *Tis*AFP8 and *Tis*AFP6, respectively, which corresponds to the area indicated in (a) and (d). Carbon, oxygen and nitrogen atoms in the area corresponding to the β-sheet IBS proposed in *Tis*AFP6 are colored in yellow, red and blue, respectively. Residues in the adjacent row are shown in slate for carbon atoms, red for oxygen atoms and blue for nitrogen atoms. Partially ordered water molecules are shown as cyan spheres. Three troughs are labeled. The loop region is indicated. (c, f) Side view of the b-face of *Tis*AFP8 and *Tis*AFP6, respectively. For *Tis*AFP8, the position of Phe43 is labeled with side chain by the stick model. The position of Ser43 for *Tis*AFP6 is also labeled.

Side chains of residues at the first (A^{20}, T^{211}, T^{193}, G^{175}, G^{148}, S^{124}), second (G^{21}, A^{212}, A^{194}, A^{176}, T^{149}, P^{125}), fourth (S^{23}, A^{214}, T^{196}, S^{178}, G^{151}) and sixth (V^{25}, Q^{216}, K^{198}, E^{180}) row of the β-sheets face the solvent. Side chains on the third (V^{22}, V^{213}, V^{195}, V^{177}, L^{150}) and fifth (T^{24}, L^{215}, L^{197}, I^{179}, L^{152}) row are directed towards the interior of the β-helix to form the hydrophobic core. As a result, this β-sheet IBS presents an out-out-in-out-in-out pattern, which forms three tiny troughs on the molecular surface that are parallel to the helical axis (Fig. 2.6b).

The β-sheet IBS region of two *Tis*AFP isoforms is composed of 32 residues. Twenty-four of these residues are preserved and share a sequence identity of 78%, which is slightly lower than the overall identity of 83.4%. There are 17 hydrophobic residues located in the β-sheet IBS of *Tis*AFP8, whereas 13 hydrophobic residues occupy corresponding positions in *Tis*AFP6. The four additional hydrophobic residues (Ala20, Phe43, Pro125 and Ala212) are located in the first and second row of the β-sheet. *Tis*AFP8 has two additional hydrophobic residues (Ala39 and Ala147) in the row of residues (Pro38, Ala39, Ser19, Gln210, Lys192, Ala174, Ala147 and Thr123) (shown in slate in Fig. 2.6a and b), which constitute the loop region together with the first and second row of the β-sheet IBS. In total, the ice-binding β-sheet and the adjacent loop region of *Tis*AFP8 bears more hydrophobic character than those of *Tis*AFP6.

Despite the extreme structural diversity of the various known AFPs, a structural feature common to their IBSs has been identified; they are extensive, relatively flat and hydrophobic. The putative IBS of *Tis*AFP8 conforms to this feature (Fig. 2.6c). Side chains of A^{20}, A^{39}, A^{212} and Phe^{43} form a hydrophobic patch whereas hydrophilic residues occupy the corresponding sites for *Tis*AFP6 (T^{20}, S^{43} and S^{212}) (Fig. 2.6a and d). The bulky side chain of Phe^{43}, which is located at the edge of a joint area between the β-sheet IBS and the adjacent loop region of *Tis*AFP8, protrudes from the molecular surface to form a tiny bulge (Fig. 2.6b and c). In the crystal structure of the AFP from *Rhagium inquisitor* (*Ri*AFP, PDB ID: 4DT5) residues with

long side chains (His and Arg) are located at the edge of the IBS. Thus, high hydrophobicity in IBS appears to play a key role for retaining the antifreeze activity of *Tis*AFP8.

2.4.6 Site-directed mutagenesis of the putative IBS of *Tis*AFP8

We focused on the β-sheet of *Tis*AFP8 as its putative IBS because of its extremely high sequence identity (83.4 %) and structural similarity (RMSD of 0.38 Å for all Cα atoms) to *Tis*AFP6. A series of single mutants were prepared where residues Ala^{20}, Pro^{125}, Ala^{147}, Gly^{151}, Ser^{178} and Ala^{212}, which are located on the β-sheet IBS of *Tis*AFP8, were mutated to the corresponding residues of *Tis*AFP6, namely Thr^{20}, Ser^{125}, Asp^{147}, Asp^{151}, Asn^{178} and Ser^{212} (Fig. 2.7a and Fig. 2.8a). One of the inward-pointing side chains, Leu^{152}, was mutated to Val^{152} as a reference. The major object of these experiments was to determine the role of each residue and how these residues influence TH activity. To further examine the contribution of the residues on the loop region of *Tis*AFP8 in antifreeze activity, four mutants were prepared by multiple mutations (A20T/A212S, A20T/P125S/A212S, A20T/A147D/A212S and A20T/P125S/A147D/A212S). Each mutant was purified and analyzed for its TH activity in comparison with wild-type *Tis*AFP8. As shown in Fig. 2.9, the CD spectra of all mutants were almost identical to that of the wild-type protein, indicating that the overall conformation of the mutants was not affected by the mutation.

Figure 2.7b shows the TH activity of the mutants and the comparison with the wild-type*Tis*AFP8. All mutations resulted in different levels of TH activity loss. The G151D mutant showed a decrease in TH activity of 19% (to 1.61 °C) compared with that of the wild-type (1.98 °C) at 0.11 mM. Mutation L152V, which locates alongside G151D and has an inward-pointing side chain, resulted in TH activity loss of 34% at 0.11 mM. The TH activities of the S178N, A147D and P125S mutants were 63%, 63% and 58% of that of the wild type,

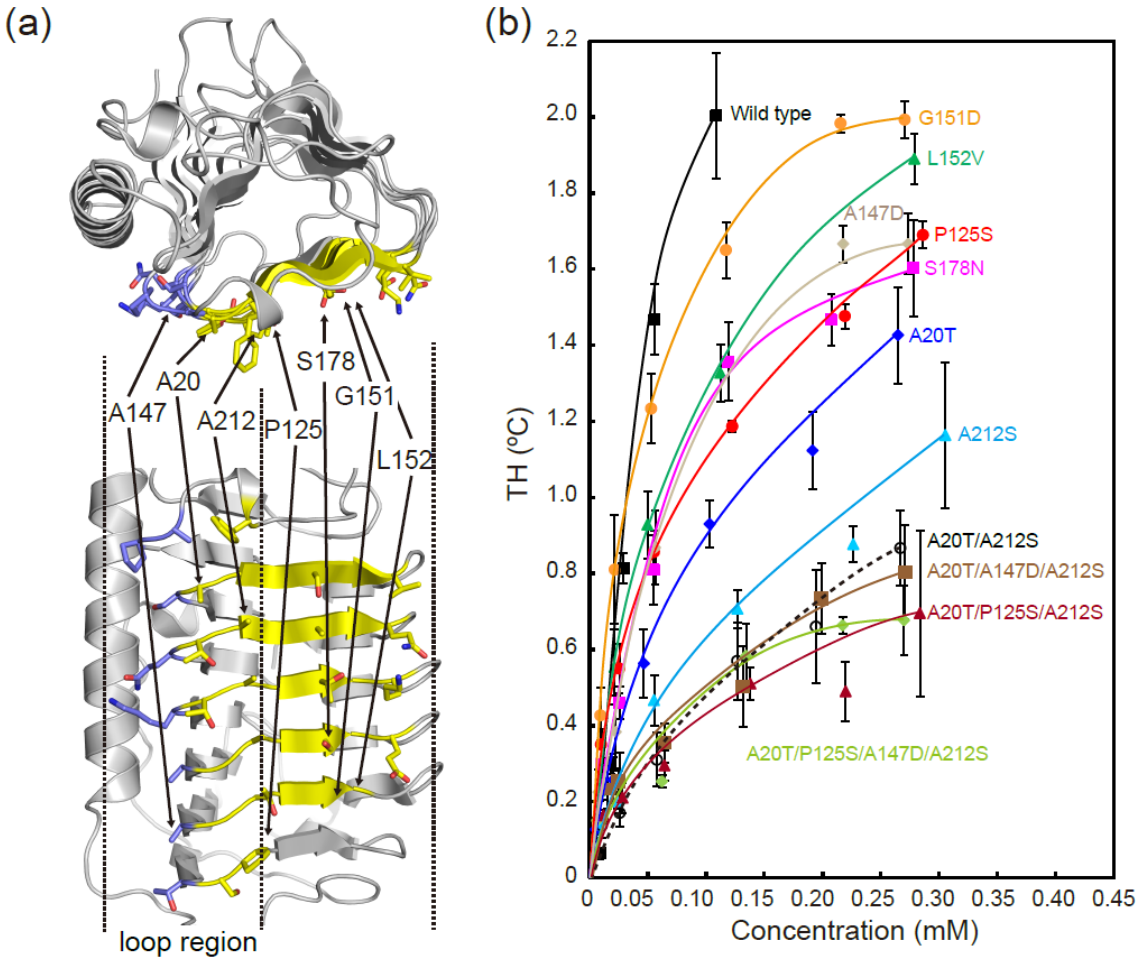

Figure 2.7 Site-directed mutants introduced to the IBS of *Tis*AFP8.

(a) The IBS of *Tis*AFP8 viewed from two different angles. The upper panel shows a top-down view along the axis of the β-helix. The lower panel shows a front view of the IBS. Putative ice-binding residues are shown as sticks. The color scheme is the same as in Fig. 2.6b and e. Mutated residues are indicated by arrows. (b) TH activities of *Tis*AFP8 wild type and mutants plotted as a function of protein concentration.

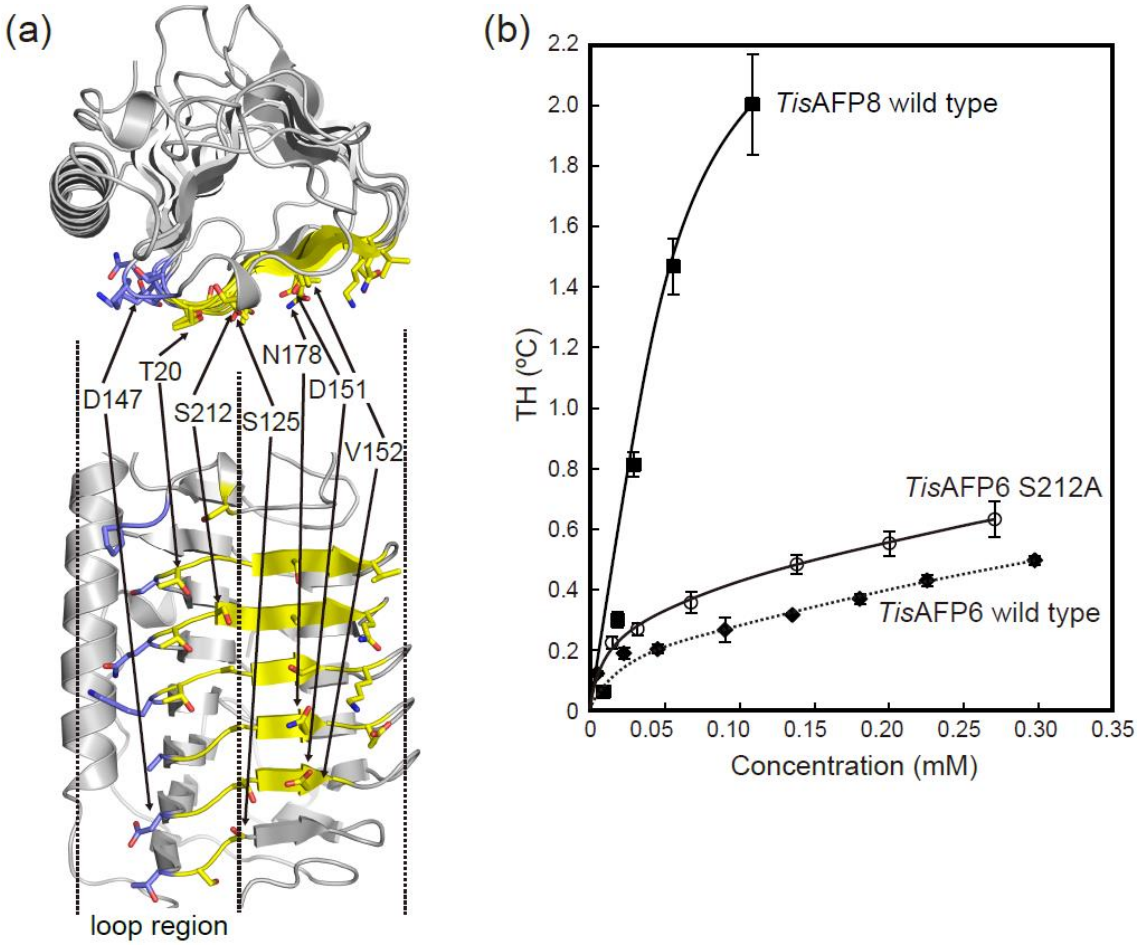

Figure 2.8 Site-directed mutants introduced to the IBS of *Tis*AFP6.

(a) The IBS of *Tis*AFP6 viewed from two different angles. The color scheme is the same as Fig. 2.7a.

(b) TH activity curve of *Tis*AFP6 mutant (S212A). Wild-type *Tis*AFP8 and *Tis*AFP6 activities are shown for comparison.

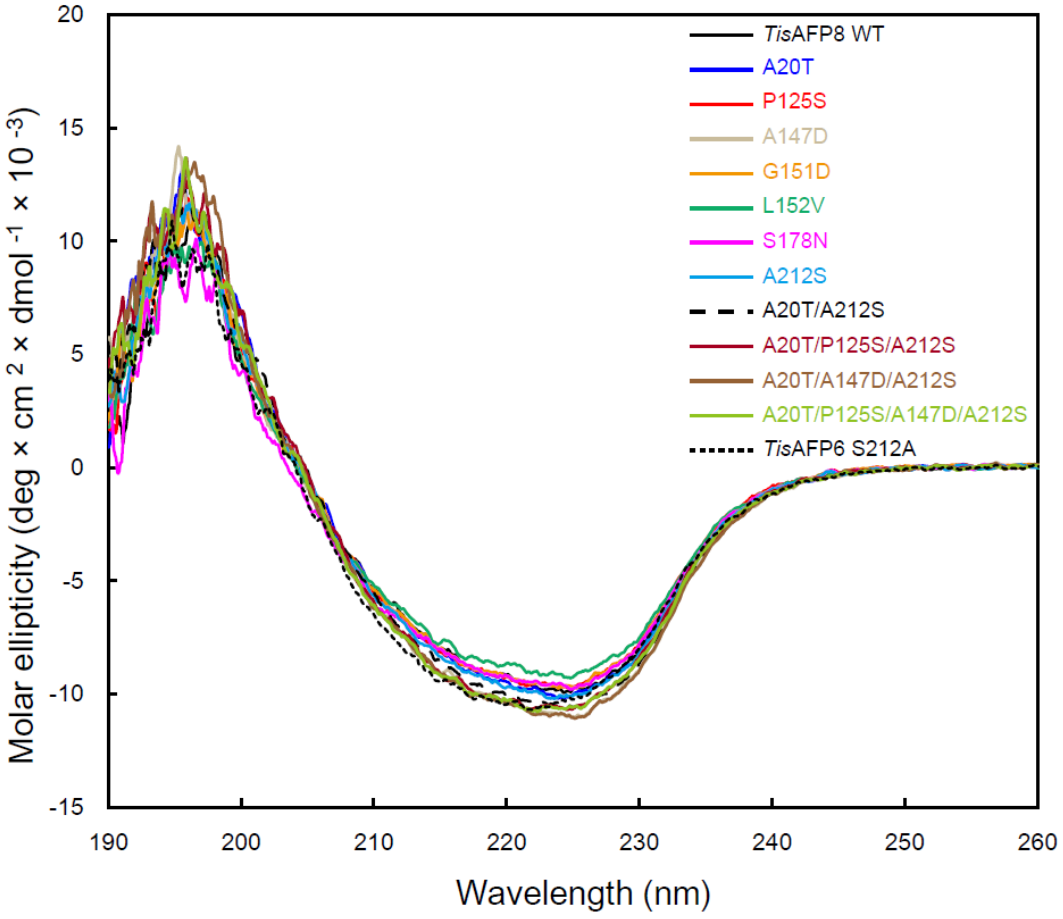

Figure 2.9 CD spectra of wild-type (WT) *Tis*AFP8 and mutants.

The CD spectra of all mutants were similar to that of wild-type *Tis*AFP8, indicating the mutations did not affect the overall conformation of the protein and the mutants adopted the native fold.

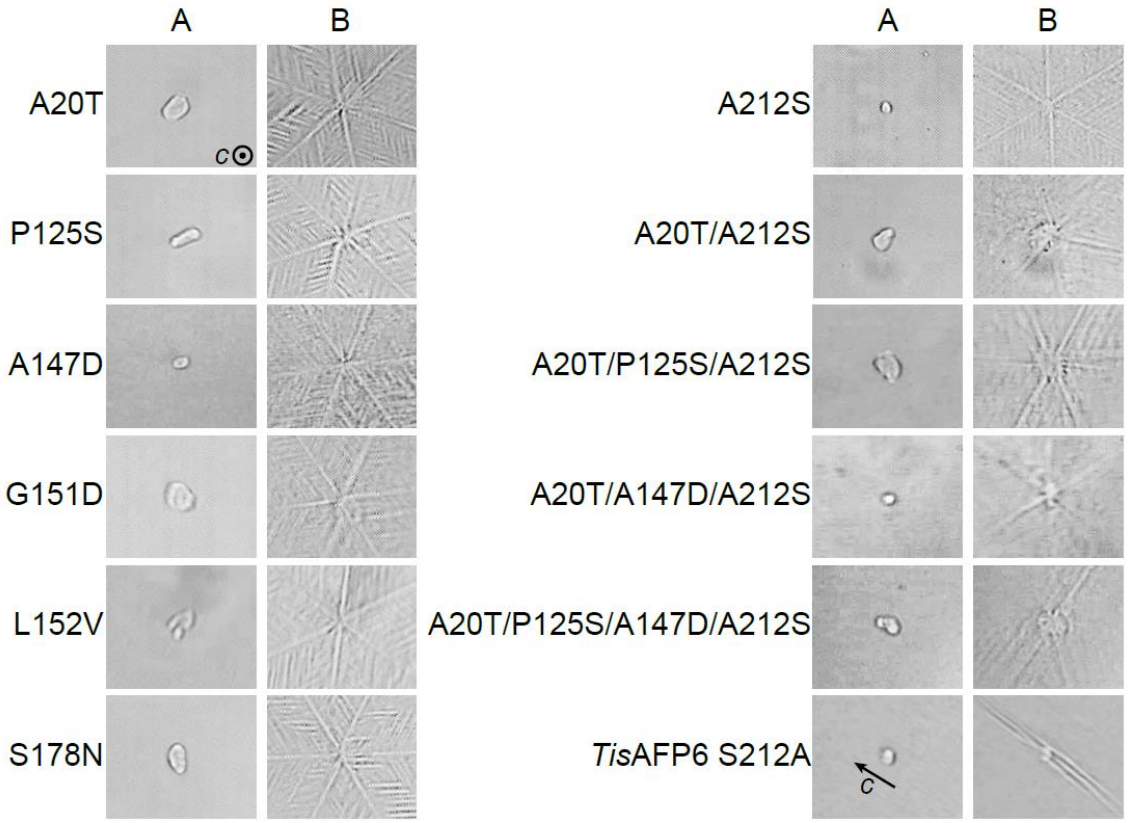

Figure 2.10 Ice crystal bursts in the presence of each mutant.

Images of ice crystals seen in frames A and B were taken before and after ice crystals rapidly exploded, respectively. The direction of the *c*-axis is shown in frame A.

respectively, and comparable to that of L152V at 0.11 mM. Among all single mutants, A20T and A212S showed the largest loss of TH activity. The A20T mutation caused a TH decrease of 54% at 0.11 mM, whereas A212S lost 68% of its TH activity when compared with the activity of the wild-type. The double mutant (A20T/A212S) showed a further decrease in TH activity, which lost 75% of the activity of wild-type *Tis*AFP8 at 0.11 mM. However, TH activities of both triple mutants (A20T/P125S/A212S and A20T/A147D/A212S) and the quadruple mutant (A20T/P125S/A147D/A212S) were nearly identical to that of A20T/A212S mutant. In the presence of each mutant, the ice crystal rapidly expanded along the *a*-axis when the sample was cooled below the TH gap, which is the same as the wild-type *Tis*AFP8 (Fig. 2.10).

Another mutant for *Tis*AFP6 was prepared, which has a backward mutation by replacing Ser^{212} with Ala in *Tis*AFP8. As shown in Fig. 2.8b, the TH value of *Tis*AFP6 S212A mutant at 0.14 mM showed a slight increase to 0.48 °C compared to that of wild-type *Tis*AFP6 (0.32 °C). Ice crystals inhibited by *Tis*AFP6 S212A burst along the *c*-axis, which was also observed in the presence of *Tis*AFP6 wild type (Fig. 2.10).

2.4.7 Characterization of the waters on the β-sheet and loop region of *Tis*AFP8

There are 34 water molecules found on the β-sheet IBS of *Tis*AFP8. Among them, 16 waters occupy the troughs formed between the side chains of the outward-pointing residues of *Tis*AFP8 (Fig. 2.6b). For *Tis*AFP6, 56 crystallographic waters were found on the IBS and exposed to the solvent region in the crystal, among which, 18 waters were located in the three tiny troughs (Fig. 2.6e) [72]. In the adjacent loop region of both *Tis*AFPs, restrained water molecules are organized in a linear pattern. In *Tis*AFP8, eight water molecules are embedded in a trough formed between two rows of residues (P^{38}, S^{19}, Q^{210}, K^{192} and A^{39}, A^{20}, T^{211}, T^{193}).

Ice lattice matching with bound waters was attempted using 24 waters that are directly bound

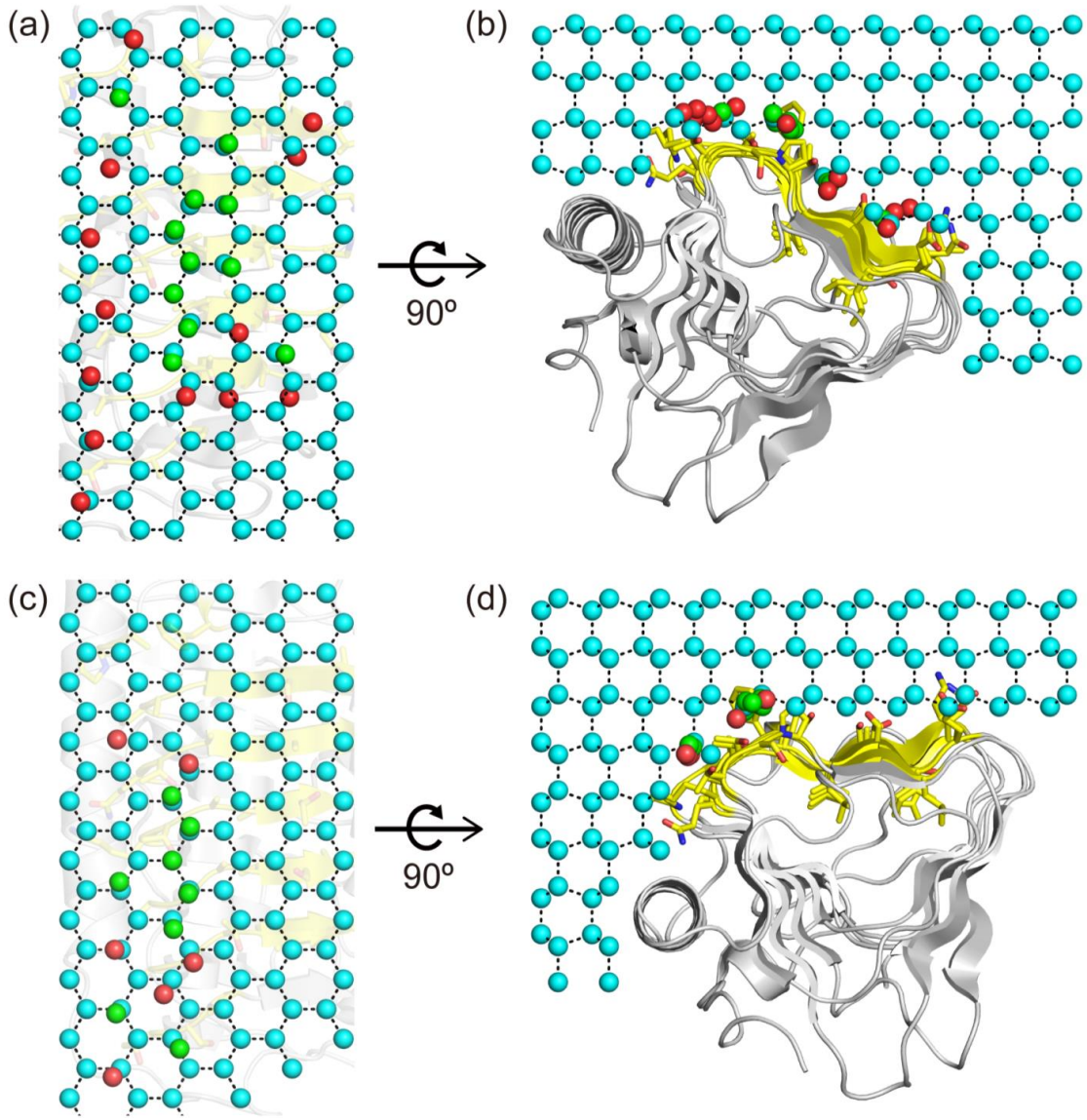

Figure 2.11 Superposing of the ice-like waters on *Tis*AFP8 to the basal plane of the ice lattice.

(a, b) 24 waters on *Tis*AFP8 are superposed to the set of water molecules on the basal plane. (a) Top-down view along the *c*-axis of the ice lattice. (b) Front view along the *a*-axis of the ice lattice. (c, d) Superposing of 14 waters on *Tis*AFP8 to the basal plane. The AFP is shown in ribbon representation. Side chains of residues on the β-sheet IBS and the loop region are shown as sticks. Waters molecules in the ice lattice are shown as cyan spheres, and the hydrogen bonds are shown as black dashed lines. Bound waters of *Tis*AFP8 that match to the ice lattice within a distance of 1 Å are represented in green spheres. Other bound waters are indicated as red spheres.

to the β-sheet IBS and the loop region. In the rotation search, the RMSD for the corresponding waters were varied from 2.0 to 1.0 Å. With the orientation giving the lowest RMSD, 11 out of 24 waters can be closely superposed to the ice lattice with a RMSD of 0.65 Å (Fig. 2.11a), nine of which are located in the first and second troughs of the β-sheet IBS (Fig. 2.11b). In this orientation, however, eight bound waters from the loop region are situated apart from the ice lattice with a slight rotation. In order to search an alternative orientation to superpose these water molecules to the ice lattice, a similar calculation was performed using 14 waters located in the loop region and the first trough of the β-sheet. In the superposition with the lowest RMSD, eight out of 14 waters are positioned to the ice lattice with a RMSD of 0.69 Å, also suggesting an ice-like network of waters in the loop region (Fig. 2.11c and d). These calculations show that bound waters in the IBS align into three rows and are divided into two groups, both of which appear to share the row of waters in the first trough on the β-sheet IBS. Each group of bound waters may separately anchor the protein to the ice lattice (Fig. 2.11b and d).

2.4.8 Ice-docking model

To gain insight into the ice-binding properties of *Tis*AFP8 and *Tis*AFP6, binding models were searched using the rigid docking program HEX 8.0.0 [120]. The basal plane of an ice crystal was selected as the docking partner because the basal plane affinity is thought to be the basis for the hyperactivity of AFPs [22]. Figure 2.12 illustrates the docking model calculated using the coordinates of *Tis*AFP8 and *Tis*AFP6, including water molecules around their IBSs. In the case of *Tis*AFP6, the docking result showed that *Tis*AFP6 recognizes the basal plane through two IBSs and surrounding water molecules. The first IBS (β-sheet IBS) (Fig. 2.12a) consists of residues on the β-sheet IBS, whereas the second (Fig. 2.12b) involves the loop IBS and the first and second row of the β-sheet IBS. On the other hand, the calculation for *Tis*AFP8 indicated

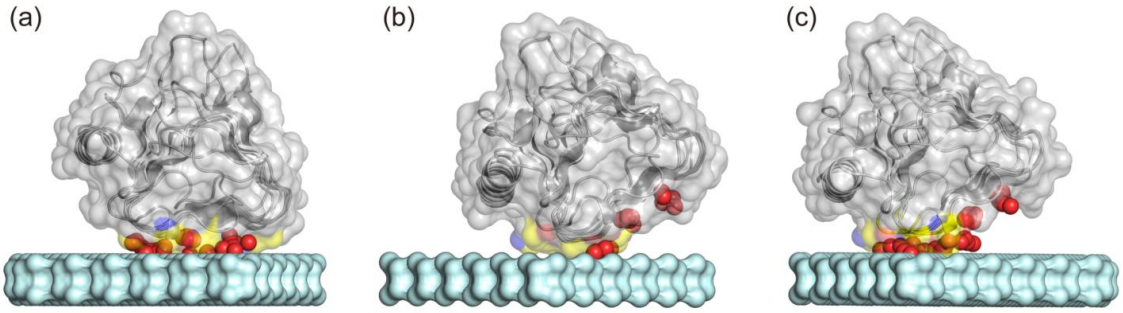

Figure 2.12 Docking of *Tis*AFP8 and *Tis*AFP6 to the basal plane of ice.

(a) The ice-binding interface (the β-sheet) of *Tis*AFP6. The residues involved in ice binding are colored in yellow for carbon, red for oxygen and blue for nitrogen. Bound water molecules are colored in red. (b) The ice-binding interface (the loop region) of *Tis*AFP6. The color scheme is the same as in (a). (c) The ice-binding interface (the loop region) of *Tis*AFP8. The color scheme is the same as in (a).

that the docked model binds the basal plane only through the loop IBS (Fig. 2.12c). The *S*c value, which evaluates the complementarity between AFP and the ice interface, for the *Tis*AFP6-ice interface on the β-sheet IBS was 0.50 with a buried surface area of 1066 Å^2. The *Tis*AFP6-ice interface on the loop IBS has an *S*c of 0.49 with a buried surface area of 783 Å^2. On the other hand, the docking result for *Tis*AFP8 shows only a model that adsorbs to the basal plane via the loop IBS, with an *S*c value of 0.55 and a buried surface area of 960 Å^2, even if the mutagenesis results indicate the participation of the sheet IBS in ice binding. This inconsistency may arise from the hydrophobic bulge formed by the aromatic side chain of Phe43 disrupting the planarity of both the β-sheet and loop IBSs. Moreover, the β-sheet IBS was involved in crystal packing, which displaced or constrained the bound waters on this surface. As a result, with the assistance of water molecules, the loop IBS matches better with the basal plane than the β-sheet IBS.

2.5 Discussion

2.5.1 General comparison between *Tis*AFP8 and *Tis*AFP6

We previously reported the crystal structure and ice-binding site of one isoform, *Tis*AFP6, derived from a snow mold fungus, *T. ishikariensis*. Here, we extended our work to gain insight into AFP-ice associations by crystal structure analysis of another isoform, *Tis*AFP8, and combined this structural data with characterization of its antifreeze activity and site-directed mutagenesis. The structure of *Tis*AFP8 exhibits high similarity to *Tis*AFP6 (RMSD of 0.38 Å for all Cα atoms), despite the distinct differences in their ice-binding abilities. This suggests that the variation of the ice-binding residues is a determinant for the differences in their antifreeze

activity.

2.5.2 Mutations on hydrophobic residues of *Tis*AFP8 caused TH decrease

In the present study, a series of single residue substitutions on the flattest β-sheet of *Tis*AFP8 with its counterpart of *Tis*AFP6 resulted in thermal hysteresis (TH) loss when compared with that of the wild-type protein, indicating that the β-sheet participates in ice binding. Furthermore, introducing a hydrophilic group to particular side chains (Ala20 to Thr, Pro125 to Ser, Gly151 to Asp, Ala212 to Ser) appears to be unfavorable for *Tis*AFP8 ice-binding capacity. Thus, the hydrophobic effect might be a dominant driving force in the interaction between *Tis*AFP8 and ice crystals. Moreover, two mutated sites, Ala20 and Ala212, are located in the loop region adjacent to the β-sheet ice-binding site (IBS) to constitute a hydrophobic patch with Phe43, Ala194 and Ala176. The largest loss in TH activity was observed for those multiple mutants, suggesting that the loop region plays a significant role in *Tis*AFP8 ice crystal-binding activity. The increased antifreeze activity caused by the mutation from Ser^{212} of *Tis*AFP6 to Ala also supports this view.

2.5.3 *Tis*AFPs may recognize ice through a compound IBS

Garnham *et al*. originally proposed that type III AFP binds to ice planes through a compound IBS, which is a combination of two adjoining flat surfaces at an angle of 150° to each other [79]. One of these surfaces binds to the primary prism plane of ice, while the other binds the pyramidal plane. Hanada *et al*. suggested *Col*AFP, a homolog of *Tis*AFPs, binds to the primary prism, secondary prism, pyramidal and basal planes of ice crystals through a compound IBS located on the flat β-sheet and the adjacent loop region [75].

Bound waters around *Tis*AFP are mainly buried in the troughs of the protein surface. The

water arrangement ordered by the IBS bears a resemblance with that of the basal plane of the ice lattice. These waters are termed anchored clathrate waters, which have been postulated to make contributions to the adsorption of AFP to ice. Further, the bound waters around the IBS of *Tis*AFP can be divided into two groups, which are in accordance with the distribution of the two IBSs: the β-sheet and loop IBS. This result supports our hypothesis that *Tis*AFP recognizes ice planes through a combination of two IBSs.

2.5.4 Bound waters on the compound IBS of *Tis*AFP8 form an ice-like network

Water molecules that encompass the IBS of *Mp*AFP and insect AFP are found to be equivalently spaced and make an excellent match to both the basal and primary prism planes of ice [32, 52, 49]. Bound waters around the IBS of *Tis*AFP8 match the ice lattice with RMSDs of 0.65 and 0.69 Å, which might be due to its poorly conserved IBS that does not have repetitive structural motifs. It seems that these less regular surface waters are organized into an ice-like arrangement, which merges with the quasi-liquid layer in between the ice lattice and bulk water. Currently, molecular dynamics simulations and terahertz spectroscopy are used to investigate the water molecule networks that are anchored to the IBS [91, 78, 126]. The crystal structure determined in the present study provides a base architecture for the microbial AFP family, and can be used to gain detailed descriptions of the water structure by using the two above methods.

2.5.5 *Tis*AFP8 matches ice lattice better

In the present study, docking models of *Tis*AFP8 and *Tis*AFP6 suggest that *Tis*AFPs adsorb onto ice through a compound IBS including the β-sheet and loop IBSs, which is consistent with the results of the mutagenesis study. A similar binding model for *Tis*AFP8 with ice was also obtained through the ice-lattice matching calculation, in which bound waters on the IBS are an

ice-like structure and appear to anchor the protein to multiple planes of ice. The ice-binding model for *Tis*AFP8 and the basal plane by this calculation (Fig. 2.7b) exhibits a close similarity with the model obtained by the molecular docking program (Fig. 2.8c) with a slight rotation of approximately 7°.

The surface complementarity between the IBS of AFP and ice was evaluated using *S*c value. The *S*c values for the complexes of non-AFPs with ice were found to be less than 0.38 [75, 89]. The calculated *S*c values suggest a better shape complementarity of the loop IBS of *Tis*AFP8 (*S*c value of 0.55) with the basal plane than the β-sheet and loop IBS of *Tis*AFP6 (*S*c values of 0.50 and 0.49, respectively). Additionally, the interaction area (960 $Å^2$) between the loop IBS of *Tis*AFP8 and the basal plane is more extensive than that of *Tis*AFP6 (783 $Å^2$) and comparable with the buried area between the β-sheet IBS of *Tis*AFP6 and ice (1066 $Å^2$). Consistent with the direct involvement of some hydration water molecules on the IBS of certain AFPs in binding to ice [32, 52], the *S*c values were significantly improved by including some partially arrayed water molecules in the compound IBS of *Tis*AFPs.

2.5.6 *Tis*AFP8 has a more hydrophobic IBS

The hydrophobic effect is thought to be a pivotal driving force when considering the functional mechanism of AFPs [45, 127, 128]. The restrained water molecules form hydrogen-bond networks and produce "cages" around hydrophobic groups. The hydrophobic groups dip into the ice grooves on the ice surface and then the caged water molecules are released into the bulk solvent with an entropy gain, which drives the AFP-ice association. The exposed nonpolar accessible surface area (ASA) is used as a scale of hydrophobicity. The nonpolar ASA values were calculated for the IBSs (including the loop IBS and the sheet IBS) of *Tis*AFP8, *Tis*AFP6 and three other homologs by the program VADAR [129]. The nonpolar ASA

of the putative IBS of *Tis*AFP8 is 2515 Å^2, which is 13% higher than that of *Tis*AFP6 (2231 Å^2) (Table 2.4). The nonpolar ASA values for hyperactive *Col*AFP, *Ff*AFP and the moderately active *Le*AFP were 2161, 2212 and 2157 Å^2, respectively, which is comparable with that of *Tis*AFP6. Taking into consideration the extremely high sequence and structural similarities between *Tis*AFP8 and *Tis*AFP6, the difference in the hydrophobicity of their IBSs likely explains the distinct difference in antifreeze activity between these two isoforms. Furthermore, the IBS of *Tis*AFP8, with higher surface complementarity to ice, seems to organize water molecules in a more ordered structure. These bound waters can form a hydrogen-bond network with a similar arrangement to ice lattice, and also anchor the protein with a high affinity to ice surface by merging with the quasi-liquid layer. Therefore, *Tis*AFP8 is capable of adsorbing to multiple ice planes and halting ice growth within a broader TH range. In conclusion, the potent antifreeze activity of *Tis*AFP8, a hyperactive isoform, may be explained by the hydrophobic patch formed by Pro^{38}-Ala^{39}-Ala^{40}-Phe^{43}-Ala^{20}-Ala^{212} in the loop IBS and better shape complementarity with the ice surface when compared with that of *Tis*AFP6. Moreover, the bulky Phe^{43} may render *Tis*AFP8 more active than *Tis*AFP6 via anchoring the AFP to the ice surface.

2.5.7 Biological implications

Snow mold fungi are psychrophilic plant pathogens that tolerate severe winter and proliferate on their hosts under snow cover [130]. During the active season for snow mold, the aqueous environment is required to serve as a soluble nutrient for growing mycelia [131, 132]. Therefore, *T. ishikariensis* has evolved to secrete AFPs to inhibit extracellular ice formation, which contributes to survival at subzero temperatures. Despite the hyperactivity of *Tis*AFP8 identified in the present study, the TH activity of *Tis*AFP purified from the mycelial culture is comparable to moderately active AFPs, suggesting a low percentage of *Tis*AFP8 in the isoform mixture.

Table 2.4 Comparison of exposed nonpolar ASA.

Protein	Exposed nonpolar ASA of IBS ($Å^2$)
*Tis*AFP8	2515
*Tis*AFP6	2231
*Col*AFP	2161
*Ff*AFP	2212
*Le*AFP	2157

Furthermore, the TH of *Tis*AFP8 was found to be dependent on the pH condition of the solution [105]. Here we hypothesize that the association of multiple AFP isoforms with a variety of IBS residues and antifreeze activity supports *T. ishikariensis* to thrive in various habitats in cold regions.

Currently, a distinct class of AFPs, comprising homologous AFPs to *Tis*AFP, was identified from various microorganisms, including fungi, diatoms and bacteria, which encounter extreme cold environments. Raymond *et al*. found that four basidiomycetous mushrooms (shiitake, enoki, king oyster and shimeji) exhibited ice-binding activity after cold acclimation [61]. On the other hand, *Tis*AFP and its homologs share approximately 40–50% amino acid sequence identity. However, the IBS of the AFP family possesses sequence variation and lacks regularly arrayed ice-binding residues, which are present in other known AFPs. Conclusively, microbial AFPs could spread widely to various species to exhibit a wide variance in their amino acid sequence and antifreeze activity, preserving an overall structure with a β-helical domain. Our research provides a structural basis for understanding that a slight amino acid sequence discrepancy on the IBS can give rise to enhanced hydrophobicity, which improves significantly the antifreeze activity. Cold-adapted microorganisms have been shown to produce extracellular polymeric substances, mainly polysaccharides and proteins [132, 133], which may depress the freezing point and inhibit extracellular ice formation [134]. It is presumed that AFPs are associated with the extracellular polymeric substance matrix to exert sufficient antifreeze activity. As for the wide distribution of cold-adapted microorganisms, ice crystal morphology and growth pattern are likely to be strongly influenced by their habitat. The highly varied IBSs, therefore, allow microbial AFPs to recognize ice crystals in a different manner, fulfilling the requirements of survival under various environments at the sub-zero temperature.

2.6 Supplemental data

2.6.1 pH dependence study of *Tis*AFP8

Materials and methods

Effect of pH on TH activity and ice crystal morphology was examined. The antifreeze activity of *Tis*AFP8 was measured in the presence of 25 mM buffer solution at pH values ranging from 3 to 10 to assess its stability at different pH. The final concentration of *Tis*AFP8 is 50 μM. Buffer used were glycine-HCl pH 3.0, acetate-NaOH pH 4.0, acetate-NaOH pH 5.0, MES-NaOH pH 6.0, HEPES-NaOH pH 7.0, ammonium bicarbonate pH 7.9, Tris-HCl pH 9.0 and glycine-NaOH pH 10.0. TH measurements for each pH condition were repeated at least three times. Effect of pH on ice crystal morphology was recorded by a CCD camera.

Results

Figure S2.1 shows the pH-dependence of the TH values examined for recombinant *Tis*AFP8 wild type. As shown, *Tis*AFP8 wild type exhibited greatly fluctuated TH activities with pH changes. During the examined pH range, the TH activity of *Tis*AFP8 wild type was maximized at pH 10 (1.2 ºC) and minimized at pH 4 (0.56 ºC) at a concentration of 50 μM. Besides, in the presence of *Tis*AFP8 wild type, the change of pH conditions did not result in changes of ice crystal morphology and burst pattern. Xiao *et al*. previously examined the pH dependence of TH activities of *Tis*AFP8 wild type at a pH range of 2–8, where more alkaline conditions had not been experimented [105]. Their results showed a maximum TH activity of *Tis*AFP8 wild type at pH 5 and a minimum TH value at pH 2. Our results in acidic conditions also showed that the TH activity of *Tis*AFP8 wild type was maximized at pH 5 (0.9 ºC), which is in consistent with the previous result of Xiao *et al*.

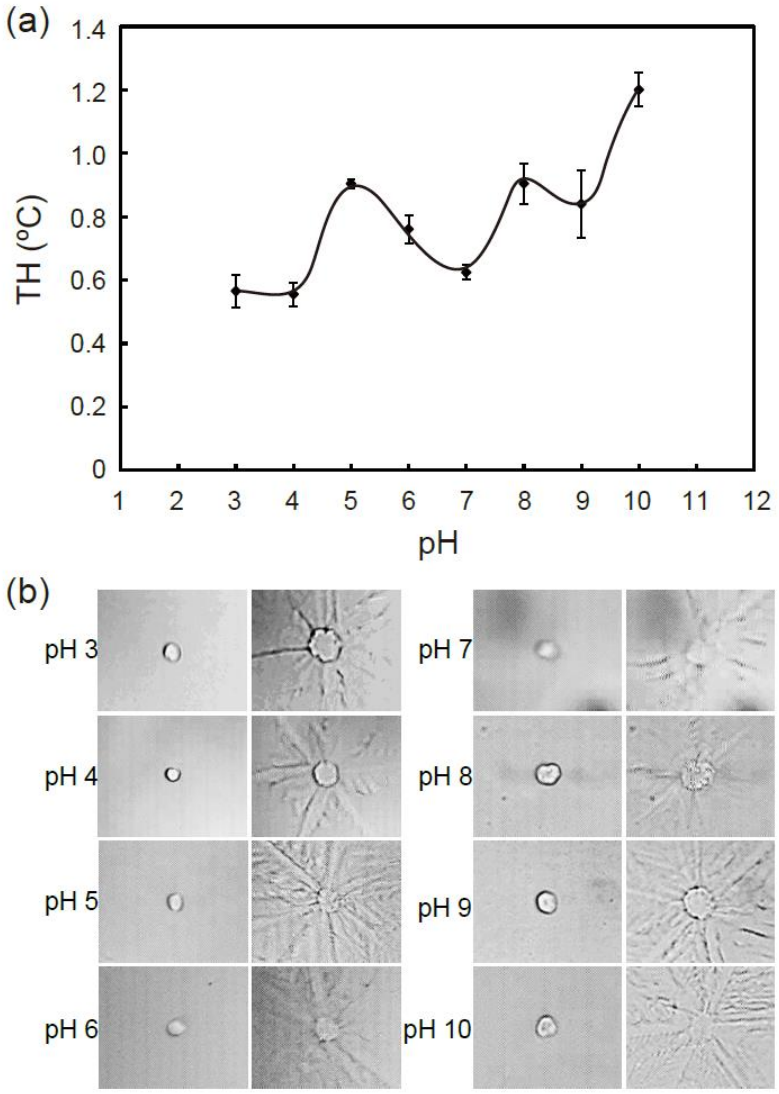

Figure S2.13 Effect of pH on TH activity and ice crystal morphology of *Tis*AFP8.

(a) *Tis*AFP8 samples of a fixed concentration (50 μM) were assayed at pH values ranging from 2 to 10. Standard deviation for the *Tis*AFP8 samples was based on triplicate measurements. (b) Ice crystals burst in the presence of *Tis*AFP8 at pH conditions ranging from 2 to 10.

Biological implications of the pH dependence

The influence of pH on the activities of several intracellular AFPs (type III AFP [135], type IV AFP [136], *Ri*AFP [137], *Cf*AFP [138]) was studied by several groups. For those AFPs, which are secreted to extracellular space (like microbial AFPs), little was known about their TH activity dependence on pH. The TH activity of *Tis*AFP8 was easily affected by pH conditions. In contrast, antifreeze activity of *Tis*AFP6 was unchanged from pH 2 to 10 (unpublished data, performed by Hanada, Y.). It indicates that the protein fold is stable over a wider pH range than that of *Tis*AFP8. It is hypothesized that *T. ishikariensis* produce several AFP isoforms to reply to and survive in inconstant, changeable extracellular environments.

2.6.2 Ice recrystallization inhibition (IRI) assay

Materials and methods

The IRI assay was performed by using sucrose sandwich method [139]. *Tis*AFP8 wild type was dissolved to 0.01–1.00 mg/ml in 25 mM ammonium bicarbonate (pH 7.9) containing 30 % sucrose. 1 μl of the sample was sandwiched between two round glass cover slips and immediately frozen entirely at ∼−20 °C using the same equipment for TH measurement. The samples were then warmed up to −6 °C and incubated for 1 h, which is near the temperature zone of maximum ice crystal formation [140]. Microscope images were captured using a CCD camera.

Results

The IRI activity of *Tis*AFP8 was measured and is shown in Fig. S2.2. After 1 h of incubation, the ice crystals formed in the control solution showed significant growth. In contrast, *Tis*AFP8 inhibited small ice crystals to gather together, keeping the sizes small. Even at a concentration

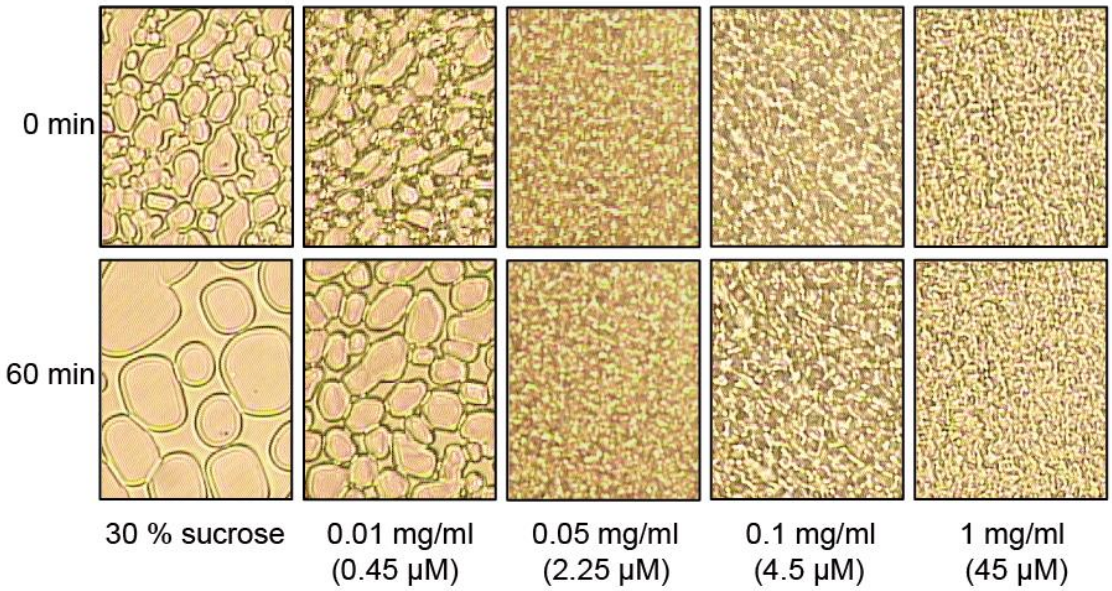

Figure S2.14 Inhibition of ice recrystallization by *Tis*AFP8.

The first lance shows IRI assays using 30 % sucrose solution as the negative control. The remaining lanes show the IRI activities of *Tis*AFP8 at four different concentrations (0.45 μM, 2.25 μM, 4.5 μM, 45 μM).

of 0.45 μM, *Tis*AFP8 showed clear IRI activity, where the recrystallization of ice crystals was inhibited and the sizes of ice crystals were obviously much smaller than those in 30 % sucrose solution. Such a capability was enhanced with increasing concentrations of *Tis*AFP8 solutions. After 1 h of incubation, the growth of the ice crystals, which formed in those solutions with *Tis*AFP8 concentrations of 2.25, 4.5 and 45μM, was completely inhibited. Therefore, *Tis*AFP8 has strong TH activity as well as effective IRI activity.

2.7 Acknowledgements

The experiments using synchrotron radiation were performed with the approval of the Photon Factory Program Advisory Committee (proposal number 2013G183). The authors thank Dr. Yoshikazu Tanaka for the practical advice about the CD spectroscopy.

Chapter 3 General discussion

3.1 *Tis*AFPs adsorb to ice surface through the anchored clathrate water mechanism

Early researches suggested that AFPs directly adsorb to the surface of ice crystals through hydrogen bonding [83-85] or hydrophobic effect [33, 45] as the main driving force. In this case, surface hydration waters on the IBS of an AFP have to be released into the bulk solvent and the IBS should make an intimate fit to the ice planes to which it binds. However, more and more recent studies presented both modelling [91, 110, 141,] and experimental [32, 41, 49, 52] evidence that ice-like waters on the IBS help the adsorption of AFPs onto ice surface. The anchored clathrate water (ACW) mechanism was first proposed by Garnham *et al*. in recent years [32]. In this mechanism, it was hypothesized that the ice-like waters are organized by the IBS through the hydrophobic effect and anchored to the protein via hydrogen bonds. These anchored waters then match the quasi-liquid layer of ice and allow an AFP to bind ice.

However, since the identification of an IBS through mutagenesis studies, its flat and hydrophobic nature results in the tendency that AFPs form protein-protein contact via IBSs during crystallization [127]. The same phenomenon was observed in the crystal packing of *Tis*AFP8, where the IBSs were packed face to face with part exposed to solvent (Fig. 5.1). In this thesis, I superposed the surface hydration water molecules on the IBS of *Tis*AFP8 with ice lattice waters, in order to obtain the water pattern on the IBS. The results suggested that surface waters on the IBS (including the β-sheet and loop region of the IBS) were organized into an ice-like pattern, although they were not so perfectly arrayed as seen in hyperactive bacterial *Mp*AFP [32] and insect *Ri*AFP [52]. Besides, these bound waters seemed to be divided into two groups, one located in the β-sheet IBS and another one located in the loop IBS. Each group of water molecules may separately anchor the protein to ice. Therefore, the ACW mechanism can

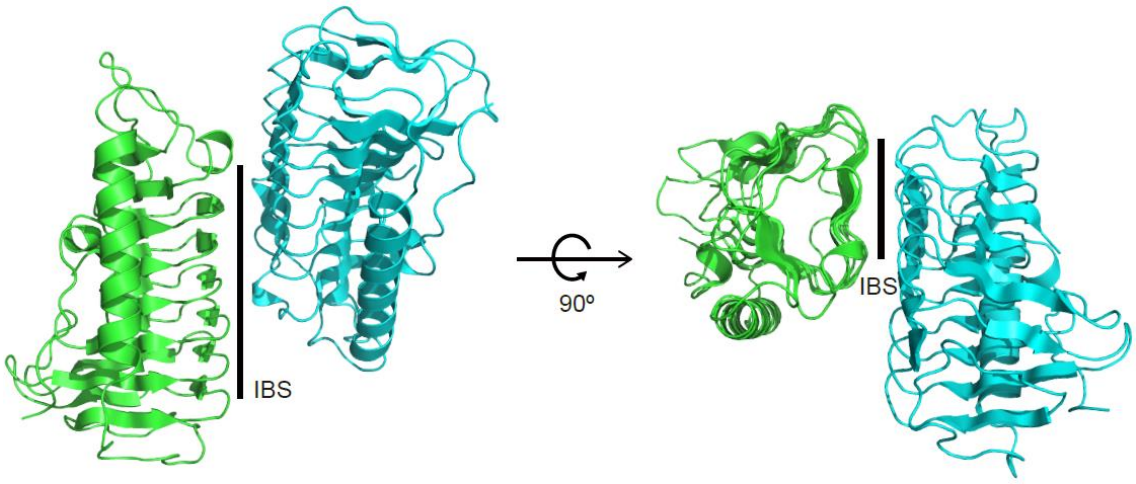

Figure 3.1 Crystal packing of TisAFP8 observed in the asymmetric unit of the crystal.

The IBSs of the two molecules in the asymmetric unit were involved in crystal packing, with part exposed to solvent.

also be applied to microbial *Tis*AFP8.

Although not examined, surface waters on the IBS of *Tis*AFP6, whose arrangement was highly similar with that of *Tis*AFP8, might possess the ice-like character. Hyperactive *Tis*AFP8 is able to order water molecules to allow it to bind to multiple planes of ice, including the basal planes. Moderately active *Tis*AFP6 orders water molecules to enable it to adsorb to the prism planes, as well as the basal planes (with a longer time, several hours). And the slight difference between the water arrangements of *Tis*AFP8 and *Tis*AFP6 may explain the above antifreeze activity differences.

In conclusion, the evaluation about the surface water molecule pattern performed in this thesis provides additional support for the ACW mechanism by which AFPs bind to ice.

3.2 Hyperactive *Tis*AFP8 Vs moderately active *Tis*AFP6

Homologous AFPs to *Tis*AFP6 have been identified from fungus, diatom, yeast and bacteria. They form a unique AFP family and have a growing number of homologs which share ~40–50 % sequence identity. Crystal structures of *Tis*AFP6 and *Le*AFP were the first determined structures within this AFP family, both of which were identified to be moderately active AFP [72, 73]. It is interesting to find that *Ff*AFP and *Col*AFP from this family exhibit hyperactive antifreeze activity [74, 75]. The IBSs of this AFP family share a common feature that they are complex and lack repetitive ice-binding motifs which can be seen in other hyperactive insect and bacteria AFPs. Attempts have been made to propose a universal mechanism for the concomitant of hyperactive and moderately active AFPs in one AFP family, as well as the hyperactivity of microbial AFPs without regular IBSs. Our understanding about the above doubts, although

advanced, remains incomplete.

As described in this thesis, *Tis*AFP8 and *Tis*AFP6 exhibited remarkably different antifreeze activities in spite of their extremely high sequence identity. In the present study, I first constructed the expression system of *Tis*AFP8 and mutants in the yeast *Pichia pastoris*, purified and characterized their antifreeze activities. Nevertheless, the purity of recombinant *Tis*AFP8 and mutants was low. And some contaminants from culture media could not be removed by purification, which influenced the antifreeze activities of the proteins. As a result, I performed the above experiments in *E. coli* expression system again and found expressed proteins in this system can be easily purified. On this basis, crystallization and structure determination of *Tis*AFP8 were carried out.

By comparing with *Tis*AFP6, the mutagenesis studies and ice-docking studies reported in this thesis provides a structural basis for understanding the antifreeze mechanism of *Tis*AFPs and new insights into the reasons for the higher antifreeze activity of *Tis*AFP8 compared with *Tis*AFP6. It is proposed that the difference in TH activity between *Tis*AFP8 and *Tis*AFP6 may arise from the more hydrophobic amino-acid composition of the IBS of *Tis*AFP8 and its better shape complementarity with ice.

3.3 Biological implications

The ambient environment under snow cover remains near 0 ºC, resulting in more freeze-thaw cycles [142]. Ordinary phytopathogenic fungi survive the severe winter in the form of spores and sclerotia and attack their host plants in the following spring. Opposite to ordinary phytopathogenic fungi, snow molds develop mycelia in winter [132]. Although *Typhula*

ishikariensis can grow at temperatures below -5 ºC, the growth of mycelia is arrested in a frozen environment. Therefore, it is necessary for *T. ishikariensis* to develop freezing resistance strategies under dark, humid and temperature fluctuated environment during winter. *T. ishikariensis* adapts to harsh winters by producing *Tis*AFPs to extracellular space. Given that *Tis*AFPs show distinct activities (concentration-dependence, pH-dependence and so on), they allow *T. ishikariensis* to adapt to temperature fluctuated ambient environment and thrive in diverse habitats in cold areas. It was also reported that *T. ishikariensis* produces extracellular polysaccharides, covering mycelia [132, 143]. It is presumed that AFPs are concentrated in the polysaccharide matrix, therefore inhibiting the diffusion of AFPs and sufficiently preserving surrounding aqueous environment [143].

Acknowledgements

In the first place, I would like to sincerely thank my supervisor, Dr. Hidemasa Kondo, for his kind, patient and considerate advice, discussion and technical guidance. I have learned a tremendous amount from him and I would be forever grateful for what he has taught me. I would also like to thank Dr. Sakae Tsuda for accepting me as a graduate student in his great laboratory. Dr. Tsuda is a very supporting professor and excellent scientist. It has been my pleasure to work and study under his guidance.

I am also very thankful to everybody in the Tsuda lab, past and present. Especially, I would like to thank Dr. Yuichi Hanada and Dr. Nan Xiao for their kind advice and guidance both in daily life and research in Sapporo. I would like to thank Dr. Mami Sakashita, Dr. Yoshiyuki Nishimiya and Dr. Tamotsu Hoshino for their helpful technical assistance and guidance. I would also like to thank Mrs. Ai Miura for her fundamental supports for years. I am also very grateful to all students in this lab for their accompanying, supporting and encouraging every day.

I am grateful for the financial support afforded me by Chinese Government Scholarship and Iwatani Naoji Foundation for the international students.

Finally, my thanks would go to my beloved family for their loving considerations and great confidence in me all through these years. I also owe my sincere gratitude to my friends both in China and in Sapporo who gave me their help and time in listening to me and helping me work out my problems during my daily life in Japan. And I would like to thank my hamsters, Kintarou and Momotarou, for always being lovely.

References

1. DeVries, A. L. and Wohlschlag, D. E. (1969) Freezing resistance in some Antarctic fishes. *Science* **163**, 1073-1075.
2. Guo, S., Garnham, C. P., Whitney, J. C., Graham, L. A. and Davies, P. L. (2012) Re-evaluation of a bacterial antifreeze protein as an adhesin with ice-binding activity. *PLoS ONE* **7**, e48805.
3. Clarke, C.J., Buckley, S.L. and Lindner, N. (2002) Ice structuring proteins - a new name for antifreeze proteins. *Cryo Letters* **23**, 89-92.
4. Lindow, S. E., Arny, D. C. and Upper, C. D. (1982) Bacterial ice nucleation: a factor in frost injury to plants. *Plant Physiol*. **70**, 1084-1089.
5. Warren, G. and Wolber, P. (1991) Molecular aspects of microbial ice nucleation. *Mol. Microbiol.* **5**, 239-243.
6. Govindarajan, A. G. and Lindow, S. E. (1988) Size of bacterial ice-nucleation sites measured in situ by radiation inactivation analysis. *Proc. Natl. Acad. Sci. U.S.A.* **85**, 1334-1338.
7. Venketesh, S. and Dayananda, C. (2008) Properties, potentials, and prospects of antifreeze proteins. *Crit. Rev. Biotechnol.* **28**, 57-82.
8. Regand, A., and Goff, H. D. (2006) Ice recrystallization inhibition in ice cream as affected by ice structuring proteins from winter wheat grass. *J. Dairy Sci.* **89**, 49-57.
9. Hassas-Roudsari, M. and Goff, H. D. (2012) Ice structuring proteins from plants: Mechanism of action and food application. *Food Res. Int.* **46**, 425-436.
10. Kamijima, T., Sakashita, M., Miura, A., Nishimiya, Y. and Tsuda, S. (2013) Antifreeze

protein prolongs the life-time of insulinoma cells during hypothermic preservation. *PLoS ONE* **8**, e73643.

11. Amir, G., Rubinsky, B., Horowitz, L., Miller, L., Leor, J., Kassif, Y., Mishaly, D., Smolinsky, A. K. and Lavee, J. (2004) Prolonged 24-hour subzero preservation of heterotopically transplanted rat hearts using antifreeze proteins derived from arctic fish. *Ann. Thorac. Surg*. **77**, 1648-1655.
12. Pham, L., Dahiya, R. and Rubinsky, B. (1999. An in vivo study of antifreeze protein adjuvant cryosurgery. *Cryobiology*, **38**, 169-175.
13. Huang, T., Nicodemus, J., Zarka, D. G., Thomashow, M. F., Wisniewski, M. and Duman, J. G. (2002) Expression of an insect (*Dendroides canadensis*) antifreeze protein in Arabidopsis thaliana results in a decrease in plant freezing temperature. *Plant Mol. Biol*. **50**, 333-344.
14. Esser-Kahn, A. P., Trang, V. and Francis, M. B. (2010) Incorporation of antifreeze proteins into polymer coatings using site-selective bioconjugation. *J. Am. Chem. Soc*. 132, 13264–13269.
15. Gordienko, R., Ohno, H., Singh, V. K., Jia, Z., Ripmeester, J. A. and Walker, V. K. (2010) Towards a green hydrate inhibitor: imaging antifreeze proteins on clathrates. *PLoS ONE* **5**, e8953.
16. Ohno, H., Susilo, R., Gordienko, R., Ripmeester, J. and Walker, V. K. (2010) Interaction of antifreeze proteins with hydrocarbon hydrates. *Chem. Eur. J.* **16**, 10409-10417.
17. Bindslev-Jensen, C., Sten, E., Earl, L. K., Crevel, R. W. R., Bindslev-Jensen, U., Hansen, T. K., Skov, P. S. and Poulsen, L. K. (2003) Assessment of the potential allergenicity of ice structuring protein type III HPLC 12 using the FAO/WHO 2001 decision tree for novel foods. *Food Chem. Toxicol.* **41**, 81-87.

18. Meldolesi, A. (2009) News: GM fish ice cream. *Nature Biotechnol.* **27**, 682.

19. Tyshenko, M. G. and Walker, V. K. (2004) Hyperactive spruce budworm antifreeze protein expression in transgenic *Drosophila* does not confer cold shock tolerance. *Cryobiology* **49**, 28-36.

20. Raymond, J. A. and DeVries, A. L. (1977) Adsorption inhibition as a mechanism of freeze resistance in polar fishes. *Proc. Natl. Acad. Sci. U.S.A.* **74**, 2589-2593.

21. Knight, C. A., Cheng, C. C. and DeVries, A. L. (1991) Adsorption of α-helical antifreeze peptides on specific ice crystal surface planes. *Biophys. J.* **59**, 409-418.

22. Scotter, A. J., Marshall, C. B., Graham, L. A., Gilbert, J. A., Garnham, C. P. and Davies, P. L. (2006) The basis for hyperactivity of antifreeze proteins. *Cryobiology* **53**, 229-239.

23. Bar-Dolev, M., Celik, Y., Wettlaufer, J. S., Davies, P. L. and Braslavsky, I. (2012) New insights into ice growth and melting modifications by antifreeze proteins. *J. R. Soc. Interface* **9**, 3249-3259.

24. Knight, C.A., Wen, D. and Laursen, R.A. (1995) Nonequilibrium antifreeze peptides and the recrystallization of ice. *Cryobiology* **32**, 23-34.

25. Jia, Z. and Davies, P. L. (2002) Antifreeze proteins: an unusual receptor–ligand interaction. *Trends Biochem. Sci.* **27**, 101-106.

26. Yu, S. O., Brown, A., Middleton, A. J., Tomczak, M. M., Walker, V. K. and Davies, P. L. (2010) Ice restructuring inhibition activities in antifreeze proteins with distinct differences in thermal hysteresis. *Cryobiology* **61**, 327-334.

27. Worrall, D., Elias, L., Ashford, D., Smallwood, M., Sidebottom, C., Lillford, P., Telford, J., Holt, C. and Bowles, D. (1998) A carrot leucine-rich-repeat protein that inhibits ice recrystallization. *Science* **282**, 115-117.

28. Sidebottom, C., Buckley, S., Pudney, P., Twigg, S., Jarman, C., Holt, C., Telford, J.,

MaArthur, A., Worrall, D., Hubbard, R. and Lillford, P. (2000) Heat-stable antifreeze protein from grass. *Nature* **406**, 256.

29. Maki, L. R., Galyan, E. L., Chang-Chien, M.-M. and Caldwell, D. R. (1974) Ice nucleation induced by *Pseudomonas syringae*. *Appl. Microbiol.* **28**, 456-459.

30. Graether, S. P. and Jia, Z. (2001) Modeling *Pseudomonas syringae* ice-nucleation protein as a β-helical protein. *Biophys. J.* **80**, 1169-1173.

31. Garnham, C. P., Campbell, R. L., Walker, V. K. and Davies, P. L. (2011) Novel dimeric β-helical model of an ice nucleation protein with bridged active sites. *BMC Struct. Biol.* **11**, 36.

32. Garnham, C. P., Campbell, R. L. and Davies, P. L. (2011) Anchored clathrate waters bind antifreeze proteins to ice. *Proc. Natl. Acad. Sci. U.S.A.* **108**, 7363-7367.

33. Garnham, C. P., Gilbert, J. A., Hartman, C. P., Campbell, R. L., Laybourn-Parry, J. and Davies, P. L. (2008) A Ca^{2+}-dependent bacterial antifreeze protein domain has a novel β-helical ice-binding fold. *Biochem. J.* **411**, 171-180.

34. Gilbert, J. A., Davies, P. L. and Laybourn-Parry, J. (2005) A hyperactive, Ca^{2+}-dependent antifreeze protein in an Antarctic bacterium. *FEMS Microbiol. Lett.* **245**, 67-72.

35. Vance, T. D., Olijve, L. L., Campbell, R. L., Voets, I. K., Davies, P. L. and Guo, S. (2014) Ca^{2+}-stabilized adhesin helps an Antarctic bacterium reach out and bind ice. *Biosci. Rep.* **34**, e00121.

36. Chen, L., DeVries, A. L. and Cheng, C.-H. C. (1997) Convergent evolution of antifreeze glycoproteins in Antarctic notothenioid fish and Arctic cod. *Proc. Natl. Acad. Sci. U.S.A.* **94**, 3817-3822.

37. Logsdon, J. M. and Doolittle, W. F. (1997) Origin of antifreeze protein genes: a cool tale in molecular evolution. *Proc. Natl. Acad. Sci. U.S.A.* **94**, 3485-3487.

38. Yang, D. S., Sax, M., Chakrabartty, A. and Hew, C. L. (1988) Crystal structure of an antifreeze polypeptide and its mechanistic implications. *Nature* **333**, 232-237.

39. Sicheri, F., and Yang, D. S. (1995) Ice-binding structure and mechanism of an antifreeze protein from winter flounder. *Nature* **375**, 427-431.

40. Marshall, C. B., Fletcher, G. L. and Davies, P. L. (2004) Hyperactive antifreeze protein in a fish. *Nature* **429**, 153.

41. Sun, T., Lin, F. H., Campbell, R. L., Allingham, J. S. and Davies, P. L. (2014) An antifreeze protein folds with an interior network of more than 400 semi-clathrate waters. *Science* **343**, 795-798.

42. Gronwald, W., Loewen, M. C., Lix, B., Daugulis, A. J., Sönnichsen, F. D., Davies, P. L. and Sykes, B. D. (1998) The solution structure of type II antifreeze protein reveals a new member of the lectin family. *Biochemistry* **37**, 4712-4721.

43. Nishimiya, Y., Kondo, H., Takamichi, M., Sugimoto, H., Suzuki, M., Miura, A. and Tsuda, S. (2008) Crystal structure and mutational analysis of Ca^{2+}-independent type II antifreeze protein from longsnout poacher, *Brachyopsis rostratus*. *J. Mol. Biol.* **382**, 734-746.

44. Sönnichsen, F. D., Sykes, B. D., Chao, H. and Davies, P. L. (1993) The nonhelical structure of antifreeze protein type III. *Science* **259**, 1154-1157.

45. Sönnichsen, F. D., DeLuca, C. I., Davies, P. L. and Sykes, B. D. (1996) Refined solution structure of type III antifreeze protein: hydrophobic groups may be involved in the energetics of the protein–ice interaction. *Structure* **4**, 1325-1337.

46. Jia, Z., DeLuca, C. I., Chao, H. and Davies, P. L. (1996) Structural basis for the binding of a globular antifreeze protein to ice. *Nature* **384**, 285-288.

47. Deng, G., Andrews, D. W. and Laursen, R. A. (1997) Amino acid sequence of a new type of antifreeze protein, from the longhorn sculpin *Myoxocephalus octodecimspinosis*. *FEBS*

Lett. **402**, 17-20.

48. Cheng, C.-H. C. and Chen, L. (1999) Evolution of an antifreeze glycoprotein. *Nature* **401**, 443-444.

49. Liou, Y. C., Tocilj, A., Davies, P. L. and Jia, Z. (2000) Mimicry of ice structure by surface hydroxyls and water of a β-helix antifreeze protein. *Nature* **406**, 322-324.

50. Graether, S. P., Kuiper, M. J., Gagné, S. M., Walker, V. K., Jia, Z., Sykes, B. D. and Davies, P. L. (2000) β-helix structure and ice-binding properties of a hyperactive antifreeze protein from an insect. *Nature* **406**, 325-328.

51. Zachariassen, K. E., Li, N. G., Laugsand, A. E., Kristiansen, E. and Pedersen, S. A. (2008) Is the strategy for cold hardiness in insects determined by their water balance? A study on two closely related families of beetles: Cerambycidae and Chrysomelidae. *J. Comp. Physiol. B* **178**, 977-984.

52. Hakim, A., Nguyen, J. B., Basu, K., Zhu, D. F., Thakral, D., Davies, P. L., Isaacs, F. J., Modis, Y. and Meng, W. (2013) Crystal structure of an insect antifreeze protein and its implications for ice binding. *J. Biol. Chem.* **288**, 12295-12304.

53. Graham, L. A. and Davies, P. L. (2005) Glycine-rich antifreeze proteins from snow fleas. *Science* **310**, 461.

54. Pentelute, B. L., Gates, Z. P., Tereshko, V., Dashnau, J. L., Vanderkooi, J. M., Kossiakoff, A. A. and Kent, S. B. (2008) X-ray structure of snow flea antifreeze protein determined by racemic crystallization of synthetic protein enantiomers. *J. Am. Chem. Soc.* **130**, 9695-9701.

55. Mok, Y. F., Lin, F. H., Graham, L. A., Celik, Y., Braslavsky, I. and Davies, P. L. (2010) Structural basis for the superior activity of the large isoform of snow flea antifreeze protein. *Biochemistry* **49**, 2593-2603.

56. Basu, K., Graham, L. A., Campbell, R. L. and Davies, P. L. (2015) Flies expand the repertoire of protein structures that bind ice. *Proc. Natl. Acad. Sci. U.S.A.* **112**, 737-742.

57. Basu, K., Wasserman, S. S., Jeronimo, P. S., Graham, L. A. and Davies, P. L. (2016) Intermediate activity of midge antifreeze protein is due to a tyrosine-rich ice-binding site and atypical ice plane affinity. *FEBS J.* **283**, 1504-1515.

58. Middleton, A. J., Marshall, C. B., Faucher, F., Bar-Dolev, M., Braslavsky, I., Campbell, R. L., Walker, V. K. and Davies, P. L. (2012) Antifreeze protein from freeze-tolerant grass has a beta-roll fold with an irregularly structured ice-binding site. *J. Mol. Biol.* **416**, 713-724.

59. Hoshino, T., Kiriaki, M., Ohgiya, S., Fujiwara, M., Kondo, H., Nishimiya, Y., Yumoto, I. and Tsuda, S. (2003) Antifreeze proteins from snow mold fungi. *Can. J. Bot.* **81**, 1175-1181.

60. Lee, J. K., Park, K. S., Park, S., Park, H., Song, Y. H., Kang, S. H. and Kim, H. J. (2010) An extracellular ice-binding glycoprotein from an Arctic psychrophilic yeast. *Cryobiology* **60**, 222-228.

61. Raymond, J. A. and Janech, M. G. (2009) Ice-binding proteins from enoki and shiitake mushrooms. *Cryobiology* **58**, 151-156.

62. Janech, M. G., Krell, A., Mock, T., Kang, J. S. and Raymond, J. A. (2006) Ice-binding proteins from sea ice diatoms (*Bacillariophyceae*). *J. Phycol.* **42**, 410-416.

63. Gwak, I. G., sic Jung, W., Kim, H. J., Kang, S. H. and Jin, E. (2010) Antifreeze protein in Antarctic marine diatom, *Chaetoceros neogracile*. *Mar. Biotechnol.* **12**, 630-639.

64. Raymond, J. A. and Morgan-Kiss, R. (2013). Separate origins of ice-binding proteins in Antarctic *Chlamydomonas* species. *PLoS ONE* **8**, e59186.

65. Jung, W., Gwak, Y., Davies, P. L., Kim, H. J. and Jin, E. (2014) Isolation and

characterization of antifreeze proteins from the Antarctic marine microalga *Pyramimonas gelidicola*. *Mar. Biotechnol.* **16**, 502-512.

66. Raymond, J. A., Fritsen, C. and Shen, K. (2007) An ice-binding protein from an Antarctic sea ice bacterium. *FEMS Microbiol. Ecol.* **61**, 214-221.

67. Raymond, J. A., Christner, B. C. and Schuster, S. C. (2008) A bacterial ice-binding protein from the Vostok ice core. *Extremophiles* **12**, 713-717.

68. Do, H., Lee, J. H., Lee, S. G. and Kim, H. J. (2012) Crystallization and preliminary X-ray crystallographic analysis of an ice-binding protein (FfIBP) from *Flavobacterium frigoris* PS1. *Acta Crystallogr., Sect. F: Struct. Biol. Cryst. Commun.* **68**, 806-809.

69. Kiko, R. (2010) Acquisition of freeze protection in a sea-ice crustacean through horizontal gene transfer? *Polar Biol.* **33**, 543-556.

70. Raymond, J. A. and Kim, H. J. (2012) Possible role of horizontal gene transfer in the colonization of sea ice by algae. *PLoS ONE* **7**, e35968.

71. Bayer-Giraldi, M., Uhlig, C., John, U., Mock, T. and Valentin, K. (2010) Antifreeze proteins in polar sea ice diatoms: diversity and gene expression in the genus *Fragilariopsis*. *Environ. Microbiol.* **12**, 1041-1052.

72. Kondo, H., Hanada, Y., Sugimoto, H., Hoshino, T., Garnham, C. P., Davies, P. L. and Tsuda, S. (2012) Ice-binding site of snow mold fungus antifreeze protein deviates from structural regularity and high conservation. *Proc. Natl. Acad. Sci. U.S.A.* **109**, 9360-9365.

73. Lee, J. H., Park, A. K., Do, H., Park, K. S., Moh, S. H., Chi, Y. M. and Kim, H. J. (2012) Structural basis for antifreeze activity of ice-binding protein from arctic yeast. *J. Biol. Chem.* **287**, 11460-11468.

74. Do, H., Kim, S. J., Kim, H. J. and Lee, J. H. (2014) Structure-based characterization and antifreeze properties of a hyperactive ice-binding protein from the Antarctic bacterium

Flavobacterium frigoris PS1. *Acta Crystallogr., Sect. D: Biol. Crystallogr.* **70**, 1061-1073.

75. Hanada, Y., Nishimiya, Y., Miura, A., Tsuda, S. and Kondo, H. (2014) Hyperactive antifreeze protein from an Antarctic sea ice bacterium Colwellia sp. has a compound ice-binding site without repetitive sequences. *FEBS J.* **281**, 3576-3590.

76. Raymond, J. A., Janech, M. G. and Fritsen, C. H. (2009) Novel ice-binding proteins from a psychrophilic Antarctic alga (*Chlamydomonadaceae*, *Chlorophyceae*). *J. Phycol.* **45**, 130-136.

77. Petrenko, V. F. (1993) Structure of Ordinary Ice I_h. Part 1: Ideal Structure of Ice. Report No. 93-25, U.S. Army Corps of Engineers, Cold Regions Research and Engineering Laboratory, Hanover, NH.

78. Nada, H. and Furukawa, Y. (2005) Anisotropy in growth kinetics at interfaces between proton-disordered hexagonal ice and water: A molecular dynamics study using the six-site model of H_2O. *J. Cryst. Growth* **283**, 242-256.

79. Garnham, C. P., Natarajan, A., Middleton, A. J., Kuiper, M. J., Braslavsky, I. and Davies, P. L. (2010) Compound ice-binding site of an antifreeze protein revealed by mutagenesis and fluorescent tagging. *Biochemistry* **49**, 9063-9071.

80. Basu, K., Garnham, C. P., Nishimiya, Y., Tsuda, S., Braslavsky, I. and Davies, P. (2014) Determining the ice-binding planes of antifreeze proteins by fluorescence-based ice plane affinity. *J. Vis. Exp.* **83**, e51185.

81. Antson, A. A., Smith, D. J., Roper, D. I., Lewis, S., Caves, L. S., Verma, C. S., Buckley, S. L., Lillford, P. L. and Hubbard, R. E. (2001) Understanding the mechanism of ice binding by type III antifreeze proteins. *J. Mol. Biol.* **305**, 875-889.

82. Pertaya, N., Marshall, C. B., Celik, Y., Davies, P. L. and Braslavsky, I. (2008) Direct visualization of spruce budworm antifreeze protein interacting with ice crystals: basal

plane affinity confers hyperactivity. *Biophys. J.* **95**, 333-341.

83. DeVries, A. L. (1971) Glycoproteins as biological antifreeze agents in Antarctic fishes. *Science* **172**, 1152-1155.

84. DeVries, A. L. and Lin, Y. (1977) Structure of a peptide antifreeze and mechanism of adsorption to ice. *Biochim. Biophys. Acta* **495**, 388-392.

85. Knight, C. A., Driggers, E. and DeVries, A. L. (1993) Adsorption to ice of fish antifreeze glycopeptides 7 and 8. *Biophys. J.* **64**, 252-259.

86. Chao, H., Houston, M. E., Hodges, R. S., Kay, C. M., Sykes, B. D., Loewen, M. C., Davies, P. L. and Sönnichsen, F. D. (1997) A diminished role for hydrogen bonds in antifreeze protein binding to ice. *Biochemistry* **36**, 14652-14660.

87. Haymet, A. D., Ward, L. G., Harding, M. M. and Knight, C. A. (1998) Valine substituted winter flounder 'antifreeze': preservation of ice growth hysteresis. *FEBS Lett.* **430**, 301-306.

88. Sönnichsen, F. D., Sykes, B. D. and Davies, P. L. (1995) Comparative modeling of the three-dimensional structure of type II antifreeze protein. *Protein Sci.* **4**, 460-471.

89. Leinala, E. K., Davies, P. L. and Jia, Z. (2002) Crystal structure of β-helical antifreeze protein points to a general ice binding model. *Structure* **10**, 619-627.

90. Leinala, E. K., Davies, P. L., Doucet, D., Tyshenko, M. G., Walker, V. K. and Jia, Z. (2002) A β-helical antifreeze protein isoform with increased activity. Structural and functional insights. *J. Biol. Chem.* **277**, 33349-33352.

91. Nutt, D. R. and Smith, J. C. (2008) Dual function of the hydration layer around an antifreeze protein revealed by atomistic molecular dynamics simulations. *J. Am. Chem. Soc.* **130**, 13066-13073.

92. Garnham, C. P., Nishimiya, Y., Tsuda, S. and Davies, P. L. (2012) Engineering a naturally

inactive isoform of type III antifreeze protein into one that can stop the growth of ice. *FEBS Lett.* **586**, 3876-3881.

93. Sun, T., Gauthier, S. Y., Campbell, R. L. and Davies, P. L. (2015) Revealing Surface Waters on an Antifreeze Protein by Fusion Protein Crystallography Combined with Molecular Dynamic Simulations. *J. Phys. Chem. B* **119**, 12808-12815.

94. Davies, P. L. and Hew, C. L. (1990) Biochemistry of fish antifreeze proteins. *FASEB J.* **4**, 2460-2468.

95. Duman, J. G. and DeVries, A. L. (1976) Isolation, characterization, and physical properties of protein antifreezes from the winter flounder, *Pseudopleuronectes americanus*. *Comp. Biochem. Physiol. B* **54**, 375-380.

96. Hew, C. L., Joshi, S. and Wang, N. C. (1984) Analysis of fish antifreeze polypeptides by reversed-phase high-performance liquid chromatography. *J. Chromatogr.* **296**, 213-219.

97. Li, X. M., Trinh, K. Y., Hew, C. L., Buettner, B., Baenziger, J. and Davies, P. L. (1985) Structure of an antifreeze polypeptide and its precursor from the ocean pout, *Macrozoarces americanus*. *J. Biol. Chem.* **260**, 12904-12909.

98. Hew, C. L., Wang, N. C., Joshi, S., Fletcher, G. L., Scott, G. K., Hayes, P. H., Buettner, B. and Davies, P. L. (1988) Multiple genes provide the basis for antifreeze protein diversity and dosage in the ocean pout, *Macrozoarces americanus*. *J. Biol. Chem.* **263**, 12049-12055.

99. Nishimiya, Y., Sato, R., Takamichi, M., Miura, A. and Tsuda, S. (2005) Co-operative effect of the isoforms of type III antifreeze protein expressed in Notched-fin eelpout, *Zoarces elongatus Kner*. *FEBS J.* **272**, 482-492.

100. Kumble, K. D., Demmer, J., Fish, S., Hall, C., Corrales, S., DeAth, A., Elton, C., Prestidge, R., Luxmanan, S., Marshall, C. J. and Wharton, D. A. (2008) Characterization

of a family of ice-active proteins from the ryegrass, *Lolium perenne*. *Cryobiology* **57**, 263-268.

101. Andorfer, C. A. and Duman, J. G. (2000) Isolation and characterization of cDNA clones encoding antifreeze proteins of the pyrochroid beetle *Dendroides canadensis*. *J. Insect Physiol.* **46**, 365-372.

102. Doucet, D., Tyshenko, M. G., Kuiper, M. J., Graether, S. P., Sykes, B. D., Daugulis, A. J., Davies, P. L. and Walker, V. K. (2000) Structure–function relationships in spruce budworm antifreeze protein revealed by isoform diversity. *Eur. J. Biochem.* **267**, 6082-6088.

103. Bayer-Giraldi, M., Weikusat, I., Besir, H. and Dieckmann, G. (2011) Characterization of an antifreeze protein from the polar diatom *Fragilariopsis cylindrus* and its relevance in sea ice. *Cryobiology* **63**, 210-219.

104. Wang, L. and Duman, J. G. (2005) Antifreeze proteins of the beetle *Dendroides canadensis* enhance one another's activities. *Biochemistry* **44**, 10305-10312.

105. Xiao, N., Suzuki, K., Nishimiya, Y., Kondo, H., Miura, A., Tsuda, S. and Hoshino, T. (2010) Comparison of functional properties of two fungal antifreeze proteins from *Antarctomyces psychrotrophicus* and *Typhula ishikariensis*. *FEBS J.* **277**, 394-403.

106. Knight, C. A. (2000) Structural biology: adding to the antifreeze agenda. *Nature* **406**, 249-251.

107. Griffith, M. and Ewart, K. V. (1995) Antifreeze proteins and their potential use in frozen foods. *Biotechnol. Adv.* **13**, 375-402.

108. Graham, L. A., Liou, Y. C., Walker, V. K. and Davies, P. L. (1997) Hyperactive antifreeze protein from beetles. *Nature* **388**, 727-728.

109. Graether, S. P. and Sykes, B. D. (2004) Cold survival in freeze-intolerant insects. *Eur. J.*

Biochem. **271**, 3285-3296.

110. Smolin, N. and Daggett, V. (2008) Formation of ice-like water structure on the surface of an antifreeze protein. *J. Phys. Chem. B* **112**, 6193-6202.

111. Xiao, N., Hanada, Y., Seki, H., Kondo, H., Tsuda, S. and Hoshino, T. (2014) Annealing condition influences thermal hysteresis of fungal type ice-binding proteins. *Cryobiology* **68**, 159-161.

112. Park, K. S., Do, H., Lee, J. H., Park, S. I., Kim, E., Kim, S.-J., Kang, S.-H. and Kim, H. J. (2012) Characterization of the ice-binding protein from Arctic yeast *Leucosporidium* sp. AY30. *Cryobiology* **64**, 286-296.

113. Takamichi, M., Nishimiya, Y., Miura, A. and Tsuda, S. (2007) Effect of annealing time of an ice crystal on the activity of type III antifreeze protein. *FEBS J*. **274**, 6469-6476.

114. McPherson, A. (1990) Current approaches to macromolecular crystallization. *Eur. J. Biochem*. **189**, 1-23.

115. Otwinowski, Z. and Minor, W. (1997) Processing of X-ray diffraction data collected in oscillation mode. *Methods Enzymol*. **276**, 307-326.

116. Winn, M. D., Ballard, C. C., Cowtan, K. D., Dodson, E. J., Emsley, P., Evans, P. R., Keegan, R. M., Krissinel, E. B., Leslie, A. G., McCoy, A., McNicholas, S. J., Murshudov, G. N., Pannu, N. S., Potterton, E. A., Powell, H. R., Read, R. J., Vagin, A. and Wilson, K. S. (2011) Overview of the CCP4 suite and current developments. *Acta Crystallogr., Sect. D: Biol. Crystallogr*. **67**, 235-242.

117. Adams, P. D., Afonine, P. V., Bunkóczi, G., Chen, V. B., Davis, I. W., Echols, N., Headd, J. J., Hung, L. W., Kapral, G. J., Grosse-Kunstleve, R. W., McCoy, A. J., Moriarty, N. W., Oeffner, R., Read, R. J., Richardson, D. C., Richardson, J. S., Terwilliger, T. C. and Zwart, P. H. (2010) PHENIX: a comprehensive Python-based system for macromolecular

structure solution. *Acta Crystallogr., Sect. D: Biol. Crystallogr*. **66**, 213-221.

118. Emsley, P., Lohkamp, B., Scott, W. G. and Cowtan, K. (2010) Features and development of Coot. *Acta Crystallogr., Sect. D: Biol. Crystallogr*. **66**, 486-501.

119. Murshudov, G. N., Vagin, A. A. and Dodson, E. J. (1997) Refinement of macromolecular structures by the maximum-likelihood method. *Acta Crystallogr., Sect. D: Biol. Crystallogr*. **53**, 240-255.

120. Ritchie, D. W. and Kemp, G. J. L. (2000) Protein docking using spherical polar Fourier correlations. *Proteins: Struct. Funct. Genet*. **39**, 178-194.

121. Lawrence, M. C. and Colman, P. M. (1993) Shape complementarity at protein/protein interfaces. *J. Mol. Biol*. **234**, 946-950.

122. Drori, R., Celik, Y., Davies, P. L. and Braslavsky, I. (2014) Ice-binding proteins that accumulate on different ice crystal planes produce distinct thermal hysteresis dynamics. *J. R. Soc. Interface* **11**, 20140526.

123. Matthews, B. W. (1968) Solvent content of protein crystals. *J. Mol. Biol*. **33**, 491-497.

124. Brünger, A. T. (1992) Free R value: a novel statistical quantity for assessing the accuracy of crystal structures. *Nature* **355**, 472-475.

125. Chen, V. B., Arendall, W. B. 3rd, Headd, J. J., Keedy, D. A., Immormino, R. M., Kapral, G. J., Murray, L. W., Richardson, J. S. and Richardson, D. C. (2010) MolProbity: all-atom structure validation for macromolecular crystallography. *Acta Crystallogr., Sect. D: Biol. Crystallogr*. **66**, 12-21.

126. Meister, K., Ebbinghaus, S., Xu, Y., Duman, J. G., DeVries, A., Gruebele, M., Leitner, D. M. and Havenith, M. (2013) Long-range protein–water dynamics in hyperactive insect antifreeze proteins. *Proc. Natl. Acad. Sci. U.S.A.* **110**, 1617-1622.

127. Davies, P. L. (2014) Ice-binding proteins: a remarkable diversity of structures for stopping

and starting ice growth. *Trends Biochem. Sci*. **39**, 548-555.

128. Jorov, A., Zhorov, B. S. and Yang, D. S. (2004) Theoretical study of interaction of winter flounder antifreeze protein with ice. *Protein Sci*. **13**, 1524-1537.

129. Wishart, D. S., Willard, L., Richards, F. M. and Sykes, B. D. (1994) VADAR: a comprehensive program for protein structure evaluation, version 1.2. University of Alberta, Edmonton, Alberta, Canada.

130. Hsiang, T., Matsumoto, N. and Millett, S. M. (1999) Biology and management of Typhula snow molds of turfgrass. *Plant Dis*. **83**, 788-798.

131. Snider, C. S., Hsiang, T., Zhao, G. and Griffith, M. (2000) Role of ice nucleation and antifreeze activities in pathogenesis and growth of snow molds. *Phytopathology* **90**, 354-361.

132. Hoshino, T., Xiao, N. and Tkachenko, O. B. (2009) Cold adaptation in the phytopathogenic fungi causing snow molds. *Mycoscience* **50**, 26-38.

133. Riedel, A., Michel, C. and Gosselin, M. (2006) Seasonal study of sea-ice exopolymeric substances on the Mackenzie shelf: implications for transport of sea-ice bacteria and algae. *Aquat. Microbial Ecol*. **45**, 195-206.

134. Krembs, C. E., Eicken, H., Junge, K. and Deming, J. W. (2002) High concentrations of exopolymeric substances in Arctic winter sea ice: implications for the polar ocean carbon cycle and cryoprotection of diatoms. *Deep-Sea Res. Part I* **49**, 2163-2181.

135. Chao, H., Sönnichsen, F. D., DeLuca, C. I., Sykes, B. D. and Davies, P. L. (1994) Structure-function relationship in the globular type II antifreeze protein: Identification of a cluster of surface residues required for binding to ice. *Protein Sci*. **3**, 1760-1769.

136. Deng, G. and Laursen, R. A. (1998) Isolation and characterization of an antifreeze protein from the longhorn sculpin, *Myoxocephalus octodecimspinosis*. *Biochim. Biophys. Acta*

1388, 305-314.

137. Kristiansen, E., Ramløv, H., Hagen, L., Pedersen, S. A., Andersen, R. A. and Zachariassen, K. E. (2005) Isolation and characterization of hemolymph antifreeze proteins from larvae of the longhorn beetle *Rhagium inquisitor* (L). *Comp. Biochem. Physiol. B* **142**, 90-97.

138. Gauthier, S. Y., Kay, C. M., Sykes, B. D., Walker, V. K. and Davies, P. L. (1998) Disulfide bond mapping and structural characterization of spruce budworm antifreeze protein. *Eur. J. Biochem.* **258**, 445-453.

139. Smallwood, M., Worrall, D., Byass, L., Elias, L., Ashford, D., Doucet, C. J., Holt, C., Telford, J., Lillford, P. and Bowles, D. J. (1999) Isolation and characterization of a novel antifreeze protein from carrot (*Daucus carota*). *Biochem. J.* **340**, 385-391.

140. Kiani, H. and Sun, D.-W. (2011) Water crystallization and its importance to freezing of foods: a review. *Trends Food Sci. Technol.* **22**, 407-426.

141. Yang, C. and Sharp, K.A. (2004) The mechanism of the type III antifreeze protein action: a computational study. *Biophys. Chem*. **109**, 137–148.

142. Decker, K. L. M., Wang, D., Waite, C. and Scherbatskoy, T. (2003) Snow removal and ambient air temperature effects on forest soil temperatures in Northern Vermont. *Soil Sci. Soc. Am*. **67**, 1234–1242.

143. Hoshino, T., Xiao, N., Yajima, Y., Kida, K., Tokura, K., Murakami, R., Tojo, M. and Matsumoto, N. (2013) Ecological strategies of snow molds to tolerate freezing stress. In *Plant and Microbe Adaptations to Cold in a Changing World* (pp. 285-292). Springer New York.